

# Hamiltonian theory of integrable generalizations of the nonlinear Schrödinger equation

V. G. Marikhin

*L. D. Landau Institute of Theoretical Physics, Russian Academy of Sciences, 142432 Chernogolovka, Moscow Region, Russia*

(Submitted 9 October 1997; resubmitted 30 October 1997)

Pis'ma Zh. Éksp. Teor. Fiz. **66**, No. 11, 673–678 (10 December 1997)

A method for constructing integrable systems and their Bäcklund transformations is proposed. The case of integrable generalizations of the nonlinear Schrödinger equation in the one-dimensional case and the possibility of extending the method to higher dimensions are discussed in detail. The existence of Bäcklund transformations of a definite type in the systems considered is used as a criterion of integrability. This leads to “gauge fixing” — the number of physically different integrable systems is strongly diminished. The method can be useful in constructing the admissible nonlinear terms in some models of quantum field theory, e.g., in Ginzburg–Landau functionals. © 1997 American Institute of Physics. [S0021-3640(97)00123-0]

PACS numbers: 03.70.+k, 03.65.Ge

## 1. INTEGRABILITY CRITERION AND CHOICE OF GAUGE

The nonlinear Schrödinger equation (NSE) and a number of systems which generalize the NSE, of which several tens are known (see, for example, Ref. 1), are well known in the theory of integrable systems. There exist many integrability criteria for such systems. Because these criteria obviously are related with one another, it is natural to choose a criterion which, on the one hand, will make it possible to distinguish systems that are truly different and which, on the other, does not obscure the physical reason for the integrability of these systems.

The following criterion is used in the present letter: There exists a canonical transformation that does not change the Hamiltonian of the system. The action  $S = \int dt dx (pq_t - H)$  is thereby invariant and hence the transformation obtained is a Bäcklund transformation (BT) (see Refs. 2 and 6 for a discussion of the relation between BTs and the inverse-problem method) for the given system, i.e., it transforms one solution into another.

The objective of the present letter is not so much to construct a complete classification of integrable systems (though such a classification will be obtained in a simple and condensed form for one-dimensional systems of the NSE type) as to determine in a physically transparent form their discrete symmetries, which play almost the same role in the theory of integrable systems as continuous symmetries play in gauge theories.

At the end of this letter we will examine the possibility of extending the method to two dimensions, specifically, we will give the form of the Hamiltonian and the BT for the

Davey–Stewartson system and discuss possible physical applications.

So, consider a system of the form

$$\begin{aligned} u_t &= u_{xx} + F(u_x, v_x, u, v), \\ -v_t &= v_{xx} + G(u_x, v_x, u, v). \end{aligned} \quad (1)$$

It is easy to see that the substitution

$$F = uv^2, \quad G = u^2v, \quad u = \psi, \quad v = \psi^*$$

transforms the system (1) into an ordinary nonlinear Schrödinger equation. As another interesting example, the substitutions<sup>1</sup>

$$n_- = 2/(u-v), \quad n_+ = -2uv/(u-v), \quad n_3 = (u+v)/(u-v)$$

transform the well-known Heisenberg model (or the  $n$ -field model,  $\mathbf{n}_t = \mathbf{n}_{xx} \times \mathbf{n}$ ) into an  $u-v$  system, if  $F = -2u_x^2/(u-v)$  and  $G = 2v_x^2/(u-v)$ . The standard method of proving integrability is to determine the functions  $F$  and  $G$  for which Eqs. (1) are a simultaneous system. However, here we proceed immediately to the Hamiltonian formalism. We require that the first Hamiltonian equation, specifically,  $q_t = \delta H / \delta p$ , immediately give one of the equations of the  $u-v$  system (1) (for example, the equation for  $v$ ). This requirement already strongly limits the form of the Hamiltonian:

$$H = p_x q_x + h(q_x, q, p). \quad (2)$$

Here  $q = v$  and the momentum  $p$  must be expressed in terms of  $u$  and  $v$ , but it is important that the function  $h$  not depend on  $p_x$ .

It is obvious that there also exists a representation that is dual to Eq. (2), specifically,

$$\hat{H} = -\hat{p}_x \hat{q}_x + \hat{h}(\hat{q}_x, \hat{q}, \hat{p}), \quad \hat{q} = u, \quad \hat{p} = \hat{p}(u, v), \quad (3)$$

which on variation with respect to  $\hat{p}$  gives the equation for  $u$  in the system (1). In order to specify even more the form of the Hamiltonian and also to relate the Hamiltonians  $H$  and  $\hat{H}$ , I shall formulate the integrability conditions:

1. There exist BTs  $B(p, q) = (\tilde{p}, \tilde{q})$  under which the Hamiltonian and Poisson brackets are invariant (in the case of NSE-type systems the trivial Poisson brackets  $\{p, q\} = 1$  can always be chosen; however, it is technically more convenient not to follow the brackets but rather to require that the temporal part of the action, in this case  $p q_t$ , be invariant).

2. The transformations  $B$  can be represented in the form of a composition of two “gauge” transformations  $B_p$  and  $B_q$ , such that

$$\begin{aligned} B_p(p, q) &= (\tilde{p}, q): \quad p = \tilde{p} + \frac{\delta T[q]}{\delta q}, \\ B_q(\tilde{p}, q) &= (\tilde{p}, \tilde{q}): \quad q = \tilde{q} + \frac{\delta S[\tilde{p}]}{\delta \tilde{p}}, \\ B &= B_q B_p. \end{aligned} \quad (4)$$

3. The next condition is duality. Under the transformations  $B_p$  and  $B_q$  the Hamiltonian transforms as

$$H(p, q) \rightarrow \hat{H}(\tilde{p}, q) \rightarrow H(\tilde{p}, \tilde{q}). \quad (5)$$

We note that the transformations  $B_p$  and  $B_q$  are strongly reminiscent of a gauge transformation of the vector potential  $A_\mu = \tilde{A}_\mu + \partial_\mu f$ . Drawing an analogy reveals an interesting fact — the action of the integrable system is gauge-invariant literally: The Hamiltonian  $H$  does not change at all under the canonical transformation  $B$ !

The next problem is to find the specific form of the transformations (1) and indicate possible functions  $h$ .

## BACKLUND TRANSFORMATIONS AND HAMILTONIANS OF $u-v$ SYSTEMS

On account of the form of  $B_p$ , the Hamiltonian is a quadratic polynomial in  $p$ :

$$H = p_x q_x + a(q_x, q) p^2 + b(q_x, q) p + c(q_x, q). \quad (6)$$

All Hamiltonians (6) can be divided into two classes:

1. The first class consists of systems with translational invariance. In this case, the coefficients  $a$ ,  $b$ , and  $c$  are independent of  $q$  and depend only on  $q_x$ . These systems possess “density-current” type conservation laws and the BTs are especially simple:

$$B_p : \frac{\delta T}{\delta q} = \frac{q_{xx}}{a(q_x)}. \quad (7)$$

Duality in this case has the form  $p \rightarrow q_x$ . So, the most general form of integrable Hamiltonians with the translational invariance is

$$H = p_x q_x + p^2 a(q_x) + p b(q_x) + c(q_x). \quad (8)$$

On account of duality, the functions  $a$ ,  $b$ , and  $c$  are quadratic polynomials in  $q_x$ .

2. “Magnetic” systems are a more complicated example of integrable  $u-v$  systems. It can be shown that in this case the quantities  $b$  and  $c$  depend only on  $q$  and are independent of  $q_x$ . The quantity  $a$  has the form  $a = q_x^2 + r(q)$ . The Hamiltonian in this case is

$$H = p_x q_x - p^2 q_x^2 - p^2 r(q) - p \frac{r'(q)}{2} - \frac{r''(q)}{12}. \quad (9)$$

The BTs are quite simple in this case also:

$$p = \tilde{p} - \frac{q_{xx} + r'(q)}{q_x^2 + r(q)}, \quad q = \tilde{q} + \frac{1}{\tilde{p}}.$$

We have obtained an important result: In terms of the Hamiltonian there exist only two integrable systems of the NSE type, specifically, the Hamiltonian (8) with a momentum conservation law and the Hamiltonian (9) without such a law. To understand which

$u-v$  systems are integrable, it is necessary to construct the correspondence  $(p, q) \rightarrow (u, v)$ . In the next sections I shall discuss possible variants and also indicate the corresponding  $u-v$  systems.

### 3. TRANSITIONS TO $u-v$ SYSTEMS

This transition can be made in two different ways — it can be assumed that duality is equivalent to identity, i.e., we can study the case  $p = \hat{p}$  or the general case. Of course, the first method is simpler,  $p = g(u-v)$ . I give immediately the answers for the cases with a momentum conservation law

$$u_t = u_{xx} + 2a(u_x)g(u-v) + b(u_x), \quad -v_t = v_{xx} + 2a(v_x)g(u-v) + b(v_x), \quad (10)$$

where  $g' = \tilde{a}(g)$  is a quadratic polynomial, and without a momentum conservation law (Landau–Lifshitz model<sup>1</sup>)

$$u_t = u_{xx} - 2 \frac{u_x^2 + r(u)}{u-v} + \frac{r'(u)}{2}, \quad -v_t = v_{xx} + 2 \frac{v_x^2 + r(v)}{u-v} + \frac{r'(v)}{2}, \quad (11)$$

where  $r$  is a biquadratic polynomial. In the next section I shall examine the most non-trivial generalization of the NSE — the case without a momentum conservation law and with a nontrivial dependence of the momentum on  $u$  and  $v$  — a generalized Landau–Lifshitz model. In the present section I shall derive this dependence for  $p$  and  $\hat{p}$  and construct “magnetic” (the momentum  $p$  depends on the velocity  $u_x, v_x$ )  $u-v$  systems with translational invariance. It can be shown that the momenta  $p$  and  $\hat{p}$  have the form

$$p = f(u-v)u_x + g(u-v), \quad \hat{p} = f(u-v)v_x + g(u-v). \quad (12)$$

Indeed,  $\hat{p} - p$  is a total derivative, i.e., the momenta are related by a gauge transformation. In this case integrability is expressed in terms of duality as

$$H(p, q) = \hat{H}(\hat{p}, \hat{q}), \quad (13)$$

which gives relations for the functions  $f$  and  $g$

$$2g = f'/f + \alpha f, \quad (f')^2 = \gamma f^4 + c_1 f^3 + c_2 f^2, \\ a(x) = x^2 + \alpha x + \beta, \quad \gamma = \alpha^2 - 4\beta. \quad (14)$$

### 4. HAMILTONIAN AND TRANSFORMATIONS OF THE GENERALIZED LANDAU–LIFSHITZ MODEL

Let us examine a generalized Landau–Lifshitz model (see, for example, Ref. 1) in the form of a  $u-v$  system:

$$u_t = u_{xx} + \frac{1}{h}(2v_x - h_u)(u_x^2 + r(u)) + \frac{r'(u)}{2}, \\ -v_t = v_{xx} - \frac{1}{h}(2u_x + h_v)(v_x^2 + r(v)) + \frac{r'(v)}{2}. \quad (15)$$

Here  $h(u,v)$  is a symmetric quadratic polynomial in each of the variables and  $r(u) = 1/4(2h_{vv}h - h_v^2)$ .

I shall show that the system (15) is a consequence of two pairs of Hamiltonian equations. Let

$$q = v, \quad p = -\frac{1}{h}\left(\hat{q}_x + \frac{h_q}{2}\right), \quad \hat{q} = u, \quad \hat{p} = -\frac{1}{h}\left(q_x - \frac{h_{\hat{q}}}{2}\right),$$

$$h = h(\hat{q}, q). \tag{16}$$

I now construct the two Hamiltonians

$$H = p_x q_x - p^2(q_x^2 + r(q)) - p \frac{r'(q)}{2} - \frac{r''(q)}{12},$$

$$\hat{H} = -\hat{p}_x \hat{q}_x - \hat{p}^2(\hat{q}_x^2 + r(\hat{q})) + \hat{p} \frac{r'(\hat{q})}{2} - \frac{r''(\hat{q})}{12}. \tag{17}$$

It is easy to show that variation of  $H$  with respect to  $p$  gives the equation for  $v$  in the system (15). Similarly, variation of  $\hat{H}$  with respect to  $\hat{p}$  gives the equation for  $u$ . But the main point is that, to within total derivatives, the Hamiltonians  $H$  and  $\hat{H}$  are identical

$$\hat{H}(\hat{p}, \hat{q}) = H(p, q), \tag{18}$$

and moreover, the Lagrangians are also identical:  $\hat{L} = L$ .

Evidently, some clarifications are in order: One would think that it would be natural to choose one of the Hamiltonians, for example  $H$ , vary it with respect to  $p$  and  $q$ , and obtain immediately the system (15). Certain difficulties arise in so doing: The equation for  $v$  is obtained immediately, but instead of the equation for  $u$  we would obtain its covariant consequence (i.e., an equation of the form  $(\partial_x - f)(u_t - u_x x - F \times (u_x, v_x, u, v)) = 0$ ; see Eq. (1)). Comparing now Eqs. (9) and (17) shows that in terms of the Hamiltonian the systems (11) and (15) are identical.

The Bäcklund transformations

$$\hat{p}(U, V) - p(u, v) = \frac{v_{xx} + r'(v)/2}{v_x^2 + r(v)}, \quad U = v, \tag{19}$$

transform the solution of the  $(u, v)$  system (15) into the solution  $(U, V)$ .

## 5. CONCLUSIONS

I have made use of the invariance of the action under Bäcklund transformations to construct integrable systems and their BTs. Since these transformations were assumed to be canonical, the invariance of the action is equivalent to invariance of the Hamiltonian. Moreover, such a choice of the BTs decreased substantially (to within substitutions) the list of integrable systems by fixing the gauge. The method can be easily applied to one-dimensional integrable systems such as the KdV, sine-Gordon, etc. systems, and moreover the method can be extended to two dimensions. It should be noted that in the

two-dimensional case the pair of variables  $p$  and  $q$  is insufficient; nonlocal variables must be introduced (compare with Ref. 3). I give a specific example: The well-known two-dimensional Davey–Stewartson  $u-v$  system

$$u_t = u_{xx} + 2(uV)_x, \quad v_t = -v_{xx} + (V^2)_y + 2u_x, \quad V_y = v_x, \quad (20)$$

has a simple Hamiltonian representation

$$H = p_x q_x + p q_x^2 + p P_x, \quad (21)$$

where  $P_y = p$ ,  $v = q_y$ , and  $u = p$ . This fits completely within the scheme described above, provided that  $a$ ,  $b$ , and  $c$  in Eq. (6) can be not only functions but also self-adjoint operators, in this case,  $a = \partial_x \partial_y^{-1}$ .

The BTs obtained above make it possible to “reproduce” solutions of the systems considered, an indication, apparently, of their integrability. Moreover, the Miura transformations,<sup>4</sup> which make it possible to obtain matched pairs of Poisson brackets and carry out the standard Lenard–Magri scheme<sup>5</sup> for constructing the first integrals, are closely related with the BTs.

Apparently, the method can be applied, for example, to the classification of possible types of interactions in the action of a field theory. Consider, for example, the Ginzburg–Landau functional with time dependence. Just as in the standard NSE, the choice of the quadratic terms in this functional is unique, which cannot be said of the higher-order terms. Of course, the theory developed cannot be extended directly to high dimensions in the symmetric (with respect to the derivatives) case, but it can be conjectured that the form of the vacuum Ginzburg–Landau solutions far from a transition point, where higher order terms are important, can be estimated from the one-dimensional solution. An example where this conjecture works is a disordered metal, where far from the mobility edge a symmetric instanton makes the main contribution to the density of states. It is well known that the asymptotic behavior and the contribution to the action for such an instanton are identical, to within a numerical factor, for any dimension and are determined by the symmetry of the fourth-order term. Therefore, once the symmetry of such terms is analyzed, the method developed above can be used to attempt a continuation of the Ginzburg–Landau theory with time dependence into a region far from the transition point.

In closing, I wish to thank A. B. Shabat for formulating the problem and for helpful discussions.

<sup>1</sup>A. V. Mikhaïlov, A. B. Shabat, and R. I. Yamilov, *Usp. Mat. Nauk* **42**(4), 3 (1987).

<sup>2</sup>R. M. Miura, *Lect. Notes Math.* **515** (1976).

<sup>3</sup>A. B. Shabat and R. I. Yamilov, *Phys. Lett. A* **227**, 15 (1997).

<sup>4</sup>R. M. Miura, *J. Math. Phys.* **9**, 1202 (1968).

<sup>5</sup>F. A. Magri, *J. Math. Phys.* **19**, 1156 (1978).

<sup>6</sup>A. B. Shabat and V. É. Adler, *Teor. Mat. Fiz.* **113** (3), 323 (1997).

Translated by M. E. Alferieff

## Spherical striations in a glow discharge

O. A. Nerushev, S. A. Novopashin,<sup>a)</sup> V. V. Radchenko, and G. I. Sukhinin  
*Institute of Thermal Physics, Siberian Branch of the Russian Academy of Sciences,  
630090 Novosibirsk, Russia*

(Submitted 15 September 1997; resubmitted 17 October 1997)  
*Pis'ma Zh. Éksp. Teor. Fiz.* **66**, No. 11, 679–682 (10 December 1997)

The stratification of a volume glow discharge is observed experimentally. Spherically symmetric stationary striations are detected. © 1997  
*American Institute of Physics.* [S0021-3640(97)00223-5]

PACS numbers: 52.80.Hc

The appearance of glowing and dark regions (striations) in the positive column of a glow discharge in a tube is a well-known phenomenon, first observed in 1843.<sup>1</sup> It has now been established that the striations are due to ionizational instability, and the phenomenon is known as ionization waves.<sup>2–6</sup> As far as we know, stratification of a volume glow discharge has still not been investigated theoretically or experimentally.

We report in this letter the experimental observation of three-dimensional striations consisting of a series of nearly spherical, glowing surfaces, one surface enclosing another.

The experiments were performed in a cylindrical steel vacuum chamber 60 cm high and 50 cm in diameter (Fig. 1). The lowest pressure to which it could be evacuated was  $10^{-2}$  Pa. After evacuation, the volume could be filled with different gases. The experiments were performed under static (no gas flow) conditions in the pressure range 2–50 Pa. A high-voltage cable without braided shielding was inserted into the chamber along the radial direction at mid-height. The uninsulated end, 0.3 cm in diameter and 1 cm long, was located at the geometric center of the chamber. The inner surface of the vacuum chamber served as the cathode. A high-voltage regulable power supply with a maximum voltage of 1 kV powered the discharge. The current was set by a regulating ballast resistance and could be varied up to a maximum value of 40 mA. The voltage drop across the discharge was about 400 V. The vacuum chamber was equipped with flanges with four glass windows, 15 cm in diameter, positioned at mid-height for visual observation and photographing from different angles.

When the voltage on the inner electrode is positive, a collection of concentric, spherical glowing regions (striations), one enclosing another, is observed around the electrode. The spherical symmetry of the glowing regions is based on observations from different windows. A photograph of the observed phenomenon is displayed in Fig. 2. The characteristic size of the glowing region is 10 cm (the feed cable, whose diameter equals 9 mm, can be seen by carefully examining the photograph). The number of striations observed in the experiment ranged from a single striation up to more than 10 (four striations can be seen in Fig. 2). A stationary glow pattern can be observed for several minutes.

The size of the striations depends on the pressure and composition of the gas. The

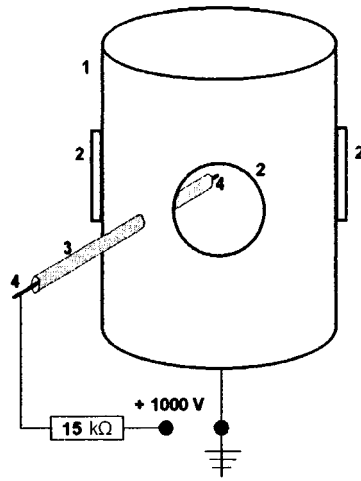


FIG. 1. Experimental apparatus: 1 — Vacuum chamber, 2 — windows, 3 — insulator, 4 — central electrode.

absolute radius of a striation is close to inversely proportional to the pressure. The dependence of the radius of a striation on the number of the striation is shown in Fig. 3. The radii are normalized to the radius of the central glowing zone. Starting at the second striation, the dependence can be approximated as

$$r_n/r_0 = \alpha^n = e^{\beta n}, \quad (1)$$

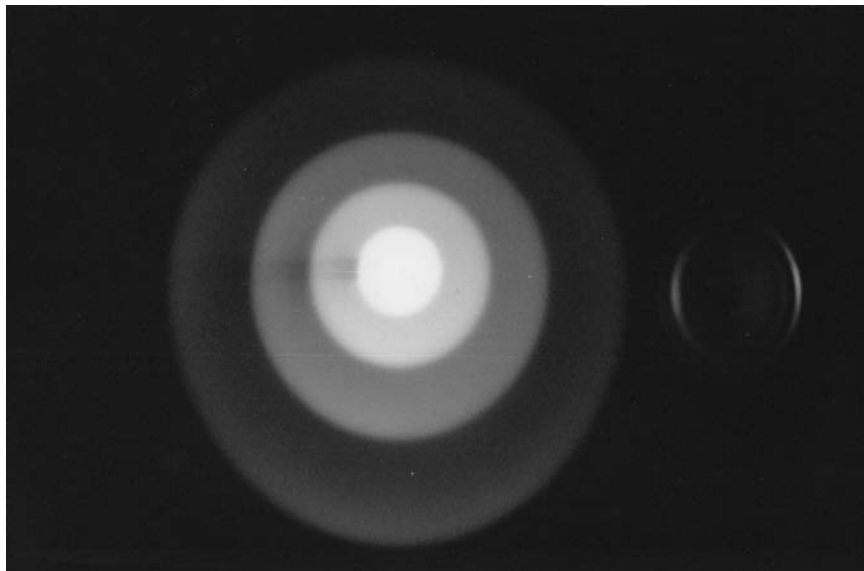


FIG. 2. Glow of a stratified discharge.

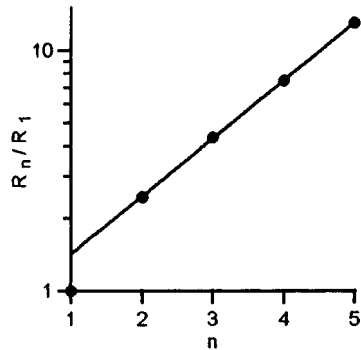


FIG. 3. Radius of the striations versus the number of the striation.

The coefficients  $\alpha$  and  $\beta$  depend on the discharge burning conditions. The experimental values of  $\alpha$  lie in the range 1.4–2. Striations were observed in molecular gases: air, nitrogen, CO<sub>2</sub>. Adding a high-molecular gas (acetone, benzene vapors) increases the number of striations and decreases their size (the coefficient  $\alpha$  in Eq. (1) decreases). Striations were not observed in pure argon in the experimental pressure range. However, adding a molecular gas resulted in the appearance of striations. Striations are also not observed with a different polarity of the power supply. Under these conditions the discharge voltage is much higher (about 1 kV) and the current is much lower (about 2 mA). In concluding the experimental part, it should be noted that there is an analogy between the observed phenomenon and double layers,<sup>7</sup> which were observed in a volume glow discharge in argon, but under conditions of gas flow and a gas density gradient in the discharge region.

We shall now present some estimates of the discharge parameters. It is known that for a stratified discharge in tubes the voltage drop between the striations is positive. This jump in the voltage is due to electron energy losses in inelastic collisions.<sup>4,6</sup> Let us assume that the same situation is also realized in the three-dimensional case. Using the experimentally measured dependence of the distance between striations on the discharge voltage  $\Phi$ , it is possible to estimate the dependence of the potential on the radius (the presence of a volume charge changes the distribution of the potential) and the distribution  $\rho(r)$  of the volume charge. The electrical potential of  $n$ -th striation can be represented, taking account of Eq. (1), as

$$\varphi(r_n) = \Phi - \varphi_0 n = \Phi - \varphi_0 \ln(r_n/r_0)/\beta.$$

The quantity  $\varphi_0$  depends on the type of and energy spectrum of the gas and the electron energy loss cross sections. Ordinarily,  $\varphi_0$  equals several electron volts and is correlated with the energy  $\epsilon_1$  of the first electronic excitation (or ionization potential of the gas). Let us assume that the smoothed potential between the anode and cathode layers can be represented by a similar expression

$$\varphi(r) = \Phi - \varphi_0 \ln(r/r_0)/\beta, \quad E(r) = -\partial\varphi(r)/\partial r = \varphi_0/\beta r. \quad (2)$$

The Poisson equation gives the volume-charge distribution  $\rho(r) = \varphi_0/4\pi\beta r^2$ . It is easy to see that the breakdown of the quasineutrality of the plasma is due to the presence of excess ions.

Assuming that the discharge current  $J$  is due predominantly to the electrons, we estimate the electron density  $n_e(r)$  from the relation

$$j_e(r) = J/4\pi r^2 = -en_e(r)\mu_e E(r), \quad (3)$$

where  $j_e(r)$  is the electron current density and  $\mu_e$  is the electron mobility. Comparing Eqs. (2) and (3) shows that the electron density is inversely proportional to the radius. Substituting numerical values for the mobility  $\mu_e$  (Ref. 5) and the current density  $j_e(r)$ , we obtain that for all distances, starting with the radius of the anode, the breakdown of quasineutrality is small:

$$\rho(r) = \rho_i(r) - \rho_e(r) \ll \rho_e(r).$$

In conclusion, we shall make several general remarks. First, the spherically symmetric stratification of the discharge is stable (the experiments were performed in a cylindrical chamber and the striations have a clearly expressed spherical symmetry).

Second, despite the smallness of the breakdown of neutrality the presence of a volume charge apparently strongly influences the potential distribution, leading to the self-similar law (1) in the spatial arrangement of the striations.

Third, the existence of three-dimensional striations simplifies the solution of the problem of stratification of a glow discharge in connection with the absence of walls. Mathematically, the problem becomes one-dimensional.

Fourth, the longitudinal electric field in the positive column of a glow discharge in tubes is virtually constant (translational symmetry holds approximately). For this reason, the observation of stationary striations for a discharge in tubes is due to the presence of inhomogeneities of some type in the region of the positive column.<sup>4-6</sup> For the three-dimensional case, strong gradients of the electric field themselves serve as an inhomogeneity. This is apparently the reason why only stationary striations were observed in our experiments.

Financial support for this work was provided by the Russian Fund for Fundamental Research under Grant No. 96-02-19045.

<sup>a)</sup>e-mail: sanov@itp.nsc.ru

<sup>1</sup>M. Abria, *Ann. Chim. Phys.* **7**, 462 (1943).

<sup>2</sup>A. V. Nedospasov, *Usp. Fiz. Nauk* **94**, 439 (1968) [*Sov. Phys. Usp.* **11**, 174 (1968)].

<sup>3</sup>L. Pekarek, *Usp. Fiz. Nauk* **94**, 463 (1968) [*Sov. Phys. Usp.* **11**, 188 (1968)].

<sup>4</sup>L. D. Tsandin, *Plasma Sources Sci. Technol.* **4**, 200 (1995).

<sup>5</sup>Yu. P. Raizer, *The Physics of Gas Discharges* [in Russian], Nauka, Moscow, 1987.

<sup>6</sup>Yu. V. Golubovskii and S. U. Nisimov, *Zh. Tekh. Fiz.* **66**(7), 20 (1996) [*Tech. Phys.* **41**, 645 (1996)].

<sup>7</sup>L. Conde and L. Leon, *Phys. Plasmas* **1**(8), 2441 (1994).

Translated by M. E. Alferieff

## Dependence of the specific heat of a $\text{La}_{1.85}\text{Sr}_{0.15}\text{CuO}_4$ superconducting single crystal on the magnetic field direction in the $a$ - $b$ plane

M. N. Khlopkin, G. Kh. Panova, N. A. Chernoplekov, and A. A. Shikov  
*Kurchatov Institute Russian Science Center, 123182 Moscow, Russia*

(Submitted 14 October 1997)

*Pis'ma Zh. Éksp. Teor. Fiz.* **66**, No. 11, 683–687 (10 December 1997)

The low-temperature specific heat of a  $\text{La}_{1.85}\text{Sr}_{0.15}\text{CuO}_4$  superconducting single crystal was investigated in magnetic fields up to 8 T and with four orientations — in the  $a$ - $b$  plane (along the (100) and (110) directions) and at angles of  $45^\circ$  and  $90^\circ$  with respect to the  $a$ - $b$  plane (along the (103) and (001) directions). Anisotropy was observed in the field dependence of the specific heat in the  $a$ - $b$  plane. The specific heat was found to be minimum with the field oriented in the direction of the  $a$  axis and maximum with the field oriented in a direction making an angle of  $45^\circ$  with the  $a$  axis. This can be explained by the anisotropy of the energy gap, whose minimum lies along the (110) direction. For all orientations of the magnetic field the specific heat of the mixed state at low temperatures is a nonlinear function of the magnetic field strength.

© 1997 American Institute of Physics. [S0021-3640(97)00323-X]

PACS numbers: 74.72.Dn, 74.25.Bt, 65.40.+g

The study of the anisotropic properties of high- $T_c$  superconductors in a magnetic field has become important in recent years in connection with questions concerning the symmetry of the superconducting gap, including the two-dimensional anisotropy of the gap in the  $a$ - $b$  plane. Experiments on photoemission spectroscopy,<sup>1</sup> Raman scattering,<sup>2</sup> quasiparticle tunneling,<sup>3</sup> heat conduction,<sup>4</sup> and magnetoresistance<sup>5</sup> attest to the anisotropic behavior of the gap in the  $a$ - $b$  plane. It should be noted that experiments on the direct observation of gap anisotropy, which were performed by tunneling spectroscopy<sup>3</sup> and angle-resolved photoemission<sup>1</sup> methods, give contradictory information concerning the direction in which the gap width has its maximum value. For this reason, experimental investigations of manifestations of gap anisotropy by a new, independent method are undoubtedly of interest. An important, though indirect, manifestation of the nontrivial symmetry of the superconducting gap could be anisotropy of the specific heat of a superconductor in a mixed state with the magnetic field lying in the  $a$ - $b$  plane of the crystal.

We note that investigations of the thermal properties of superconductors (specific heat and thermal conductivity), in contrast to electric investigations, remain informative at temperatures far below the superconducting transition temperature. In the case of investigations in magnetic fields, thermal measurements are, as a rule, less sensitive to pinning than are magnetic measurements (since the external magnetic field remains un-

changed during the measurement process), so that the results should be more reliable.

Our objective in the present work was to investigate the anisotropy of the superconducting properties of a  $\text{La}_{1.85}\text{Sr}_{0.15}\text{CuO}_4$  single crystal, specifically, the field dependence of the specific heat with field orientation in the  $a$ - $b$  plane along the  $a$  axis and at an angle of  $45^\circ$  with respect to the  $a$  axis. The choice of this choice is dictated by two circumstances: 1) The upper critical field in them is not very high, which makes it possible to perform investigations in a quite representative region of the  $H_{c2}$ - $T$  diagram and 2) the parasitic magnetic anomaly in the specific heat is small.

The investigations were performed on one of the bulk  $\text{La}_{1.85}\text{Sr}_{0.15}\text{CuO}_4$  single crystals investigated previously,<sup>6,7</sup> which had been grown by the floating-zone technique.

According to x-ray structural analysis, the sample at room temperature possessed tetragonal structure (F4/mmm) with lattice parameters  $a=b=3.773(1)$  Å and  $c=13.233(2)$  Å. The experimental crystal consisted of several blocks, whose disorientation along the  $a$  and  $c$  axes was of the order of  $10^\circ$ .

The superconducting transition temperature  $T_c$  and the transition width  $\Delta T_c$  were  $T_c=39.2$  K and  $\Delta T_c=0.5$  K with respect to the magnetic susceptibility and resistivity and  $T_c=38$  K and  $\Delta T_c=2$  K with respect to specific heat. A clear jump corresponding to a superconducting transition with amplitude  $\Delta C/T_c=9$  mJ/mole·K<sup>2</sup> was observed in the temperature dependence of the specific heat.

The specific heat of the sample in magnetic fields of up to 8 T was determined by the adiabatic method with pulsed heating.<sup>8</sup> The measurement error was equal to 2% in the temperature range 1.5–4 K, 1% in the range 4–10 K, and 0.2–0.5% in the range 10–50 K.

The specific-heat investigations were performed for four directions of the magnetic field: parallel to the  $a$ - $b$  plane along the  $a$  axis — (100) and at an angle of  $45^\circ$  to the  $a$  axis — (110) as well as at an angle of  $90^\circ$  with respect to the  $a$ - $b$  plane along the  $c$  axis — (001) and at an angle of  $45^\circ$  — (103). We estimate that the total error in determining the orientation and in the positioning of the sample with respect to the field did not exceed  $10^\circ$ .

Experimental data on the low-temperature specific heat in magnetic fields of 0 and 4 T are presented in Fig. 1 in the coordinates  $C/T$  versus  $T^2$  for all four experimental directions of the magnetic field. The magnetic field increases the specific heat, the effect being smaller with field orientation along (100), i.e., along the  $a$  axis in the  $a$ - $b$  plane. The influence of the field is higher in the case of the three other orientations, but the scale is approximately the same. Comparing these results for the two directions (along the  $a$  axis and at an angle of  $45^\circ$  with respect to the  $a$  axis) indicates strong anisotropy of the electronic specific heat in the  $a$ - $b$  plane.

The temperature dependences of the specific heat in the interval 2–8 K are approximated well by a function of the form  $C = \gamma^*(H)T + \beta T^3 + \alpha T^5$  for all values of the magnetic field  $H$ . This makes it possible to determine the coefficient  $\gamma^*(H)$  of the electronic specific heat. The field dependence  $\gamma^*(H)$  is presented in Fig. 2 for four directions of the magnetic field. As one can see from the figure, this dependence is strongly nonlinear for all four orientations of the magnetic field:  $\gamma^*(H)$  grows rapidly

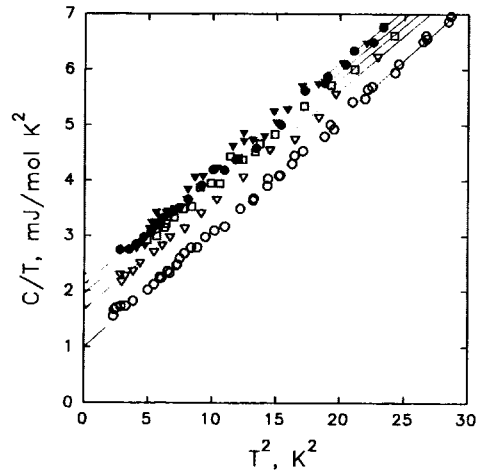


FIG. 1. Temperature dependence of the specific heat of  $\text{La}_{1.85}\text{Sr}_{0.15}\text{CuO}_4$  at low temperatures in magnetic fields 0 and 4 T for four orientations of the field  $H$ :  $\circ$  —  $H=0$ ;  $\nabla$  —  $H\parallel(100)$ ;  $\square$  —  $H\parallel(110)$ ;  $\bullet$  —  $H\parallel(001)$ ;  $\blacktriangledown$  —  $H\parallel(103)$ .

with the field in weak fields and its variation with increasing field is weaker in strong fields. Note that such a dependence is observed for all four directions of the magnetic field. The observed effect of a magnetic field on the specific heat of the experimental sample at low temperatures is different from the Abrikosov theory,<sup>9</sup> which predicts a nearly linear variation of  $\gamma^*$  as a function of  $H$ .

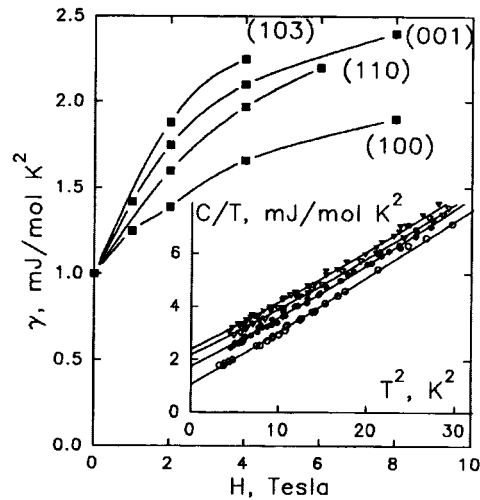


FIG. 2. The coefficient  $\gamma^*(H)$  for four orientations of the field  $H$ . The orientations are indicated in the figure. Inset: Temperature dependence of the specific heat of  $\text{La}_{1.85}\text{Sr}_{0.15}\text{CuO}_4$  at low temperatures with a fixed orientation of the field — parallel to the (100) axis — in different magnetic fields  $H$ :  $\circ$  —  $H=0$ ;  $\bullet$  —  $H=2$ ;  $\nabla$  —  $H=4$ ;  $\blacktriangledown$  —  $H=6$  T.

Comparing the results shows that the  $a$  axis is a distinguished direction. In this direction the effect of a magnetic field on the specific heat is weakest and  $\gamma^*(H)$  has its minimum value. For all other orientations of the magnetic field, the values of  $\gamma^*(H)$  are close to one another and are much higher than the values along the  $a$  axis.

Square-root extrapolation of the magnetic-field dependences of the coefficient of electronic specific heat  $\gamma^*(H)$  which we observed in the mixed state to the value  $\gamma_n$  corresponding to the normal state of the superconductor gives estimates of  $H_{c2}(0)$  which are substantially different for two directions of the field in the  $a$ - $b$  plane, also indicating a  $H_{c2}$  anisotropy in the  $a$ - $b$  plane. As a result, the upper critical field  $H_{c2}$  and energy gap anisotropies as functions of direction in momentum space and the difference in the values of the gap in the  $a$ - $b$  plane can be estimated by studying the field dependence of the electronic specific heat as a function of angle with respect to the crystallographic axes  $a$  and  $c$  in the single crystal.

It should be noted that the anisotropy of the resistive upper critical magnetic field with four-fold symmetry has been observed experimentally in a  $\text{La}_{1.85}\text{Sr}_{0.15}\text{CuO}_4$  single crystal in fields up to 6 T, the scale of the anisotropy in  $H_{c2}(\parallel 100)/H_{c2}(\parallel 110)$  being 10% at 35 K.<sup>5</sup> The anisotropy which we observed has the same sign but a much larger scale. One possible reason for the difference in the values of the anisotropy between our investigations and in Ref. 5 could be the different temperature interval: In Ref. 5 the investigations were performed near  $T_c$ , whereas in our work the investigations were performed substantially below  $T_c$ .

According to the works of Volovik<sup>10,11</sup> and Maki,<sup>12</sup> a nontrivial symmetry of the superconducting gap is manifested in the anomalous behavior of both the low-temperature specific heat of the superconductor in a mixed state and the upper critical field. Both phenomena should exhibit four-fold symmetry upon rotation of the field in the  $a$ - $b$  plane. In Ref. 11 it is shown that in the case of  $d$  pairing there exist two regimes of the influence of the magnetic field on the thermodynamic properties of a superconductor: strong-field ( $x \ll 1$ ) and weak-field ( $x \gg 1$ ). The crossover parameter  $x$  can be expressed in terms of the temperature  $T$ , the magnetic field  $H$ , the critical temperature  $T_c$ , and the upper critical field  $H_{c2}$  as

$$x \sim \frac{T}{T_c} \left( \frac{H_{c2}}{H} \right)^{1/2}.$$

An estimate of the crossover temperature  $T_x$ , determined by the relation  $x \sim 1$ , for  $\text{La}_{1.85}\text{Sr}_{0.15}\text{CuO}_4$  ( $H_{c2} \sim 200$  T,  $T_c = 38$  K) in an external field of 6 T gives a value of the order of 7 K. In Ref. 5 the critical resistive magnetic fields were investigated in fields up to 6 T at temperatures above 30 K, corresponding to the weak-field regime. Our estimates of the anisotropy were based on data obtained in fields up to 8 T but at temperatures 2–8 K, which is below the crossover temperature  $T_x$ , and they pertain to the strong-field regime.

Let us summarize. The specific heat was investigated experimentally in a superconducting  $\text{La}_{1.85}\text{Sr}_{0.15}\text{CuO}_4$  single crystal in a mixed state for four orientations of the field relative to the crystallographic axes: along the  $a$  axis and at an angle of  $45^\circ$  with respect to the  $a$  axis in the  $a$ - $b$  plane and also along the  $c$  and (103) axes. For all orientations of

the magnetic field, the specific heat of the mixed state at low temperatures is a nonlinear function of the magnetic field strength. This is not described by the standard theory of the influence of a magnetic field on superconductivity. From measurements of the specific heat in magnetic fields, we observed anisotropy of the field dependence  $\gamma^*(H)$  for a single-crystalline sample of  $\text{La}_{1.85}\text{Sr}_{0.15}\text{CuO}_4$  in magnetic fields with orientation along the  $a$  axis and at an angle of  $45^\circ$  with respect to the  $a$  axis in the  $a$ - $b$  plane as well as along the  $c$  and (103) axes. A strong anisotropy in the  $a$ - $b$  plane appears in the dependence  $\gamma^*(H)$ , whose value is smallest in the direction of the  $a$  axis and largest in a direction making an angle of  $45^\circ$  with the  $a$  axis; the anisotropy is much larger than in ordinary superconductors.

We call attention to one other important result. Tunneling spectroscopy<sup>3</sup> and angle-resolved photoemission<sup>1</sup> experiments on the direct observation of gap anisotropy give contradictory information about the direction in which the gap has its largest value. The results of our investigations of the specific-heat anisotropy in a  $\text{La}_{1.85}\text{Sr}_{0.15}\text{CuO}_4$  single crystal confirmed the angle-resolved photoemission results: The gap is largest along the Cu-O bond and not at an angle of  $45^\circ$  with respect to this bond; this confirms the predictions of  $d$ -pairing superconductivity models of high- $T_c$  superconductors.

In the future, we would like to continue measurements of the angular dependence of the upper critical field  $H_{c2}(T)$  in the  $a$ - $b$  plane in these and other high- $T_c$  superconductors in order to determine the origin of this anisotropy.

We thank A. M. Balbashov and D. A. Shulyatev for preparing the  $\text{La}_{1.85}\text{Sr}_{0.15}\text{CuO}_4$  samples and V. F. Shamraï and O. E. Parfenov for determining the orientation of the samples.

This work is supported by the Scientific Council on the problem of high- $T_c$  superconductors and was performed as part of Project 96039 in the direction "Superconductivity" of the State Science and Technology Program "Topical Problems in the Condensed-Matter Physics."

<sup>1</sup>Z. X. Shen, D. S. Dessau, B. O. Wells *et al.*, Phys. Rev. Lett. **70**, 1553 (1993).

<sup>2</sup>J. C. Irwin, X. K. Chen, H. J. Trodahl *et al.*, J. Supercond. **8**, 495 (1995).

<sup>3</sup>J. Kane and K. W. Ng, Phys. Rev. B **53**, (1996).

<sup>4</sup>H. Aubin, K. Behnia, M. Ribault *et al.*, Phys. Rev. Lett. **78**, 2624 (1997).

<sup>5</sup>T. Hanaguri, T. Fukase, Y. Koike *et al.*, Physica B **165-166**, 1449 (1990).

<sup>6</sup>A. M. Balbashev, D. A. Shulyatev, G. Kh. Panova *et al.*, Physica C **197**, 303 (1996).

<sup>7</sup>M. N. Khlopkin, G. Kh. Panova, N. A. Chernoplekov *et al.*, Zh. Èksp. Teor. Fiz. **112**, 1386 (1997) [JETP **85**, 775 (1997)].

<sup>8</sup>M. N. Khlopkin, N. A. Chernoplekov, and P. A. Cheremykh, "Low-temperature calorimeter for specific heat measurements in magnetic fields up to 20 T" [in Russian], Preprint IAÉ-3549/10, Kurchatov Institute of Atomic Energy, Moscow, 1982.

<sup>9</sup>A. A. Abrikosov, *Fundamentals of the Theory of Metals*, North-Holland, Amsterdam, 1988 [Russian original, Nauka, Moscow, 1987].

<sup>10</sup>G. E. Volovik, JETP Lett. **58**, 469 (1993).

<sup>11</sup>G. E. Volovik, JETP Lett. **65**, 491 (1997).

<sup>12</sup>K. Maki and H. Won, J. Phys. I France **6**, 2317 (1996).

Translated by M. E. Alferieff

# Dynamic self-organization of magnetic domains in amorphous films with perpendicular anisotropy

G. S. Kandaurova<sup>a)</sup> and V. E. Ivanov

*Ural State University, 620083 Ekaterinburg, Russia*

(Submitted 20 October 1997)

*Pis'ma Zh. Éksp. Teor. Fiz.* **66**, No. 11, 688–692 (10 December 1997)

Dynamic self-organization of magnetic domains is observed in amorphous gadolinium–cobalt films in narrow temperature intervals on both sides of the magnetic compensation point. Spiral dynamic domains form in a limited range of ac magnetic field amplitudes and frequencies. © 1997 American Institute of Physics.

[S0021-3640(97)00423-4]

PACS numbers: 75.60.Ch, 75.50.Kj

1. The dynamic self-organization of a system of interacting moving magnetic domains has been discovered in an investigation of the domain structure of iron garnet (IG) films in an ac magnetic field.<sup>1,2</sup> Further investigations showed a great diversity of ordered dynamic domain structures, the most remarkable of which are spiral dynamic domains (SDDs). Spiral domains form in IG films in a definite bounded region of ac field amplitudes  $H_0$  and frequencies  $f$ . In this ( $H_0$ – $f$ ) region the films pass into an excited state, termed in Ref. 3 the Anger state. The most characteristic indications of this state were determined in Ref. 3: self-organization of a dynamic aggregate of magnetic domains and evolution of this aggregate. Evolution is manifested primarily in that as long as an ac field is present, SDDs arise and vanish with a frequency that is much lower than the pump frequency. Investigation of this phenomenon led to the discovery of many new effects: the formation of ideally ordered two-dimensional domain arrays (lattices) composed of domains with different geometry; unusual pulsations of dumbbell-shaped domains;<sup>4,5</sup> transformation of the sources of dynamic domains;<sup>6,7</sup> unusual dynamic hysteresis properties<sup>8,9</sup> — dynamic single-domainness<sup>7,9,10</sup> induced by the bias field of the Anger state.<sup>11</sup> All this was obtained in an investigation of IG films with perpendicular anisotropy. It was essential to search for and study dynamic self-organization and the Anger state in other single-domain magnetic media. Only then is it possible to talk about universality of this phenomenon in the physics of magnetic domains.

2. We chose as the objects of investigation amorphous gadolinium–cobalt ( $Gd_xCo_{1-x}$ ) films with perpendicular anisotropy. These films can have a wide spectrum of magnetic properties, since in  $Gd_xCo_{1-x}$  systems  $x$  can vary continuously and the temperature  $T_c$  of compensation of the magnetic moment is a linear function of  $x$ . Gd–Co films containing “low-anisotropy” Gd ions are distinguished from other rare-earth–transition element films (for example, Tb–Fe–Co, Dy–Co, and others) by the comparatively “low” coercive force. They have been investigated intensively as alternatives to IG films for use in storage devices based on mobile bubbles. The study of domain-containing media, including IG and Gd–Co films, has remained important to this

day in connection with possible applications of such films in magneto-optic systems,<sup>12</sup> specifically, for visualizing nonuniform magnetic fields<sup>13</sup> and for topographic study of spatially nonuniform temperature fields.<sup>14</sup> On the basis of its static properties, a Kittel-type domain structure in Gd–Co films is the analog of the domain structure of IG films with a perpendicular anisotropy.<sup>15</sup> At the same time, IG films differ substantially from Gd–Co films with respect to microstructure and many other physical properties. The dynamic behavior of the domain structure in Gd–Co films cannot be predicted a priori for the following reasons. Epitaxial IG films are actually single-crystalline dielectrics and, magnetically, three-sublattice ferrimagnets. Gd–Co films are metallic amorphous films with a complicated hierarchy of structural nonuniformities.<sup>16</sup> Magnetically, these are two-sublattice ferrimagnets. Moreover, the coercivity  $H_c$  of domain walls in amorphous films is approximately an order of magnitude higher than in IG films. Films in which  $T_c$  does not differ much from room temperature can be obtained by varying the composition of the system Gd–Co. In this case it becomes possible to vary the saturation magnetization  $M_s$ , the saturation field  $H_s$ , the coercive force  $H_c$ , and the period  $2d_0$  of the domain structure in the demagnetized case over very wide limits by moderately varying the temperature of the sample. This increases the likelihood of finding a combination of these parameters for which SDDs could form in an ac field. This formulation of the experiment led to success in the present work.

3. The experimental Gd–Co films were deposited by ion–plasma sputtering in an argon atmosphere on water-cooled glass substrates coated by a  $0.05 \mu\text{m}$  thick protective layer of  $\text{SiO}_2$ . As a rule, the Gd–Co films, in which a domain structure already formed during sputtering, exhibit stabilization of domain walls.<sup>17</sup> This imposes a substantial limitation on the motion of the walls and rearrangement of the entire domain structure. For this reason, to exclude any parasitic influence of this effect, the films were sprayed on in the presence of a magnetic field oriented perpendicular to their surface. Domain structure was observed with a polar magneto-optic Kerr effect. A spatially uniform sinusoidal ac magnetic field  $H = H_0 \sin(2\pi ft)$  was oriented in a direction normal to the film. The frequency  $f$  of the ac field varied from 0.05 to 50 kHz, and the amplitude  $H_0$  varied from 0 to 300 Oe. The temperature of the samples ranged from  $-20$  to  $150^\circ\text{C}$ . The exposure time for photographing the domain structure was equal to several seconds. The systematization of the experimental data done in Ref. 18 indicates that SDDs form in the presence of a certain combination of magnetic properties, specifically, domain width  $d_0$  and characteristic length of the material.<sup>4</sup> For this reason, in the present work we also took the domain width as the main characteristic associated with the formation of SDDs.

4. We shall demonstrate the obtained results for the example of a  $\text{Gd}_{22}\text{Co}_{78}$  film with perpendicular anisotropy. The thickness of the film was  $L = 0.4 \mu\text{m}$  and the compensation temperature was equal to  $55^\circ\text{C}$ . Figure 1 shows the temperature dependence of the half-period  $d_0$  of the domain structure in the demagnetized state. In the temperature interval  $(T_c - 30, T_c + 30)^\circ\text{C}$  the domain structure is irregular. The configuration and dimensions of the domains are determined mainly by the distribution of the defects on which the domain walls are pinned. The effect of an ac magnetic field at these temperatures is to produce an uncorrelated oscillatory motion of the domain walls near some positions of equilibrium. Increasing the amplitude of the field at all experimental frequencies completely washes out the pattern of the domain structure; this is observed visually as

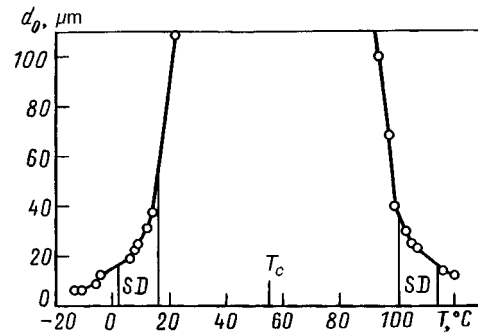


FIG. 1. Temperature dependence of domain width in the demagnetized state of the experimental amorphous gadolinium-cobalt film.

a gray background. Away from  $T_c$  the domain structure becomes labyrinthine, which is typical for films with perpendicular anisotropy. In the temperature ranges  $(1 - 15) ^\circ\text{C}$  and  $(100 - 113) ^\circ\text{C}$  (marked by the letters *SD* in Fig. 1) and in the frequency range 10–50 kHz, SDDs form as the amplitude  $H_0$  increases up to a critical value (curve 1 in Fig. 2). Examples of the patterns of the domain structure in the initial demagnetized state and SDDs at the same temperature  $T = 110 ^\circ\text{C}$  are presented in Figs. 3a and 3b, respectively. Very small SDDs (1–2 loops) are short-lived. They arise and vanish, arise once again, and so on while the pump field acts. The characteristic times for the Anger state, the lifetime  $T_g$  and the waiting time  $T_w$ ,<sup>3</sup> equal 1–2 s. In Fig. 3b such single-loop spirals are seen at the top of the photograph. Relatively large SDDs, consisting of three and more loops (Fig. 3b), are long-lived. For them  $T_g$  was longer than the observation time, which was equal to 10 s at fixed temperature. It was observed that these SDDs are localized in the region of space where they were engendered. There are approximately the same number of SDDs with positive and negative topological charge.<sup>3</sup> When  $H_0$  reaches the second critical value (curve 2 in Fig. 2), the SDDs decay. At higher amplitudes a gray background is seen visually. The amplitude–frequency ( $H_0$ – $f$ ) range of existence of

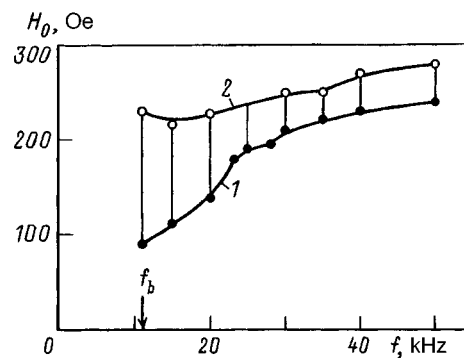


FIG. 2. Amplitude–frequency region of existence of spiral dynamic domains in an amorphous gadolinium-cobalt film at  $100 ^\circ\text{C}$ .

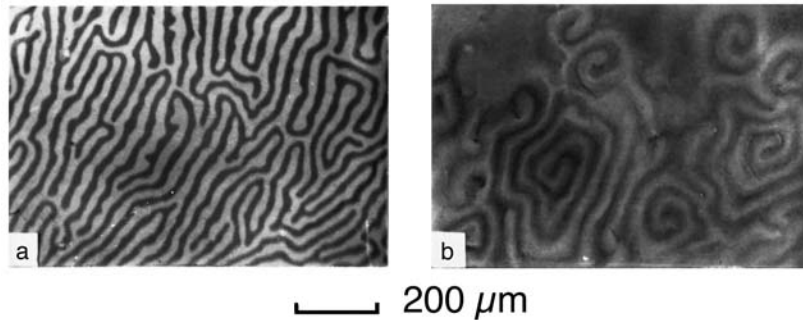


FIG. 3. Photographs of domain structure at temperature  $T=110^\circ\text{C}$  in the same section of the sample in a demagnetized state (a) and in an ac magnetic field with  $H_0=180$  Oe and  $f=30$  kHz (b).

SDDs, presented in Fig. 2, has a sharp limit on the left-hand side at the frequency  $f_b = 10$  kHz. This means that to the left of  $f_b$  and above the curve 2 in Fig. 2 space–time chaos appears in the system of domains. Domains and domain walls in the disordered domain structure move in different directions and with different velocities. Chaos  $\leftrightarrow$  order transitions occur in the region between curves 1 and 2. Here ordered dynamic structures — spiral domains — form; the domain walls oscillate around stable positions of equilibrium. The quantitative characteristics of the  $(H_0-f)$  region change with temperature, remaining qualitatively similar to the region presented in Fig. 2. The frequency  $f_b$  remains quite high:  $f_b > 10$  kHz. The  $(H_0-f)$  region is cut off on the right-hand side by the frequency  $f = 50$  kHz. This is due to the limitations of the method employed to excite the ac field. It is evident from Fig. 1 that the temperature intervals where the SDDs are stable are arranged virtually symmetrically with respect to  $T_c$  and they correspond to the sections of the curve  $d_0(T)$  that are symmetric within the limits of the measurement error.

5. Comparison with IG films shows the following. In IG films, as the amplitude and frequency of the magnetic field change, a large diversity of the ordered SDDs is observed visually; in other words, they have very complicated dynamic domain phase diagrams.<sup>10</sup> So far we have observed only SDDs in the experimental Gd–Co films, and at higher frequencies than in the IG films. Furthermore, spatial localization of multiloop SDDs occurs in Gd–Co films, in contrast to IG films where such SDDs can move relatively freely through the sample and interact with one another. Finally, the maximum number of loops in the SDDs in the experimental Gd–Co films is four or five, while in IG films the number of loops in the SDDs can reach 15–20.

In summary, we have studied the low-frequency dynamics of an aggregate of magnetic domains in amorphous Gd–Co films with perpendicular anisotropy and the investigations were performed in a temperature interval encompassing the magnetic compensation point. Self-organization of a dynamic array of magnetic domains and formation of spiral structures in magnetic films sharply differing in microstructure and many magnetic properties from previously studied IG films was demonstrated. This gives grounds for believing that the phenomenon of dynamic self-organization of multidomain magnetic media is universal.

We thank E. A. Rusinov for assisting in this work.

This work was supported by the Russian Fund for Fundamental Research (Grant 96-02-16199a).

<sup>a)</sup>e-mail: Gerta.Kandaurova@usu.ru

- 
- <sup>1</sup>G. S. Kandaurova and A. É. Sviderskiĭ, JETP Lett. **47**, 490 (1988).  
<sup>2</sup>G. S. Kandaurova and A. É. Sviderskiĭ, Pis'ma Zh. Tekh. Fiz. **14**, 777 (1988) [Sov. Tech. Phys. Lett. **14**, 346 (1988)].  
<sup>3</sup>G. S. Kandaurova and A. É. Sviderskiĭ, Zh. Éksp. Teor. Fiz. **97**, 1218 (1990) [Sov. Phys. JETP **70**, 684 (1990)].  
<sup>4</sup>F. V. Lisovskiĭ, E. G. Mansvetova, and E. P. Nikolaev, Zh. Éksp. Teor. Fiz. **103**, 213 (1993) [JETP **76**, 116 (1993)].  
<sup>5</sup>F. V. Lisovskiĭ, E. G. Mansvetova, and Ch. M. Pak, Zh. Éksp. Teor. Fiz. **108**, 1031 (1995) [JETP **81**, 567 (1995)].  
<sup>6</sup>G. S. Kandaurova, Fiz. Met. Metalloved. **79**, 158 (1995).  
<sup>7</sup>G. S. Kandaurova and Zh. A. Kipshakbaeva, Fiz. Tverd. Tela (St. Petersburg) **37**, 1058 (1995) [Phys. Solid State **37**, 574 (1995)].  
<sup>8</sup>G. S. Kandaurova and V. Kh. Osadchenko, Pis'ma Zh. Tekh. Fiz. **20**, 24 (1994) [Tech. Phys. Lett. **20**(21), 864 (1994)].  
<sup>9</sup>G. S. Kandaurova and V. Kh. Osadchenko, Pis'ma Zh. Tekh. Fiz. **21**, 11 (1995) [Tech. Phys. Lett. **21**(20), 819 (1995)].  
<sup>10</sup>G. S. Kandaurova and A. A. Rusinov, Dokl. Ross. Akad. Nauk **340**, 610 (1995).  
<sup>11</sup>G. S. Kandaurova and A. A. Rusinov, JETP Lett. **65**, 63 (1997).  
<sup>12</sup>V. V. Randoshkin and A. Ya. Chervonenkis, *Applied Magneto-optics* [in Russian], Énergoatomizdat, Moscow, 1990.  
<sup>13</sup>A. Ya. Chervonenkis and N. F. Kubrakov, Pis'ma Zh. Tekh. Fiz. **8**, 696 (1982) [Sov. Tech. Phys. Lett. **8**, 303 (1982)].  
<sup>14</sup>V. E. Ivanov and G. S. Kandaurova, Fiz. Met. Metalloved. **82**(3), 21 (1996).  
<sup>15</sup>R. J. Hasegawa, J. Appl. Phys. **45**, 3109 (1974).  
<sup>16</sup>V. V. Yudin, *Stochastic Magnetic Structure of Films with a Microporous System* [in Russian], Nauka, Moscow, 1987.  
<sup>17</sup>V. E. Ivanov, G. S. Kandaurova, and M. F. Karimov, Fiz. Met. Metalloved. **79**(3), 59 (1995).  
<sup>18</sup>G. S. Kandaurova, A. E. Sviderskiĭ, and V. P. Klin, J. Magn. Magn. Mater. **140-144**, 2135 (1995).

Translated by M. E. Alferieff

# Influence of the quantum size effect for grazing electrons on the electronic conductivity of metal films

G. M. Mikhaïlov,<sup>a)</sup> I. V. Malikov, and A. V. Chernykh

*Institute of Problems of Microelectronics Technology and High-Purity Materials, Russian Academy of Sciences, 142432 Chernogolovka, Moscow Region, Russia*

(Submitted 7 October 1997; resubmitted 6 November 1997)

*Pis'ma Zh. Éksp. Teor. Fiz.* **66**, No. 11, 693–698 (10 December 1997)

The thickness dependence of the electronic conductivity of thin (5–150 nm) single-crystal (100) films of refractory metals is investigated at different temperatures ranging from 4.2 K to room temperature. Regions of square-root, quasilinear, and quadratic dependences are observed. The quasilinear thickness dependence is explained by the influence of quantum effects on the transverse motion of electrons in the case when electron scattering by the film surfaces dominates. For macroscopic film thicknesses 30–50 nm, much greater than the Fermi wavelength of an electron, quantum corrections to the electronic conductivity reach values of the order of 50%. This is a consequence of the quantum size effect for grazing electrons, which leads to an anomaly in electron scattering by the film surfaces. The region of the quadratic thickness dependence corresponds to the quantum limit, and the square-root region corresponds to the classical limit. The effect is explained in a quasiclassical two-parameter model (the effective angle  $\alpha^*$  for small-angle electrons and the parameter  $\gamma$ , equal to the ratio of this angle to the diffraction angle) that takes into account the diffraction angular limits for grazing electrons. The effect occurs for parameters  $\alpha^* \ll 1$  and  $\gamma \sim 1$  and differs from the “ordinary” quantum size effect.  
© 1997 American Institute of Physics. [S0021-3640(97)00523-9]

PACS numbers: 73.50.Dn, 73.61.At

## INTRODUCTION

The interpretation of the classical size effect in the electronic conductivity of films has for a long time been based on the Fuchs model,<sup>1,2</sup> where the ratio of the diffuse and specular scattering of all conduction electrons by the film surfaces was determined by a single effective parameter — the specular coefficient. However, even in Ref. 3 it was indicated that this parameter is different for different groups of electrons and that it is necessary to make allowance for the dependence of the specular coefficient on the angle of incidence of the electrons on the surface. Many authors have elaborated the Fuchs model and also investigated the conditions of its applicability in the classical limit (see Ref. 4 and references cited therein). In Ref. 4, it was also shown that for a sufficiently long electron mean free path  $l$  it is impossible to introduce an average specular coefficient to describe the electronic conductivity in films. The conductivity of films in this case is determined by small-angle electrons and the electronic conductivity of the film is

a square-root function of the thickness. The size effect in the electronic conductivity of perfect single-crystalline plate-like whiskers has been investigated, for example, in Ref. 5 and the references cited therein, where a quasilinear size dependence was observed. A similar dependence was obtained for single-crystalline films of refractory metals with large  $l$ .<sup>6-9</sup> In all of these cases a square-root thickness dependence should be observed in the classical limit,<sup>4</sup> but this is not confirmed experimentally. Until very recently, there was no satisfactory explanation for this discrepancy between theory and experiment.

Investigation of thin single-crystalline platinum films showed that a large deviation, which can be interpreted in the Fuchs model, from the classical size effect is observed for thickness  $d$  less than 5 nm.<sup>10</sup> In Refs. 11–14 theoretical models explaining these experimental results as a manifestation of the quantum effect at small film thickness, approaching the Fermi wavelength of an electron, were developed in Refs. 11–14. The case when the length  $l$  is much greater than the film thickness in both the quantum and classical limits has not been investigated.

## EXPERIMENTAL RESULTS

Thin (5–150 nm) single-crystalline (100) films of refractory metals were obtained in a process of epitaxial growth on a flat  $r$  sapphire surface in an ultrahigh vacuum by the method of pulsed laser vaporization. Films with a perfect crystalline structure, which consisted of single-crystalline blocks with a small disorientation and sizes much larger than the film thickness,<sup>8,9</sup> possessed slight average roughness (less than 1 nm) on both the inner and outer surfaces.<sup>9</sup> As a result of the interaction with the surrounding medium, the outer surface of the films was coated with a thin natural oxide. The effective residual electron mean free path in the films grown reached several microns and the mean free path in the bulk, as estimated from the Fuchs equations, was at least an order of magnitude longer.<sup>6-9</sup> Measurements of the electronic conductivity of the films were performed at low (4.2 K) and higher temperatures (right up to room temperature). The method for obtaining the films and the method for measuring the electronic conductivity are described in greater detail in previous publications.<sup>6,7</sup>

The experimental dependence of the ratio  $\sigma(d)/\sigma(150 \text{ nm})$  of the conductivities of single-crystalline (100) W films, measured at 4.2 K (curve 1), 40 K (2), 80 K (3), and 295 K (4), for film thicknesses  $d=15-150 \text{ nm}$  is shown in Fig. 1 (dots). The dotted and dashed lines in the figure show the square-root and quadratic, respectively, thickness dependences of the conductivity. As one can see from figure, for film thickness  $d < 50 \text{ nm}$  ( $T=4.2 \text{ K}$ ) the experimental dependence is quasilinear, passing into a quadratic dependence. The deviation from the square-root dependence is of the order of 50%. At  $T=40 \text{ K}$  and  $d > 50 \text{ nm}$  the experimental dependence is close to a square-root law. At higher temperatures the exponent of the thickness dependence decreases and the region of the transition from a low to a high exponent shifts to a smaller thickness. Figure 2 shows analogous experimental results for single-crystalline (100) Nb films. The deviation from the square-root dependence is substantial at thicknesses less than 30 nm (for  $T=4.2 \text{ K}$ ); in this region the dependence is quasilinear, passing into a quadratic dependence. At  $T=80 \text{ K}$  and  $d > 10 \text{ nm}$  the experimental dependence is close to a square-root law. The experimental thickness dependences exhibit general behavior: As the thickness changes from large to small, the exponent in the thickness dependence changes, starting at a value

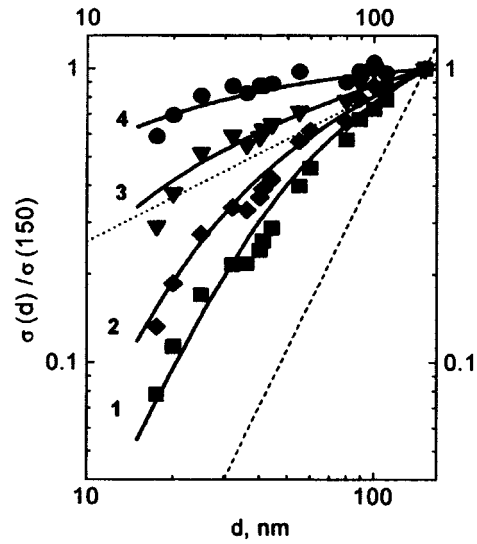


FIG. 1. Experimental normalized size dependences of the electronic conductivity of single-crystalline (100) W films (dots) at  $T=4.2$  K (curve 1), 40 K (2), 80 K (3), and 295 K (4). Solid line — Eq. (4) with  $L_0=140\,000$ , 25 000, 950, and 70, respectively, and  $\lambda_f=2$  nm. Dotted line — square-root dependence of the conductivity on the film thickness; dashed line — quadratic dependence of the conductivity on the film thickness.

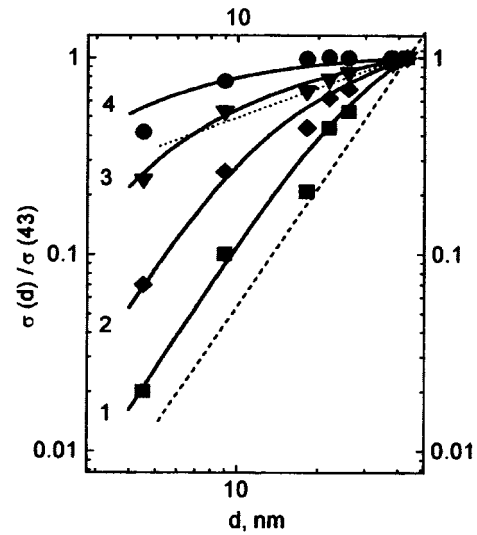


FIG. 2. Experimental normalized size dependences of the electronic conductivity of single-crystalline (100) Nb films (dots) at  $T=4.2$  K (curve 1), 40 K (2), 80 K (3), and 295 K (4). Solid line — Eq. (4) with  $L_0=35\,000$ , 25 000, 150, and 15, respectively, and  $\lambda_f=2$  nm. Dotted line — square-root dependence of the conductivity on the film thickness; dashed line — quadratic dependence of the conductivity on the film thickness.

$\sim 0.5$  (or less) and increasing up to 2. In the transitional range of thicknesses the size dependence is quasilinear. As the length  $l$  decreases (or the temperature increases), the region of the transition shifts to a smaller thickness. The value of the ratio  $d/l$  in the experiments performed lies in a range of values of the order of  $10-10^{-4}$ , where the results of Refs. 6–8 were used to estimate  $l$ .

## THEORETICAL MODEL AND DISCUSSION

The ratio of the film conductivity  $\sigma_d$  to the bulk conductivity  $\sigma_0$  for  $l \gg d$  is a square-root function of the thickness and is proportional to  $\alpha^* = \sqrt{d/Ql}$  — the effective angle; the parameter  $Q$  depends on the roughness of the film surface.<sup>4</sup> However, the transverse component of the momentum in the films is quantized because of the finite transverse motion of the electrons.<sup>12</sup> For small surface asperities, this momentum component is well determined, at least for the bottom two-dimensional subbands where the “transverse” wavelength of an electron is comparable to the thickness. From this it follows inevitably that there is a lower limit on the angle of incidence of an electron on the surface. Further, for brevity, we shall term this minimum angle  $\alpha_d = \lambda_f/2d$ , where  $\lambda_f$  is the Fermi wavelength, the diffraction angle. We also introduce the dimensionless thickness  $D = 2d/\lambda_f$ , the effective mean free path  $L_0 = 2Ql/\lambda_f$ , and the parameter

$$\gamma = \frac{\alpha^*}{\alpha_d} = \sqrt{\frac{D^3}{L_0}}. \quad (1)$$

When  $\gamma = 1$ , we obtain the following characteristic film thickness:

$$D^* = \sqrt[3]{L_0}, \quad (2)$$

for which the effective angle equals the diffraction angle. Taking  $\lambda_f \sim 1$  nm,  $Q \sim 1$  for incoherent interfaces, and mean free path  $l \sim 100$   $\mu\text{m}$ ,<sup>6–9</sup> we obtain the following possible estimate for the characteristic film thickness in metals:  $D^* \sim 100 \gg 1$ . The characteristic thickness (2) determines the spatial scale, and 1D and 2D low-dimensional objects, in which the diffraction limitations are important, can be studied. It is necessary to study the case when  $l \gg d$  in both the quantum and quasiclassical limits. This corresponds to a description of the motion of grazing electrons and the problem in this sense is analogous to studying electrons on “hopping” orbits.<sup>15</sup> For the electronic conductivity we employ the quasiclassical approximation (since  $D^* \gg 1$ ) in the isotropic case and take into account the diffraction limit on the angle for grazing electrons. Considering two scattering channels — in the volume with mean free path  $l$  and on the surface with mean free path  $l_s(\alpha)$ , depending on the angle of incidence  $\alpha$  of the electron on the surface, and introducing the effective mean free path  $(l^*)^{-1} = l^{-1} + l_s^{-1}$ , we obtain the expression

$$\frac{\sigma_d}{\sigma_0} = \int_{\in K\alpha_d} \frac{d\Omega}{1 + l/l_s(\alpha)} \cos^2 \theta, \quad (3)$$

where  $S$  is a normalization constant, equal to  $3/8\pi$  and  $3/4\pi$ , respectively, for two- and one-dimensional objects;  $K \sim 1$  is a numerical factor (see below); and,  $\theta$  is the angle between the direction of motion of an electron and the direction of the current. Integration over the entire solid angle is limited for the polar angle by the quantity  $K\alpha_d$ . The expression (3) holds for  $L_0 \gg D \gg 1$ . Moreover, to simplify the problem, it is assumed that

the correlation length for surface roughness is quite small,<sup>4</sup> so that electrons can be scattered by the film surfaces by large angles also. In Eq. (3) it is assumed that the length  $l$  on the right-hand side is the same as in the bulk conductivity  $\sigma_0$ . However, this is not true in the case of small-angle volume scattering. Electron scattering processes leading to collisional broadening of the transverse quantization levels<sup>12</sup> and interruption of the electron phase were also neglected in Eq. (3).

For  $l_s$  we use the formula<sup>4,5</sup>

$$l_s = \frac{d}{\sin \alpha (1 - P(\alpha))} \cong \frac{d}{Q \sin^2 \alpha},$$

where  $P(\alpha) = 1 - Q\alpha$  is the specular coefficient for small angles of incidence of electrons on the surface.<sup>4</sup> Substituting  $l_s$  into Eq. (3), we obtain the final formula for the electronic conductivity. For films, it follows from Eq. (3) that

$$\frac{\sigma_d}{\sigma_0} = \frac{3}{2} \alpha^{*2} \left\{ (\alpha^* + \alpha^{*-1}) \tan^{-1} \left( \frac{\gamma}{6/\pi^2 + \alpha^* \gamma} \right) - 1 \right\}, \quad (4)$$

where

$$\alpha^* = \sqrt{\frac{d}{L_0}} = \sqrt{\frac{d}{Ql}}, \quad \gamma = D \sqrt{\frac{D}{L_0}} = \frac{2d}{\lambda_f} \sqrt{\frac{d}{Ql}},$$

and the numerical factor  $K \cong 6/\pi^2$  for the correct quantum limit in the two-dimensional case. The electronic conductivity (4) of films is determined by two parameters: the effective angle  $\alpha^*$  and the parameter  $\gamma$ . For  $\gamma \gg 1$  (classical limit) expression (4) passes into the well-known formula for the conductivity of films.<sup>4</sup> The region of thick ( $\alpha^* \sim 1$ ) and thin ( $\alpha^* \ll 1$ ) films, in accordance with the classification given in Ref. 4, can be studied. For  $\alpha^* \ll 1$  and  $\gamma \sim 1$  (transitional region) a quasilinear size dependence is observed in the region of macroscopic film thicknesses; the quantum corrections ( $\sim 50\%$ ) here are large on account of the quantum size effect for grazing electrons, which leads to anomalies in the scattering of conduction electrons by the film surfaces. As the parameter  $\gamma$  decreases further ( $\gamma \ll 1$ ), the size dependence becomes quadratic and corresponds to the quantum limit. For  $\alpha^* \sim 1$  and  $\gamma \leq 1$  the characteristic film thicknesses become of the order of the Fermi wavelength, and for a sufficiently small thickness the conventional quantum size effect must also be taken into account.<sup>12,14,16</sup>

The limiting relations for expression (4) in the case of large  $l$  ( $\alpha^* \ll 1$ ), the case of interest to us, have the following form. The quantum limit with  $\gamma \ll 1$

$$\frac{\sigma_d}{\sigma_0} \xrightarrow{\lambda_f \rightarrow \infty} \frac{\pi^2}{4} \frac{D^2}{L_0} = \frac{\pi^2}{4} \gamma \alpha^*, \quad (5)$$

which corresponds to the results of Refs. 11–14 for  $D \gg 1$ . The classical limit with  $\gamma \gg 1$

$$\frac{\sigma_d}{\sigma_0} \xrightarrow{\lambda_f \rightarrow 0} \frac{3\pi}{4} \sqrt{\frac{D}{L_0}} = \frac{3\pi}{4} \alpha^*, \quad (6)$$

in agreement with the result obtained in Ref. 4. For  $\gamma \sim 1$  (transitional region) the function (4) has a point of inflection where the second derivative with respect to thickness vanishes. As a result, a numerical solution leads to the linearized expression

$$\frac{\sigma_d}{\sigma_0} \cong \frac{2.04}{D^{*2}}(d - 0.229D^*). \quad (7)$$

Hence one can see that the linear function intersects the abscissa at a positive thickness, which can be interpreted as a “dead” layer with an arbitrary quasilinear approximation of the size dependence of the conductivity.<sup>6–9</sup> However, the origin of this “layer” is connected with quantum corrections. In the general case, formula (4), which matches the functions (5)–(7), leading to a quasilinear size dependence in the transitional thickness range, must be used. This is a consequence of the quantum size effect in the conductivity for grazing electrons, located in the *bottom* two-dimensional subbands. This results in anomalies in the electron scattering by the surfaces and, correspondingly, in the size dependence of the electronic conductivity of a film. This effect is different from the conventional quantum size effect, where as the film thickness decreases, both the electron density of states at the Fermi level and, correspondingly, the electronic conductivity vary periodically as a result of the *top* two-dimensional subbands being displaced above the Fermi level.<sup>16</sup>

Qualitatively, the size dependence of the conductivity of films which is predicted by Eq. (4) corresponds to the experimental results (Figs. 1 and 2): At large thicknesses the exponent in the size dependence is small ( $\leq 0.5$ ); as the thickness decreases (when  $\alpha^* \leq 1$ ), the size dependence follows a square-root law (6); at the characteristic thickness (2) the size dependence becomes linear (7); and, in the limit of small thickness the size dependence approaches the quadratic law (5). As the length  $l$  decreases (or temperature increases), the region of characteristic thickness shifts to small values in accordance with Eq. (2). To obtain a quantitative description of the experimental results, a fit of formula (4) with variable  $L_0$  was made. Figure 1 shows the function (4) (solid line) with the adjustable parameter equal to  $L_0 = 140\,000, 25\,000, 950,$  and  $70$ , respectively, and with  $\lambda_f = 2$  nm as an average value, since a collection of Fermi wavelengths exists for the (100) surface of tungsten.<sup>17</sup> For Nb (Fig. 2) the adjustable parameters  $L_0$  were as follows: 1 — (4.2 K) 35 000, 2 — (40 K) 2500, 3 — (80 K) 150, 4 — (295 K) 15 and  $\lambda_f = 2$  nm for all fits. As one can see from the results presented, the function (4) correctly describes (Figs. 1 and 2) the region of the transition from the classical to the quantum limit and it is in satisfactory agreement with experiment.

## CONCLUSIONS

The observed quasilinear thickness dependence of the conductivity of thin (5–150 nm) single-crystalline films of refractory metals (in the case when scattering by the interfaces dominates) is explained by the large influence of the quantum size effect for grazing electrons, located in the bottom two-dimensional subbands of the energy spectrum. The characteristic size (thickness) is determined by Eq. (2) and can be much greater than the Fermi wavelength. For this thickness the quantum corrections to the conductivity reach values of the order of 50%, and the experimentally determined values of the characteristic thickness equalled 30–50 nm. Quadratic (quantum limit), quasilinear (tran-

sitional region), and square-root (classical limit) thickness dependences of the conductivity are observed experimentally. The proposed quasiclassical model, which takes account of diffraction angular limits for electrons grazing along the surface, is in satisfactory agreement with experiment.

This work was supported by the Russian Fund for Fundamental Research (Grant 97-02-17031) and grants from the science and technology programs “Physics of solid-state nanostructures” (Grant 97-1059) and “Physics of Quantum and Wave Processes” (category “Statistical Physics”).

<sup>a)</sup>e-mail: Mikhail@nano.home.chg.ru

- 
- <sup>1</sup>K. Fuchs, Proc. Cambridge Philos. Soc. **34**, 100 (1938).  
<sup>2</sup>H. Sondheimer, Adv. Phys. **1**, 1 (1952).  
<sup>3</sup>S. Soffer, J. Appl. Phys. **38**, 1710 (1967).  
<sup>4</sup>L. A. Falkovsky, Adv. Phys. **32**, 753 (1983).  
<sup>5</sup>Yu. P. Gaïdukov, in *Conduction Electrons* [in Russian], edited by M. I. Kaganov and V. S. Édel'man, Nauka, Moscow, 1985, Chapter 12, pp. 372–400.  
<sup>6</sup>G. M. Mikhailov, A. V. Chernykh, and V. T. Petrashov, J. Appl. Phys. **80**, 948 (1996).  
<sup>7</sup>G. M. Mikhaïlov, I. V. Malikov, A. V. Chernykh, and V. T. Petrashov, Fiz. Tverd. Tela (St. Petersburg) **38**, 3212 (1996) [Phys. Solid State **38**, 1754 (1996)].  
<sup>8</sup>G. M. Mikhailov, I. V. Malikov, A. V. Chernykh, and V. T. Petrashov, Thin Solid Films **293**, 315 (1997).  
<sup>9</sup>I. V. Malikov and G. M. Mikhailov, J. Appl. Phys. **82**, 5555 (1997).  
<sup>10</sup>G. Fisher and H. Hoffman, Solid State Commun. **35**, 793 (1980); H. Hoffman and G. Fisher, Thin Solid Films **36**, 25 (1976).  
<sup>11</sup>Z. Tesanovic, M. V. Jaric, and S. Maekawa, Phys. Rev. Lett. **57**, 2760 (1986).  
<sup>12</sup>N. Trivedi and N. W. Ashcroft, Phys. Rev. B **38**, 298 (1988).  
<sup>13</sup>G. Fishman and D. Calecki, Phys. Rev. Lett. **62**, 1302, (1989).  
<sup>14</sup>L. Sheng, D. Y. Xing, and Z. D. Wang, Phys. Rev. B **51**, 7325 (1995).  
<sup>15</sup>M. S. Khaïkin, Usp. Fiz. Nauk **96**, 409 (1968) [Sov. Phys. Usp. **11**, 785 (1969)].  
<sup>16</sup>V. B. Sandomirskiĭ, Zh. Éksp. Teor. Fiz. **52**, 1710 (1967) [*sic*].  
<sup>17</sup>V. S. Tsoï, in *Conduction Electrons* [in Russian], edited by M. I. Kaganov and V. S. Édel'man, Nauka, Moscow, 1985, Chapter 10, pp. 329–343.

Translated by M. E. Alferieff

## Scaling in the $ab$ resistivity of $\text{TmBaCuO}$ single crystals in the normal state

E. B. Amitin, V. Ya. Dikovskii, A. N. Lavrov, and A. P. Shelkovnikov

*Institute of Inorganic Chemistry, Siberian Branch of the Russian Academy of Sciences, Novosibirsk State University, 630090 Novosibirsk, Russia*

(Submitted 29 October 1997)

*Pis'ma Zh. Éksp. Teor. Fiz.* **66**, No. 11, 699–703 (10 December 1997)

For single crystals of the system  $\text{TmBa}_2\text{Cu}_3\text{O}_x$  with  $6.37 < x < 6.71$ , a scaling transformation is found which reduces the temperature dependences of the derivative of the resistivity in the  $ab$  plane in the normal state to a universal form which is independent of oxygen content.

© 1997 American Institute of Physics. [S0021-3640(97)00623-3]

PACS numbers: 74.72.Jt, 74.25.Fy

Crossover phenomena observed in the temperature dependences of different properties of cuprate high- $T_c$  superconductors in the normal state, including the resistivity and Hall effect,<sup>1–4</sup> magnetic susceptibility and specific heat,<sup>5</sup> NMR characteristics,<sup>6,7</sup> and others, have become a subject of wide experimental and theoretical study. Most authors attribute the observed crossovers to the appearance of gaps in the spectra of the electronic or spin subsystems of the cuprate layer in the undoped state. Recent photoemission investigations on Bi-2212 single crystals<sup>8</sup> have confirmed the existence of a pseudogap in the charge-carrier spectrum. The decrease of the pseudogap with increasing doping, observed in Ref. 9, is in qualitative agreement with the corresponding behavior of the crossover temperature  $T^*$ . The literature contains many different points of view on the origin of the characteristic features in the electronic and spin spectra of cuprate high- $T_c$  superconductors. Even to this day, however, experiment does not permit choosing among the existing models. The main obstacles in analyzing phenomena of this type are the low magnitude and monotonic behavior of the crossover contributions, making the characteristic temperature  $T^*$  uncertain. The quantitative investigation of crossover phenomena undertaken in the present work is distinguished by the facts that, first, the temperature derivative of the resistivity, which is more sensitive to the above-described temperature and concentration variations, is used for analysis and, second, the doping dependence is studied in greater detail — the measurements were performed on a single  $\text{TmBa}_2\text{Cu}_3\text{O}_x$  single crystal in which different oxygen concentrations were obtained by reannealing the sample.

### EXPERIMENTAL PROCEDURE AND RESULTS

The samples for investigating the normal-state resistivity of the compound  $\text{TmBa}_2\text{Cu}_3\text{O}_x$  were cut from single-crystalline wafers grown by the fluxed solution method and possessed dimensions  $2.0 \times 0.3 \times 0.03$  mm. The details of the procedure of growing the initial crystals are described in Ref. 10. In order to make reliable comparisons of the data obtained for different values of  $x$ , the main measurements were per-

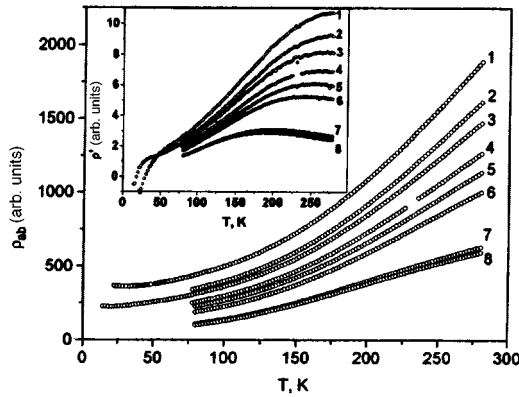


FIG. 1. Temperature dependences of the resistivity and its derivative (inset) in the  $ab$  plane of a  $\text{TmBa}_2\text{Cu}_3\text{O}_x$  single crystal for different oxygen concentrations: 1, 2 —  $x=6.37$ ; 3, 4 —  $x=6.42$ ; 5, 6 —  $x=6.47$ ; 7, 8 —  $x=6.71$ . Low-temperature equalizing annealing was performed for even numbers.

formed on the same sample, which was repeatedly reannealed so as to obtain prescribed oxygen indices. For each value of  $x$  the results were obtained with two different degrees of ordering of the chain oxygen. This was achieved by low-temperature equalizing annealing of the sample or quenching of the sample in liquid nitrogen.<sup>10</sup> The  $ab$ -plane resistivity  $\rho_{ab}$  was measured by a four-probe method. A platinum resistance thermometer was used to determine the temperature.

Data on the behavior of  $\rho_{ab}$  and its derivative  $\rho'_{ab} = d\rho_{ab}/dT$  near the normal state are presented in Fig. 1 for four oxygen concentrations:  $x = 6.37, 6.42, 6.47, \text{ and } 6.71$ . One can see that the derivative of the resistivity has a maximum whose position  $T_{\text{max}}$  shifts to higher temperatures with decreasing  $x$ . A plot of the data in the reduced coordinates  $\rho'_{ab}/\rho'_{\text{max}}$  versus  $T/T_{\text{max}}$  indicates the existence of universal behavior in the experimental ranges of the temperature and oxygen concentration. Earlier, the similarity elements were discovered in the temperature dependences of  $ab$  resistance and Hall parameters of underdoped YBCO single crystals and films in the normal state.<sup>1,2</sup> In these works, the point where the temperature dependence  $\rho_{ab}(T)$  deviates from a linear law was chosen as the characteristic temperature scale. This quantity is determined with a large error, which impedes quantitative investigation. The reduction, presented in Fig. 2a, of individual curves to a given universal curve was made using two adjustable parameters — the quantities  $T^*$  and  $\rho'_{\text{max}}$  were chosen so as to minimize the distance between the curves. It was found that the values obtained for  $T^*$  and  $\rho'_{\text{max}}$  are actually proportional to the temperature and the maximum value of  $\rho'_{ab}$  on the curves where this maximum is reached. It is noteworthy that in a wide range of temperatures the divergence between individual curves is of the same order of magnitude as the experimental error characteristic for each curve. It is also evident that the points referring to both quenched and annealed states of the sample fall on a universal curve. The values obtained for the normalizing parameters as a result of fitting vary with the oxygen content. For both parameters this variation is close to hyperbolic (see Fig. 2b). The dependences of both  $T^*$  and  $\rho'_{\text{max}}$  on the oxygen index are shifted relative to one another on the  $x$  axis for the

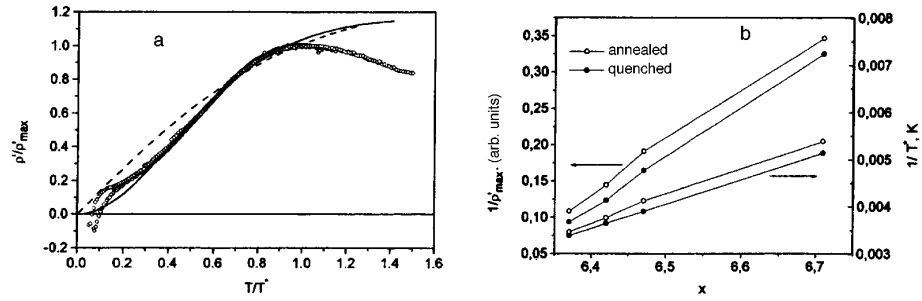


FIG. 2. a — Universal behavior of the derivative of the resistivity in the coordinates  $\rho'_{ab}/\rho'_{\max}$  versus  $T/T^*$  ( $\rho'_{\max}$  and  $T^*$  correspond to the magnitude and position of the maximum of  $d\rho_{ab}/dT$ ). The dashed and solid curves correspond to an approximation of the  $\rho'_{ab}(T)$  data according to the Moriya<sup>12</sup> and Pines<sup>14</sup> theories. b — Reciprocals of  $\rho'_{\max}$  and  $T^*$  versus the degree of doping.

quenched and annealed states by the amount  $\Delta x \approx 0.025$ . Approximately the same shift was obtained by comparing the  $x$  dependence of the superconducting transition temperatures  $T_c(x)$  of the quenched and annealed samples. Such a shift of the phase diagram agrees with the picture in which for a cuprate layer the ordering of chains in the oxygen subsystem gives an effective increase of the charge-carrier density.<sup>10</sup> It follows from the inset in Fig. 1 that obvious deviations from universality, which are manifested as a sharp decrease and even change in sign of the derivative of the resistivity, are present at low temperatures. The corresponding contributions to the resistance, which could be associated with localization effects, are most noticeable for samples with a low oxygen content. These effects will not be discussed in the present paper, since they were recently investigated in detail in Ref. 11.

Analysis of the form of the universal curve shows that its behavior on the low-temperature section is close to exponential (see Fig. 3)

$$\rho'_{ab} = \rho'_{\max} (A + B \exp(-T_A^*/T)). \quad (1)$$

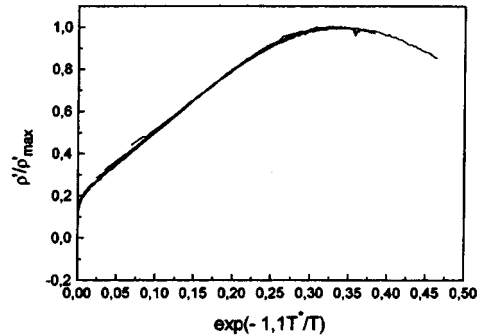


FIG. 3. Plot of the  $\rho'_{ab}/\rho'_{\max}(T/T^*)$  data on an exponential scale.

Here the constants  $A$  and  $B$  equal 0.20 and 2.9, respectively, and  $T_A^*$  and  $\rho'_{\max}$  depend on  $x$ . The values obtained for the parameter  $T_A^*$  from the approximation are close to the temperature of the maximum of the derivative of the resistivity ( $T_A^* \approx 1.1T_{\max}$  for all  $x$ ). In accordance with Eq. (1), extrapolation of the low-temperature section to  $T=0$  gives a nonzero intercept. It is interesting that the intercept is different for different oxygen concentrations but it is always proportional to  $\rho'_{\max}$ . The interval of exponential behavior increases with decreasing oxygen index. For  $x=6.37$  the approximation interval reaches  $\sim 150$  K and, as statistical analysis shows, the approximation error in this interval is of the same order of magnitude as the experimental variance.

## DISCUSSION

According to Fig. 2a, the temperature dependences obtained for the temperature coefficient of the resistivity for different oxygen concentrations can be presented in the form of a universal curve with the appropriate normalization of both the function and the argument. In other words, the derivative of the resistivity as a function of the two variables  $T$  and  $x$  can be reduced to a function of a single argument, specifically, the dimensionless ratio  $T/T^*(x)$ . The very existence of the scaling transformation that reduces the curves  $\rho'_{ab}(T)$  to a universal form indicates that in the investigated range of the phase diagram the behavior of the temperature coefficient of the resistivity is apparently determined by a single physical mechanism. Moreover, one can talk about the presence of a single energy scale in the range of oxygen indices  $6.37 < x < 6.71$  and temperatures  $1.2T_c < T < 280$  K.

In existing models there is no unique interpretation of either the existence of scaling effects in the derivative of the resistivity or the specific form of the universal curve. If the low-temperature behavior of  $\rho'_{ab}(T)$  is attributed to the existence of a gap in the spin-excitation spectrum or a pseudogap in the current-carrier spectrum, then these two possibilities lead (for ordinary magnetic metals) to, respectively, a decrease in the contribution of magnon scattering, i.e., a decrease in the resistivity, or to a decrease in the carrier density of states, i.e., a decrease in the conductivity. Qualitatively, the behavior of the derivative of the resistivity is closer to the first variant, since in the region of universality  $\rho'_{ab}$  is always positive. At the same time, for the strongly correlated electronic system of cuprate high- $T_c$  superconductors the electron-spin scattering situation may turn out to be quite complicated because of the close coupling of the electronic and spin degrees of freedom. Taking account of this coupling by the mean-field method appreciably improves the agreement between theory and experiment. The Moriya theory of electron-spin scattering<sup>12</sup> for cuprate high- $T_c$  superconductors makes it possible to describe qualitatively the behavior of  $\rho'_{ab}(T)$  (see Fig. 2a). However, quantitative agreement does not obtain and, moreover, the theory indicate directly the existence of universality. In calculations of spin scattering in the Hubbard model, however, as a rule substantial approximations are used. Thus, in the review in Ref. 13 different variants of the collective states arising as a result of self-consistency of the electronic and spin excitations are discussed. According to Ref. 13 the interaction of fermions with collective fluctuation mode results, to a first approximation, in a linear temperature dependence  $\rho_{ab}(T)$ .

An appreciably better description (but also not quantitative, see Fig. 2a) of the temperature dependences  $\rho'_{ab}(T)$  can be obtained by using the expression obtained by D.

Pines *et al.*<sup>14</sup> for the  $ab$  resistivity in an almost antiferromagnetic Fermi liquid model

$$\rho_{ab} = A \frac{T^2}{T_0 + T}, \quad (2)$$

where  $A$  accounts for the characteristic features of the carrier spectrum in the cuprate layer and  $T_0$  is the crossover temperature. In the general case  $A$  and  $T_0$  are functions of both the degree of doping and the temperature but in the simplest case, when there is no temperature evolution of the Fermi surface,  $A$  depends only on the degree of doping and  $T_0 \sim F(x)/T$ . It is easy to show that the derivative  $\rho'_{ab}(T)$  depends on the temperature only via the ratio  $T/F(x)$ , which creates conditions for universal behavior. At the same time, the observed agreement with experiment may turn out to be accidental because of the substantial simplifications employed in the derivation of expression (2). Moreover, there is no justification for neglecting the temperature dependence of the parameters of the Fermi surface for the pseudogap regime.

At present we cannot give an unequivocal explanation of the exponential behavior that we observed for the derivative of the resistivity. It is only clear that this behavior at low temperatures is most likely asymptotic. This is indicated by the circumstance that the property of universality (i.e., a single physical mechanism and a single energy scale) extends not only to the exponential section but also to the region of the maximum of  $\rho'_{ab}$ . At the same time, the presence of a dominant activation contribution at low temperatures, together with the assertion that there is only one energy scale, may mean that the temperature  $T_A^*$ , close to the point of the maximum of the derivative of the resistivity, plays the role of a single characteristic energy determining the properties of the system in the region of universality.

In summary, the derivative of the resistivity in the  $ab$  plane of a  $\text{TmBa}_2\text{Cu}_3\text{O}_x$  single crystal is characterized by universal behavior in a wide range of temperatures and oxygen indices. The behavior of the universal curve at low temperatures is close to exponential.

This work was supported by the Russian Fund for Fundamental Research (Grants 96-02-19249a and 9619227) and the Scientific Council on high- $T_c$  Superconductors (Project 93037). We thank E. V. Matizen and L. A. Boyarskiĭ for a helpful discussion.

<sup>1</sup>T. Ito, K. Takenaka, and S. Uchida, Phys. Rev. Lett. **70**, 3995 (1993).

<sup>2</sup>B. Wuyts, V. V. Moshchalkov, and Y. Bruynseraede, Phys. Rev. B **51**, 6115 (1995).

<sup>3</sup>A. Carrington, D. J. C. Walker, A. P. Mackenzie, and J. R. Cooper, Phys. Rev. B **48**, 13051 (1993).

<sup>4</sup>K. F. Quader and A. Levin, Philos. Mag. **74**, 609 (1996).

<sup>5</sup>W. Y. Liang, J. W. Loram, K. A. Mizra *et al.*, Physica C **263**, 277 (1996).

<sup>6</sup>H. Alloul, T. Ohno, and D. Mondels, Phys. Rev. Lett. **63**, 1700 (1989).

<sup>7</sup>M. Horvatic, P. Segransan, C. Berthier *et al.*, Phys. Rev. B **39**, 7322 (1989).

<sup>8</sup>D. S. Marshall, D. S. Dessau, A. G. Loeser *et al.*, Phys. Rev. Lett. **76**, 4841 (1996).

<sup>9</sup>J. M. Harris, Z.-H. Shen, P. J. White *et al.*, preprint <http://xxx.lanl.gov/abs/cond-mat/9611010>.

<sup>10</sup>A. Lavrov and L. P. Kozeeva, Physica C **248**, 365 (1995); Physica C **253**, 313 (1995).

<sup>11</sup>V. F. Gantmakher, L. P. Kozeeva, A. N. Lavrov *et al.*, JETP Lett. **65**, 870 (1997).

<sup>12</sup>T. Moriya, Y. Takahashi, and K. J. Ueda, J. Phys. Soc. Jpn. **59**, 2905 (1990).

<sup>13</sup>Yu. A. Izyumov, Usp. Fiz. Nauk **167**, 465 (1997).

<sup>14</sup>D. Pines, preprint <http://xxx.lanl.gov/abs/cond-mat/9609137>.

Translated by M. E. Alferieff

## On the electron mobility of $\delta$ layers in the presence of diamagnetic “ejection” of size-quantization levels

D. Yu. Ivanov,<sup>a)</sup> S. V. Morozov, Yu. V. Dubrovskii, S. Yu. Shapoval, V. V. Valyaev, and V. L. Gurtovoi

*Institute of Problems of the Microelectronics and Ultrapure, Materials Technology, Russian Academy of Sciences, 142432 Chernogolovka, Moscow Region, Russia*

(Submitted 29 October 1997)

*Pis'ma Zh. Éksp. Teor. Fiz.* **66**, No. 11, 704–708 (10 December 1997)

The Hall mobility of electrons is investigated as a function of the population of size-quantization subbands in the two-dimensional electron gas of a  $\delta$ -doped layer in GaAs with constant total electron density  $N_s = 3.2 \times 10^{12} \text{ cm}^{-2}$  (three initially filled subbands) at  $T = 4.2 \text{ K}$ . The population of the subbands is varied by diamagnetic “ejection” of size-quantization levels (i.e., pushing them over the Fermi level) by a magnetic field oriented parallel to the plane of the  $\delta$ -doped layer. The measurements are made in magnetic fields making small angles ( $5^\circ$ ) with the plane of the doping. The magnetic field component normal to the plane was used to measure the Hall mobility and density. It is found that the measured Hall mobility as a function of the ejecting magnetic field has a distinct maximum. This maximum is due to an increase in the electron mobility in the first subband (the ground subband is assigned the index 0) and electron redistribution between subbands with increasing ejecting magnetic field parallel to the plane of the  $\delta$  layer.

© 1997 American Institute of Physics. [S0021-3640(97)00723-8]

PACS numbers: 73.50.Dn, 73.61.Ey

Semiconductor structures with extremely nonuniform doping of homogeneous semiconductors, where the dopant is concentrated in a very narrow layer — in the limit, a monolayer, are ordinarily termed structures with  $\delta$ -doped layers or simply  $\delta$  layers. The dopant charge in a  $\delta$  layer produces a V-shaped potential well. This produces a structure with a two-dimensional electron gas (2DEG).<sup>1,2</sup> Compared with conventional structures with a 2DEG (heterostructures, MIS structures based on Si), it is possible to grow structures with  $\delta$  layers with a much higher two-dimensional electron density  $N_s > 10^{13} \text{ cm}^{-2}$ , making it possible to investigate two-dimensional electronic systems with a large number of filled size-quantization subbands.

In contrast to enriched and inversion layers at the surface of narrow-gap semiconductors, where several filled subbands have also been observed, the potential well in structures with  $\delta$  layers has a symmetric form. In  $\delta$  layers with several filled subbands scattering by ionized impurities located at the center of the potential well makes a much larger contribution to the resistance than does intersubband scattering.<sup>3</sup> Mobilities in structures with  $\delta$  layers are not high (of the order of  $1000 \text{ cm}^2/\text{V}\cdot\text{s}$ ). For this reason, the transport properties of an electron gas in a  $\delta$  layer are usually described under the

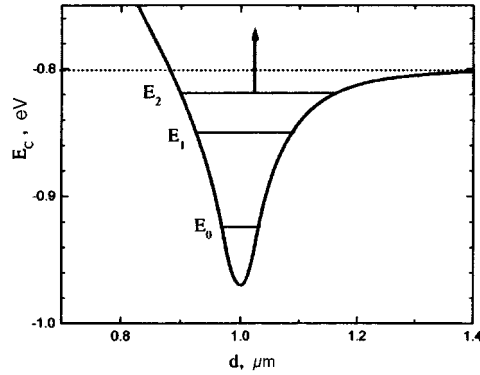


FIG. 1. Schematic band diagram of a potential well in the region of the  $\delta$  layer: Fermi level (dotted line) relative to the surface, eV; conduction-band bottom (solid curve), eV; position of the bottom of the size-quantization subband  $E_i$  ( $i=0, 1, 2$ ), eV. The arrow shows the displacement of  $E_2$  with increasing magnetic field oriented parallel to the  $\delta$  layer. The distance  $d$  (in  $\mu\text{m}$ ) from the surface is plotted along the abscissa.

assumption that each subband contains electrons with density  $n_i$  and mobility  $\mu_i$  and the conductivity is determined by simply adding the electron conductivities in different subbands:

$$\sigma = e \sum_i n_i \mu_i,$$

where  $e$  is the electron charge. It is well known<sup>4</sup> that in a magnetic field oriented parallel to the plane of a quantum well diamagnetic ejection of the upper level (Fig. 1) and electron redistribution between the subbands remaining below the Fermi level occur as the field increases. In fields in which the bottom of the ejected subband crosses the Fermi level of a two-dimensional electron gas, characteristic features are observed in the dependence of the conductivity on the parallel magnetic field.

In our work, we measured simultaneously with the longitudinal conductivity the Hall voltage in a magnetic field which was inclined by several degrees from the plane of the two-dimensional electron gas. In this case the effect of the parallel and perpendicular components of the field on the energy spectrum of the 2DEG can be regarded as being independent.<sup>5,6</sup> Thus, the magnetic-field component parallel to the plane of the 2DEG was used for electron redistribution between subbands and the perpendicular component was used to measure the Hall mobility of the electrons.

Epitaxial GaAs films with  $\delta$ -doped silicon layers were grown by MOCVD at 600 °C on semi-insulating GaAs substrates. The total thickness of the lightly doped  $n$ -GaAs epitaxial layer ( $n = 1 - 2 \times 10^{15} \text{ cm}^{-3}$ ) was equal to 600 nm. The distance between the  $\delta$  layer and the surface was equal to 100 nm. The degree of doping of the  $\delta$  layer was fixed during growth at  $3 \times 10^{12} \text{ cm}^{-2}$ . The measured value of the Hall density at  $T = 4.2 \text{ K}$  was equal to  $2.56 \times 10^{12} \text{ cm}^{-2}$ .

The measurements were performed on samples possessing Hall-bridge geometry formed by chemical etching of a mesa structure through a photoresist mask. The conducting channel was 0.4 mm wide and the potential contacts were separated by a distance

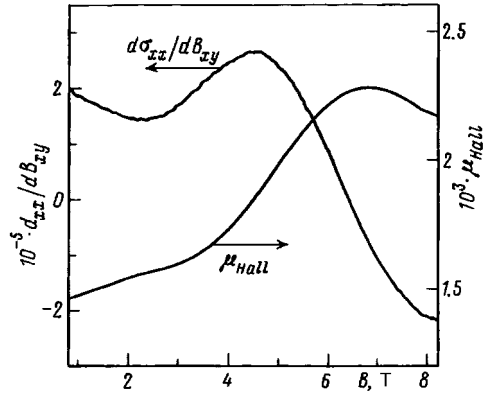


FIG. 2. Derivative of the conductivity  $\sigma_{xx}$  along a parallel surface versus the magnetic field component  $B_{xy}$ , S/T, and Hall mobility  $\mu_H$ ,  $\text{cm}^2/\text{V}\cdot\text{s}$ , versus the magnetic field  $B$ . The angle between the direction of the magnetic field  $B$  and the normal to the surface of the sample equals  $85^\circ$ .

of 1 mm. The field dependences  $\rho_{xx}(B)$  and  $\rho_{xy}(B)$  were measured at  $T=4.2$  K in fields  $B$  up to 8 T for three angles  $\varphi=0^\circ$ ,  $85^\circ$ , and  $90^\circ$  between the normal to the sample and the magnetic field. The angle was set to within  $1^\circ$  with the aid of calibration with respect to the curve  $\rho_{xy}(B)$  in weak fields. The measurements were performed with dc current not exceeding  $100 \mu\text{A}$ .

The field dependence  $\partial\sigma_{xx}/\partial B_{xy}=f(B_{xy})$ , calculated on the basis of the experimental data, where  $B_{xy}$  is the magnetic field component parallel to the plane of the  $\delta$  layer, is presented in Fig. 2. It is known<sup>4</sup> that the maxima in the field dependence  $\partial\sigma_{xx}/\partial B_{xy}$  correspond to passage of the size-quantization levels through the Fermi level. The figure also displays the Hall mobility  $\mu_H$ , measured using the magnetic field component normal to the surface, as a function of the magnitude of the parallel component. The measured Hall mobility  $\mu_H$  and Hall density  $N_H$  are related with the subband mobilities and densities  $\mu_i$  and  $n_i$  by the well-known relations

$$N_H = \frac{\left(\sum n_i \mu_i\right)^2}{\sum n_i \mu_i^2}, \quad \mu_H = \frac{\sum n_i \mu_i^2}{\sum n_i \mu_i}. \quad (1)$$

As we have already mentioned, for a 2DEG the magnetic field components  $B_z$  and  $B_{xy}$  make an independent contribution to the energy of electrons in the size-quantization subbands. In our experiments in magnetic field inclined at an angle of  $\varphi=85^\circ$  the maximum value of the normal component of the magnetic field  $(B_z)_{\text{max}}=0.7$  T and  $(\mu_i)_{\text{max}} < 6000 \text{ cm}^2/\text{V}\cdot\text{s}$ , i.e.,  $\mu B_z < 1$  for all subbands, and therefore it is correct to use the normal component of the magnetic field for measuring the Hall mobility.

The experimentally observed nonmonotonicity of the field dependence  $\mu_H=f(B_{xy})$  with  $\varphi=85^\circ$  can be explained as follows. At electron density  $3 \times 10^{12} \text{ cm}^{-2}$  three size-quantization subbands in the  $\delta$  layers are filled,<sup>7</sup> electrons in the first subband (the bottom subband is denoted by the index  $i=0$ ) having the maximum mobility. The latter circum-

stance is due to the fact that the extrema of the wave functions for odd subbands are located away from the  $\delta$ -doping plane. The mobility in the zeroth subband is low (ordinarily 500–1000 cm<sup>2</sup>/V·s) and largely depends only on the density of charged impurities.<sup>8,9</sup> For this reason, electron redistribution into this subband from higher subbands can lead only to a monotonic decrease of  $\mu_H$ . Growth of  $\mu_H$  as a function of  $B_{xy}$  can be due to electron redistribution from the second subband into the higher-mobility first subband. The maximum of the curve  $\partial\sigma_{xx}/\partial B_{xy}$  at  $B_{xy}=4.5$  T corresponds to passage of the second-subband bottom through the Fermi level. The highest rate of change of the Hall mobility is observed in this case. The maximum of the function  $\mu_H(B_{xy})$  after ejection of the second subband ( $B_{xy}>4.5$  T) is determined by two competing mechanisms: growth of the mobility in the first subband as a result of the increasing distance of the extrema of the wave functions from the scattering centers and decrease of  $\mu_H$  as a result of electron redistribution from the high-mobility first subband into the low-mobility zeroth subband. The ejection of the first subband from below the Fermi level should be observed in magnetic fields higher than those employed in our experiments.<sup>4</sup>

To obtain the dependence of the mobility in the first subband on the ejection magnetic field  $B_{xy}$ , the experimental data were analyzed as follows. First, we measured  $\rho_{xx}$  and  $\rho_{xy}$  as a function of the magnetic field  $B_z$  perpendicular to the plane of the  $\delta$  layer in order to determine the total number of electrons  $N_s$  in the  $\delta$  layer and the mobility  $\mu_0$  in the bottom subband, after which we employed a simplified description of the conductivity of the  $\delta$  layers, similar that employed in Ref. 10. It is assumed that the conductivity consists of the conductivity in the bottom subband  $(\sigma_{xx})_0$  and the conductivity in all other subbands  $(\sigma_{xx})_u$ . Electrons in the upper subbands are assigned the same mobility  $\mu_u$ . A function with four parameters

$$\sigma_{xx} = \frac{en_0\mu_0}{1 + (\mu_0 B_z)^2} + \frac{en_u\mu_u}{1 + (\mu_u B_z)^2},$$

where  $n_0$  and  $\mu_0$  are the density and mobility in the bottom subband,  $n_u$  and  $\mu_u$  are the density and mobility in the “upper” subbands, and  $n_0$ ,  $\mu_0$ ,  $n_u$ , and  $\mu_u$  do not depend on the magnetic field, was fit to the experimental data on  $\sigma_{xx}(B_z)$  with  $B_{xy}=0$ . The total number of electrons in the  $\delta$  layer was determined as  $N_s = n_0 + n_u$ .

Once the values of the mobility in the “zeroth” subband and the total electron density in the  $\delta$  layer are obtained, the electron mobility and density in the first subband can be determined from the measured values of  $N_H(B_{xy})$  and  $\mu_H(B_{xy})$  in an inclined field by means of the relations (1), assuming that, to a first approximation,  $\mu_0 = \text{const}$ , when only the two size-quantization subbands remain filled.

The computational results are presented in Fig. 3. We estimate their accuracy to be not worse than 20%. Most interesting for us is the fact that the mobility in the first subband increases with its diamagnetic ejection from the quantum well. The fact that the mobility in the first subband increases remains valid even when the electron density in the upper subbands in the  $\delta$  layer is determined with an accuracy of not worse than 100%. Qualitatively, the increase in electron mobility  $\mu_1$  in the first subband with increasing magnetic field  $B_{xy}$  can be attributed to the increase in the distance between the maxima

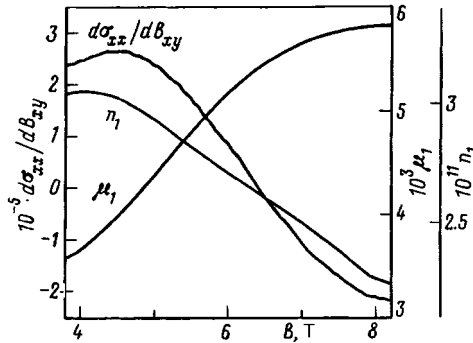


FIG. 3. Derivative of the conductivity with respect to the magnetic field  $d\sigma_{xx}/dB_{xy}$  (left-hand axis),  $S/T$ , electron mobility in the first subband (right-hand axis)  $\mu_1$ ,  $\text{cm}^2/\text{V}\cdot\text{s}$ , and electron density in the first subband  $n_1$  (additional axis on the right-hand side),  $\text{cm}^{-2}$ , versus the magnetic field  $B$ . The angle between the direction of the magnetic field  $B$  and the normal to the surface of the sample equals  $85^\circ$ .

of the wave function and the doping plane, since the bottom of this subband is ejected into a wider part of the potential well.

In summary, we have investigated the dependence of the Hall electron mobility as a function of the population of the size-quantization subbands in a two-dimensional electron gas of a  $\delta$ -doped layer with a constant total electron density  $N_s = 3.2 \times 10^{12} \text{ cm}^{-2}$  (three initially filled subbands) at  $T = 4.2 \text{ K}$ . The population of the subbands was changed by means of diamagnetic ejection of size-quantization levels by a magnetic field oriented parallel to the plane of the  $\delta$ -doped layer. The dependences of the subband mobility and density on the ejection magnetic field were obtained for high magnetic fields ( $B > 4.5 \text{ T}$ ), when only the two bottom subbands remain filled. The mobility in the first subband increases with its diamagnetic ejection from the quantum well. This is attributed to an increase in the average distance between the electrons and the plane of the scattering donor impurities.

This work was supported by the Russian Fund for Fundamental Research (Project 95-02-06328).

<sup>a)</sup>e-mail: ivanovd@ipmt-hpm.ac.ru

- <sup>1</sup>K. Ploog, J. Cryst. Growth **81**, 304 (1987).
- <sup>2</sup>E. F. Shubert, in *Semiconductor and Semimetals "Epitaxial Microstructures"*, edited by A. G. Gossard, Academic Press, New York, 1994, Vol. 40, p. 1.
- <sup>3</sup>Y. Fu and M. Willander, J. Appl. Phys. **78**, 3504 (1995).
- <sup>4</sup>A. Zrenner, H. Reisinger, F. Koch *et al.*, Phys. Rev. B **33**, 5607 (1986).
- <sup>5</sup>D. C. Tsui, Phys. Rev. B **4**, 4438 (1971).
- <sup>6</sup>F. Stern and W. E. Howard, Phys. Rev. **163**, 816 (1967).
- <sup>7</sup>G. Q. Hai, N. Studart, and F. M. Peeters, Phys. Rev. B **52**, 8363 (1995).
- <sup>8</sup>G. Q. Hai, and N. Studart, Phys. Rev. B **52**, 2245 (1995).
- <sup>9</sup>A. B. Henriques, Phys. Rev. B **53**, 16365 (1996).
- <sup>10</sup>X. Zheng, T. K. Carns, K. L. Wang, and B. Wu, Appl. Phys. Lett. **62**, 504 (1993).

Translated by M. E. Alferieff

## Double-well coherent laser with suppressed intersubband relaxation

V. F. Elesin and A. V. Tsukanov

*Moscow State Engineering Physics Institute, 115409 Moscow, Russia*

V. V. Kopaev and Yu. V. Kopaev<sup>a)</sup>

*P. M. Lebedev Physics Institute, Russian Academy of Sciences, 117924 Moscow, Russia*

(Submitted 31 October 1997)

*Pis'ma Zh. Éksp. Teor. Fiz.* **66**, No. 11, 709–713 (10 December 1997)

A theory of coherent lasing on a double-well structure with asymmetric barriers is constructed. On account of the appearance of a termination point of the bottom subband, such a structural element permits strong suppression of intersubband relaxation involving the emission of an optical phonon. It is shown that such a laser possesses low threshold currents and high lasing power, and it can operate without a population inversion. © 1997 American Institute of Physics.

[S0021-3640(97)00823-2]

PACS numbers: 42.55.Px

1. Almost twenty years after being proposed by Kazarinov and Suris,<sup>1</sup> a new type of semiconductor laser — the quantum cascade laser (QCL) — was built by Capasso *et al.*<sup>2</sup> The laser operated on diagonal transitions between levels in two neighboring wells. A model with vertical transitions in a single well was examined in Refs. 3 and 4, which are devoted to the theory of the QCL. It was found<sup>5</sup> that the laser utilizing vertical transitions possesses definite advantages. The structures realized in Refs. 2 and 5 are subjected to strong dissipation processes due to intersubband transitions with the emission of optical phonons with a short time  $\tau_{\text{ph}}$ .

However, quantum-well (dot) lasers are also capable of operating in a fundamentally different regime, since the electron residence time in them can be much shorter than  $\tau_{\text{ph}}$ . Coherent, with respect to the electronic subsystem, lasing on vertical transitions in a single well was studied in Ref. 6 and this regime inherently has low threshold currents, high power, and the possibility of operating without a population inversion. But the real conditions for realizing a coherent regime are stringent on account of the shortness of  $\tau_{\text{ph}}$ . The time  $\tau_{\text{ph}}$  can be substantially increased by using structures consisting of two quantum wells, one of which possesses asymmetric barriers.<sup>7</sup>

2. Let us consider the following model. Lasing occurs on diagonal transitions between levels in two quantum wells (see Fig. 1a). The well parameters are chosen so that the energy difference between the levels  $\epsilon_2$  and  $\epsilon_1$  approximately equals the frequency of the electromagnetic field  $\hbar\omega = \epsilon_2 - \epsilon_1$ . A stationary electron flux with density proportional to  $q$  and energy  $\epsilon$  approximately equal to  $\epsilon_2$  is incident on the system from the left-hand side.

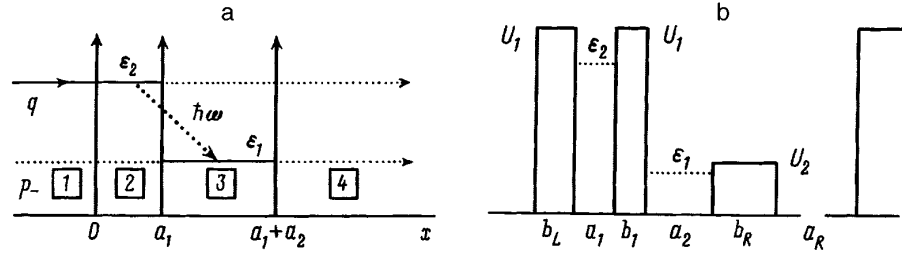


FIG. 1. Diagram of the structure with  $\delta$ -function barriers that was used for calculating the coherent lasing regime (a) and geometry of the real structure with asymmetric barriers (b).

The electromagnetic field

$$E_x(z,t) = E(t) \sin(kz) \cos(\omega t + \phi(t)) \quad (1)$$

is polarized perpendicular to the plane of the wells (i.e., along the  $x$  axis) and the wave vector lies in the plane (along the  $z$  axis). In a single-mode stationary regime the equations for the field are (see Refs. 6 and 8 for a more detailed discussion)

$$\frac{E}{2\tau_0} = -\frac{2\pi}{\kappa} J_c(k), \quad (\omega - \Omega)E = -\frac{2\pi}{\kappa} J_s(k), \quad (2)$$

where  $J_c(k)$  and  $J_s(k)$  are the Fourier components of the polarization currents,  $J_c$  in phase with the field and  $J_s$  phase shifted by  $\pi/2$ , and describe interlevel transitions;  $\tau_0$  is the photon lifetime in the cavity;  $\Omega$  is the cavity frequency; and,  $\kappa$  is the permittivity.

The currents  $J$  can be expressed in the standard manner in terms of the system wave function  $\psi(x,t)$  satisfying the equation

$$i \frac{2m^*}{\hbar} \frac{\partial \psi(x,t)}{\partial t} = -\frac{\partial^2 \psi(x,t)}{\partial x^2} + U(x) \psi(x,t) + \hat{V}(x,t) \psi(x,t), \quad (3)$$

where  $m^*$  is the electron effective mass,

$$U(x) = \alpha [\delta(x) + \gamma \delta(x - a_1) + \beta \delta(x - a_1 - a_2)]$$

is the potential energy of the barriers ( $\gamma$  and  $\delta$  are the relative strengths of the barriers), and

$$\hat{V}(x,t) = V(e^{i\omega t} - e^{-i\omega t}) \frac{\partial}{\partial x}, \quad V = -\frac{eE}{\omega},$$

is the interaction with the electromagnetic field. In what follows,  $eE/\omega p$  is assumed to be a small parameter.

We seek the solution of Eq. (3) in the form (see Ref. 6)

$$\psi(x,t) = \begin{cases} e^{-i\epsilon t}[qe^{ipx} + D_0 e^{-ipx}] + D_{-1} e^{-i(\epsilon-\omega)t - ipx}, & x < 0 \\ e^{-i\epsilon t} \psi_0(x) + \psi_{-1}(x) e^{-i(\epsilon-\omega)t}, & 0 < x < a_1 \\ e^{-i\epsilon t} \tilde{\psi}_0(x) + \tilde{\psi}_{-1}(x) e^{-i(\epsilon-\omega)t}, & a_1 < x < a_1 + a_2 \\ C_0 e^{-i\epsilon t + ip(x-a_1-a_2)} + C_{-1} e^{-it(\epsilon-\omega) + ip(x-a_1-a_2)}, & x > a_1 + a_2, \end{cases} \quad (4)$$

where  $p = (2m^* \epsilon)^{1/2}$ ,  $p_- = (2m^* (\epsilon - \omega))^{1/2}$ , and the functions  $\psi_0(x)$  and  $\psi_{-1}(x)$  satisfy the equations

$$\epsilon \psi_0 + \psi_0'' = V \psi_{-1}', \quad (\epsilon - \omega) \psi_{-1} + \psi_{-1}'' = -V \psi_0'. \quad (5)$$

The solutions of Eqs. (5) have the form

$$\psi_n(x) = A_n e^{\delta x}, \quad \tilde{\psi}_n(x) = \tilde{A}_n e^{\delta x}, \quad n = 0, -1. \quad (6)$$

We determine the coefficients  $D_n$ ,  $C_n$ ,  $A_n$ , and  $\tilde{A}_n$  from the boundary conditions obtained from the requirement that the functions (4) be continuous and the conditions imposed on the derivatives (see Ref. 6). Substituting the wave functions found above into the expression for the currents

$$J_c(x) = -\frac{ie}{2m^*} [(\psi_0^* \psi_{-1}' + \psi_{-1}^* \psi_0') - \text{h.c.}],$$

$$J_s(x) = \frac{e}{2m^*} [(\psi_{-1}^* \psi_0' - \psi_0^* \psi_{-1}') + \text{h.c.}] \quad (7)$$

(similarly for  $\tilde{\psi}_n$ ), after some calculations we find from Eq. (2) equations for the field and lasing frequency

$$\tilde{Q} \frac{\Gamma_1 \Gamma_2}{|\tilde{\Delta}(\lambda)|^2} \frac{p^2}{\alpha^2} = 1,$$

$$\tilde{Q} \frac{\Gamma_2 (\epsilon - \omega - \epsilon_1)}{\tau_0 |\tilde{\Delta}(\lambda)|^2} \frac{p^2}{\alpha^2} = \omega - \Omega, \quad (8)$$

where the dimensionless coherent-pump current is

$$\tilde{Q} = \frac{4\pi\tau_0}{\kappa} Q \eta, \quad Q = \frac{q^2 p}{m^*}, \quad \eta = \frac{32p_-^3 p^2 e^2}{\gamma^2 a_1 a_2 \omega^3} \nu_1,$$

$$\tilde{\Delta}(\lambda) = \{(\epsilon - \omega - \epsilon_1 + i\Gamma_1)(\epsilon_2 - \epsilon - i\Gamma_2) + \lambda^2\},$$

$$\lambda^2 = \frac{4p_-^2 p^2}{\alpha^2 a_1 a_2} \tilde{V}^2 \nu_2, \quad \tilde{V}^2 = \frac{2p_-^2 V^2}{\omega^2} \ll 1, \quad (9)$$

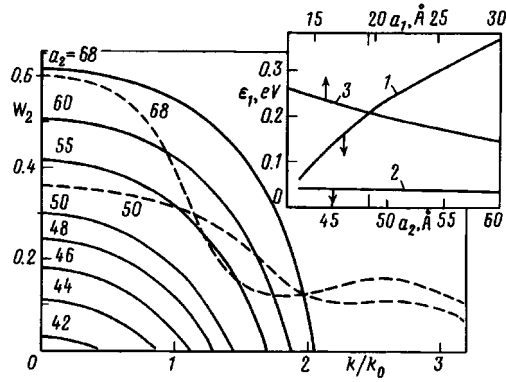


FIG. 2. Probability  $W_2$  of finding an electron in an asymmetric well versus  $k$  ( $k_0 = \sqrt{2/\hbar^2 m^* U_0}$  is the normalization wave vector,  $U_0 = 0.1$  eV) for a series of values of  $a_2$ . Inset: Energy  $\epsilon_2$  of the bottom of the top subband versus the width  $a_1$  of the symmetric well (3); energy of the bottom (2) and energy  $\epsilon_1(k_f)$  of the termination point (1) of the bottom subband versus the width  $a_2$  of the well with asymmetric barriers.

$\Gamma_1 = 2p_-^3 / \alpha^2 \beta^2 a_2$  and  $\Gamma_2 = 2p^3 / \alpha^2 a_1$  are the level widths and the quantities  $\nu_1$  and  $\nu_2$  are of the order of 1.

The equations (8) and (9) are similar to the corresponding equations for a single-well structure.<sup>6</sup> Therefore, the conclusions that the optimal lasing regime obtains with energy tuning without a population inversion, the lasing power is a linear function of the coherent-pump current, and others remain valid. A substantial difference is the presence of the small factor  $p^2 / \alpha^2$  multiplying  $\bar{Q}$ . This leads to a threshold current ( $\lambda = 0$  in Eq. (8))

$$\bar{Q}_{th} = \Gamma_1 \Gamma_2 \frac{\alpha^2}{p^2}, \quad (10)$$

that is formally greater than the value in the single-well structure.<sup>6</sup> However, on account of the suppression of relaxation in the double-well structure the actual value of  $\bar{Q}_{th}$  can be made very small (see below).

**3. Realization of the lasing mechanism examined above requires a double-well structure where the bottom subband corresponds to a well with asymmetric barriers (Fig. 1b). The termination line of the two-dimensional subband must correspond to an energy below the minimum of the upper subband, corresponding to a symmetric well.**

As a first step in choosing the structural parameters required for suppression for interband relaxation, we assume that the widths  $b_L$  and  $b_R$  of the outer barriers are infinite. Figure 2 displays the probability  $W_2$  of observing an electron with energy  $\epsilon_1$  in well 2 as a function of the wave vector  $k$  along the layers of the structure for different values of the well width  $a_2$ . The probability of a relaxation intersubband transition is proportional to  $W_2$  with  $k$  satisfying the condition  $\epsilon_1(k) \approx \epsilon_2(0)$ . For efficient lasing, the value of  $W_2$  for  $k=0$  must be large as far as possible. The calculations were performed for the system  $\text{Al}_x\text{Ga}_{1-x}\text{As}/\text{GaAs}$ , where at the right-hand barrier  $x=0.05$  ( $U_2=0.043$

eV) and at the left-hand and central barriers  $x=0.40$  ( $U_1=0.346$  eV). Starting at barrier width  $b_1>30$  Å the probabilities  $W_2$  and  $W_1$  become virtually independent of  $b_1$ . Vanishing of  $W_2$  corresponds to the termination point  $k_f$  of the two-dimensional state.<sup>7</sup> The inset in Fig. 2 displays the energy  $\epsilon_{1f}$  (curve 1), corresponding to  $k_f$ , and  $\epsilon_1(0)$  (curve 2) versus the well width  $a_2$  and the energy  $\epsilon_2(0)$  — the minimum of the upper subband — versus the width  $a_1$  of the symmetric well (curve 3). As follows from the figure, for the present system suppression of relaxation is possible if the width of the symmetric well  $a_1<a_{1c}=20$  Å and the width of the asymmetric well  $a_2<a_{2c}=49$  Å.

We have examined above a single element of a quantum cascade laser. The finiteness of  $b_L$  has virtually no effect on the position of the levels in the wells, but it does determine the probability of tunneling into well 2. To decrease the critical value  $k_f$  (and therefore  $\epsilon_{1f}$  also),  $a_2$  must be chosen so that the minimum of the subband lies near  $U_2$ . Then the wave function penetrates substantially into the right-hand barrier and therefore the barrier width  $b_R$  must be quite large in order for localization of a state in the well to occur. Moreover, the real structure of the laser must contain several (up to 50) such elements, i.e., the structure which we have examined is bounded on the right-hand side by the barrier  $U_1$  from the next element. Therefore, to describe a real structure the system examined above must be supplemented at least by a barrier  $b_R$  and a well  $a_R$  (see Fig. 1b). In such a structure the concept of a termination point in the asymmetric well 2 becomes formally meaningless. Actually, however, for  $k$  close to  $k_f$ , in the preceding structure relocation of the wave function from well 2 into well  $a_R$  occurs. The probability  $W_2$  no longer strictly vanishes, but rather it remains a finite quantity determined by the ratio  $a_2/(a_R+b_R+a_2)$ . In principle, for finite  $k$  the levels in the well  $a_R$  can fall into resonance with the levels of the well  $a_2$ . As a result, the probability  $W_2$  remains high in a much larger range of  $k$ , diminishing the relaxation suppression effect. This can be avoided by optimizing the parameters  $b_R$  and  $a_R$ . Moreover, it is possible to pick parameters such that the function  $\epsilon_1(k)$  for small values of  $k$  becomes sharper than in the case  $b_R\rightarrow\infty$  and the probability  $W_2$  with  $k=0$  remains high. As an example, the quantities  $W_2(k)$  with  $a_2=50$  and  $68$  Å for the optimal values  $b_R=200$  Å and  $a_R=340$  Å are shown in Fig. 2 (dashed curves). The calculations show that the width  $b_R$  of the barrier must exceed  $100$  Å for substantial localization of the state in the well 2 with  $k=0$ .

**4.** The suppression of relaxation ( $\tau_{\text{ph}}\rightarrow\infty$ ) substantially weakens the conditions for the existence of a coherent regime  $\Gamma_i>1/\tau_{\text{ph}}$  or  $\alpha^2/p^2<\epsilon\tau_{\text{ph}}$ , so that  $\Gamma$  and  $\alpha^2/p^2$  can be made very small. For this reason, the threshold current (10) in the double-well structure studied here

$$\bar{Q} = \frac{4p_-^2 p_2^2}{\alpha^2 a_1 a_2 \beta^2} \sim \frac{1}{\alpha^2}$$

can be made small to the degree that  $\alpha^2/p^2$  is small. This is achieved by selecting sufficiently thick barriers. It is easily verified that the structural parameters required for suppression of relaxation (see above) agree with the requirement that  $\alpha^2/p^2$  be small.

This work was supported by the Russian Fund for Fundamental Research and the Russian Interdisciplinary Science and Technology Program ‘‘Physics of Solid-State Nanostructures.’’

<sup>a)</sup>e-mail: kopaev@sci.lpi.ac.ru

- 
- <sup>1</sup>R. Kazarinov and R. Suris, *Fiz. Tekh. Poluprovodn.* **6**, 96 (1972) [*Sov. Phys. Semicond.* **6**, 120 (1972)].  
<sup>2</sup>J. Faist, F. Capasso, and D. L. Sivco, *Science* **264**, 553 (1994).  
<sup>3</sup>V. F. Elesin and Yu. V. Kopaev, *Solid State Commun.* **96**, 987 (1995).  
<sup>4</sup>V. F. Elesin and Yu. V. Kopaev, *Zh. Éksp. Teor. Fiz.* **108**, 2186 (1995) [*JETP* **81**, 1192 (1995)].  
<sup>5</sup>J. Faist, F. Capasso, C. Sirtori, *Appl. Phys. Lett.* **66**, 538 (1995).  
<sup>6</sup>V. F. Elesin, *Zh. Éksp. Teor. Fiz.* **112**, 483 (1997) [*JETP* **85**, 264 (1997)].  
<sup>7</sup>V. V. Kopaev and Yu. V. Kopaev, *JETP Lett.* **65**, 202 (1997).  
<sup>8</sup>W. E. Lamb, *Phys. Rev.* **134**, 1429 (1964).

Translated by M. E. Alferieff

## Efficient electronic energy transfer from a semiconductor quantum well to an organic material

V. M. Agranovich

*Institute for Spectroscopy, Russian Academy of Sciences, 142092 Troitsk, Moscow Region, Russia*

G. C. La Rocca<sup>a)</sup> and F. Bassani

*Scuola Normale Superiore and INFN, Piazza dei Cavalieri, I-56126 Pisa, Italy*

(Submitted 4 November 1997)

*Pis'ma Zh. Éksp. Teor. Fiz.* **66**, No. 11, 714–717 (10 December 1997)

We predict an efficient electronic energy transfer from the two-dimensional Wannier–Mott excitons confined in a semiconductor quantum well to the optically active organic molecules of the nearby medium (substrate and/or overlayer). The energy transfer mechanism is of the Förster type and, at semiconductor–organic distances of several nanometers, can easily be as fast as 100 ps, which is about an order of magnitude shorter than the average exciton lifetime in an isolated quantum well. Under such conditions, the Wannier–Mott exciton luminescence is quenched and the organic luminescence is efficiently turned on. Our calculations, combining a microscopic quantum mechanical exciton model with a macroscopic electrodynamic description of the organic medium, take into account the dielectric constant discontinuities and can be applied to any organic–inorganic multilayer structure.

© 1997 American Institute of Physics. [S0021-3640(97)00923-7]

PACS numbers: 71.35.Aa, 78.20.Bh, 78.66.Qn

A large effort has recently been devoted to the study of organic light emitting diodes<sup>1</sup> and lasers.<sup>2</sup> Förster-like energy transfer between different dye molecules in solid solutions has already been used to achieve light amplification in optically pumped organic thin films.<sup>3</sup> However, optically active organic materials have poor transport properties compared to inorganic semiconductors, and the efficient electrical pumping of such devices is a challenging problem. Prompted by the rapid advances of epitaxial growth techniques for crystalline molecular materials (even on inorganic substrates), we consider here a novel hybrid configuration in which both inorganic semiconductors and organic materials are present: the basic idea is to pump the optically active organic molecules via electronic energy transfer from the two-dimensional Wannier–Mott excitons of a semiconductor quantum well. It is hoped that in such a hybrid system it would be possible to capitalize on the efficient electrical pumping of the inorganic semiconductor material.

In organic–inorganic heterostructures, in fact, it is possible to take advantage of the complementary functional properties of both types of material. This has been shown to be the case, for instance, in the coherent hybrid Wannier–Mott/Frenkel excitons at a covalent-semiconductor/molecular-solid interface:<sup>4</sup> such novel excitations share both the

large radius of a Wannier–Mott exciton and the large oscillator strength of a Frenkel exciton, and consequently exhibit large optical nonlinearities.<sup>5</sup> The focus of the present paper is on the basic physics governing the incoherent resonant electronic energy transfer from the semiconductor quantum well to the organic material. Our model calculations, employing realistic material parameters, show that such energy transfer can be fast enough to efficiently quench the Wannier–Mott exciton luminescence and pump the organic molecule light emission.

The configuration we consider consists of a semiconductor quantum well of width  $L_w$  sandwiched between two semiconductor barriers of width  $L_b$ , the whole semiconductor structure embedded in bulk-like organic material (for the sake of simplicity, we choose a symmetric configuration and consider the organic material to be isotropic). The background dielectric constant  $\epsilon_b$  of the semiconductor material is taken to be real, whereas the organic material dielectric constant  $\tilde{\epsilon}$  has both a real and an imaginary part in the frequency region of interest. In fact, we are interested in an organic material having a broad band in the optical range overlapping the sharp resonance energy  $\hbar\omega$  of the two-dimensional Wannier–Mott exciton. The Förster-like energy transfer mechanism due to the dipole–dipole interaction can be calculated simply from the Joule losses<sup>6</sup> in the organic material. These are proportional to the imaginary part of  $\tilde{\epsilon}$  and are produced by the penetration of the electric field generated by the semiconductor exciton polarization (explicitly taken into account as a source term in the macroscopic electrostatic equations). Neglecting retardation is a valid approximation as the typical exciton center of mass in-plane wave vector  $k$  is much larger than the wave vector of the corresponding resonant light ( $k \gg \sqrt{\epsilon_b}\omega/c$ ). We also assume to be in the linear regime in which excitons can be described in the bosonic approximation.

Let  $z$  be the growth direction (with  $z=0$  corresponding to the center of the quantum well) and  $x$  be the direction of the in-plane exciton wave vector. We adopt a microscopic quantum mechanical model of a quantum well Wannier–Mott exciton, where the polarization can be taken to vanish for  $|z| > L_w/2$  and, inside the well, to be given by

$$\mathbf{P}(x,z) = \frac{d\hat{x}}{a_B\sqrt{S}} \frac{2}{L_w} \cos^2\left(\frac{\pi z}{L_w}\right) \exp(ikx), \quad (1)$$

where  $a_B$  is the exciton Bohr radius,  $S$  is the in-plane normalization area,  $d$  is the interband transition dipole moment,  $\hat{x}$  is a unit vector, and the polarization chosen is that of the  $L$  mode.<sup>4</sup> An analogous calculation can be carried out for the  $Z$  mode. The corresponding electric field  $\mathbf{E}(x,z) = -\nabla\Phi(x,z)$  can be obtained from the solution of the Poisson equation

$$\epsilon(z)\nabla^2\Phi(x,z) = 4\pi\nabla\cdot\mathbf{P}(x,z), \quad (2)$$

with the appropriate boundary conditions at  $z = \pm L_w/2$  and at  $z = \pm(L_w/2 + L_b)$ , i.e., continuity of the tangential component of the electric field  $\mathbf{E}(x,z)$  and of the normal component of the electric displacement  $\mathbf{D}(x,z) = \epsilon(z)\mathbf{E}(x,z)$ . Writing  $\Phi(x,z) = \phi(z) \times \exp(ikx)$ , we find that  $\phi(z)$  satisfies

$$\frac{d^2\phi}{dz^2} - k^2\phi = \frac{4\pi}{\epsilon_b} ik \frac{d}{a_B\sqrt{S}} \frac{2}{L_w} \cos^2\left(\frac{\pi z}{L_w}\right), \quad (3)$$

for  $|z| < L_w/2$ , and otherwise

$$\frac{d^2\phi}{dz^2} - k^2\phi = 0, \quad (4)$$

with the boundary conditions that  $\phi(z)$  and  $\epsilon(z)d\phi(z)/dz$  be continuous at the four interfaces. The corresponding solution in the organic material (from now on  $k > 0$  and  $z > L_w/2 + L_b$ ) is given by

$$\phi(z) = -i \frac{2q^3}{k(k^2 + q^2)} \frac{d}{a_B\sqrt{S}} \frac{(e^{kL_w/2} - e^{-kL_w/2})}{(\epsilon_b + \tilde{\epsilon}) - (\epsilon_b - \tilde{\epsilon})e^{-2kL_b - kL_w}} \exp(-kz), \quad (5)$$

with  $q = 2\pi/L_w$ . Thus, the electric field penetrating in the organic material is given by

$$E_x(x, z) = -ik \exp(ikx)\phi(z), \quad E_z(x, z) = k \exp(ikx)\phi(z), \quad E_y = 0. \quad (6)$$

We observe that the macroscopic approach we have taken is fully adequate, as the electric field is slowly varying on the molecular scale. It is now a simple matter to calculate the Joule losses in the organic material, the time-averaged power per unit volume being<sup>7</sup>

$$w(z) = \frac{\omega}{4\pi} \text{Im}(\tilde{\epsilon})k^2|\phi(z)|^2, \quad (7)$$

with  $\phi(z)$  given by Eq. (5). Thus the total power delivered to the organic material is

$$W = S \int_{L_w/2 + L_b}^{+\infty} dz w(z) = \frac{S\omega}{8\pi k} \text{Im}(\tilde{\epsilon})k^2|\phi(z=L_w/2 + L_b)|^2 \equiv \frac{\hbar\omega}{\tau}, \quad (8)$$

where we have introduced  $\tau$  as the average time required by an exciton to transfer its energy to an organic molecule (if the organic material in the region  $z < -L_w/2 - L_b$  is also considered,  $\tau$  would be half as long). We can see that the previous expression for  $\tau$  does not depend on the excitation density (as long as the linear regime obtains). In fact, if the bosonic exciton state is  $N$ -fold populated, then the corresponding polarization scales as  $\sqrt{N}$  and the power  $w$  as  $N$ , just as the total excitation energy  $N\hbar\omega$ ; indeed,  $N$  cancels from both sides of Eq. (8). Besides, the same expression can be derived from a fully microscopic approach considering the Förster dipole-dipole energy transfer and the appropriate averaging procedure.

We estimate the order of magnitude of  $\tau$  from Eq. (8) and Eq. (5), employing parameters representative of II-VI semiconductor quantum wells<sup>8</sup> and optically active organic condensed media such as metallophthalocyanines<sup>9</sup> or fullerenes.<sup>10</sup> Taking  $L_w \approx 60 \text{ \AA}$ ,  $L_b \approx 40 \text{ \AA}$ ,  $k \approx 3 \cdot 10^6 \text{ cm}^{-1}$  (appropriate to a thermalized exciton distribution with  $T \approx 100 \text{ K}$ ),  $d/a_B \approx 0.1e$ ,  $\epsilon_b \approx 5$ ,  $\tilde{\epsilon} \approx 4 + i3$ , we obtain for this typical case  $\tau \approx 50 \text{ ps}$ . Considering that in an isolated quantum well the exciton lifetime (for such a thermalized distribution) is a few nanoseconds,<sup>8</sup> the energy transfer mechanism here proposed turns

out to be fast enough to efficiently transfer a large fraction of the semiconductor electronic excitation energy to the adjacent organic molecules, which will eventually decay, emitting visible light.

Finally, we wish to stress that our model calculations can be easily applied to any hybrid multilayer structure and could be generalized to the case in which the structure is embedded in a microcavity and to the case in which the two-dimensional excitons are localized (i.e., in-plane translational symmetry is broken) or the semiconductor is excited in the continuum (i.e., free electron hole pairs, rather than bound excitons, are present).

V. M. A. is grateful to Scuola Normale Superiore and FORUM-INFM (Pisa, Italy) for hospitality and support. He also acknowledges partial support through Grant 96-0334049 of the Russian Fund for Fundamental Research, Grant 1-044 of the Russian Ministry of Science and Technology and INTAS Grant 93-461.

<sup>a)</sup>e-mail: larocca@ella.sns.it

---

<sup>1</sup>J. R. Sheats, *Science* **277**, 191 (1997), and references therein.

<sup>2</sup>V. G. Kozlov, V. Bulović, P. E. Burrows, and S. R. Forrest, *Nature* **389**, 362 (1997).

<sup>3</sup>M. Berggren, A. Dodabalapur, R. E. Slusher and Z. Bao, *Nature* **389**, 466 (1997).

<sup>4</sup>V. M. Agranovich, R. Atanasov, and F. Bassani, *Solid State Commun.* **92**, 295 (1994).

<sup>5</sup>G. C. La Rocca, F. Bassani, and V. M. Agranovich, *Nuovo Cimento D* **17**, 1555 (1995).

<sup>6</sup>A similar idea has been used to calculate the energy transfer from an excited dye molecule to the surrounding solution, considering the molecule as a point classical dipole and the solution as a continuous absorbing medium: M. D. Galanin and I. M. Frank, *Zh. Éksp. Teor. Fiz.* **21**, 114 (1951); M. D. Galanin, *Zh. Éksp. Teor. Fiz.* **21**, 126 (1951).

<sup>7</sup>L. D. Landau and E. M. Lifshitz, *Electrodynamics of Continuous Media*, Pergamon Press, Oxford, 1960, paragraph 61.

<sup>8</sup>P. Y. Yu and M. Cardona, *Fundamentals of Semiconductors*, Springer-Verlag, Berlin, 1996, Ch. 9.

<sup>9</sup>T. Yamada, H. Hoshi, T. Manaka *et al.*, *Phys. Rev. B* **53**, R13314 (1996).

<sup>10</sup>A. F. Hebard, R. C. Haddon, R. M. Fleming and A. R. Kortan, *Appl. Phys. Lett.* **59**, 2109 (1991).

Published in English in the original Russian journal. Edited by Steve Torstveit.

# Crossover scale of the fixed point with replica symmetry breaking in the random Potts model

S. B. Bravyi and V. S. Dotsenko

*Landau Institute of Theoretical Physics, Russian Academy of Sciences, 117940 Moscow, Russia*

(Submitted 4 November 1997)

*Pis'ma Zh. Éksp. Teor. Fiz.* **66**, No. 11, 718–723 (10 December 1997)

We study the scaling properties of the renormalization group (RG) flows in the two-dimensional random Potts model, assuming a general type of replica symmetry breaking (RSB) in the renormalized coupling matrix. It is shown that in the asymptotic regime the RG flows approach the non-trivial RSB fixed point algebraically slowly, which reflects the fact that this type of the fixed point is marginally stable. As a consequence, the crossover spatial scale corresponding to the critical regime described by this fixed point turns out to be exponentially large.

© 1997 American Institute of Physics. [S0021-3640(97)01023-2]

PACS numbers: 64.60.Ak, 75.10.Nr

After several years of extensive studies of the critical properties of the ferromagnetic random Potts model there still remains the controversy due to the fact that in the renormalization group (RG) approach one finds two types of attracting fixed points, one of which is replica symmetric (Refs. 1 and 2) while at the other the replica symmetry is broken.<sup>3</sup> In this situation, which one of the two fixed points is actually reached depends on the starting conditions for the coupling matrix in the RG equations. Recent numerical studies seems to favor the critical properties corresponding to the RSB fixed point Ref. 4. However, since the replica symmetry breaking (RSB) fixed point is only marginally stable (the spectrum of the corresponding eigenvalues starts from zero), the crossover spatial scale corresponding to the critical regime of this fixed point may turn out to be much larger than the currently usable sizes for numerical tests. To obtain a prediction for the value of the RSB crossover scale one has to derive the asymptotic behavior of the RG flows near the RSB fixed point, and it is this problem which we address in the present letter.

The random  $q$ -state Potts model is described by the following lattice Hamiltonian:

$$H[\sigma] = - \sum_{\langle i,j \rangle} J_{ij} V(\sigma_i, \sigma_j). \quad (1)$$

Here the spins  $\{\sigma_{ij}\}$  take on  $q$  values; the summation goes over the nearest-neighbor sites;  $V(\sigma, \sigma') = 1 - \delta_{\sigma, \sigma'}$  is the spin-spin interaction potential;  $\{J_{ij}\}$  are random ferromagnetic coupling constants with independent distributions characterized by a narrow width  $g_0$  around a mean value  $J_0$ . Since the randomness is assumed to be weak ( $g_0 \ll J_0$ ), in the critical region this system can be analyzed in terms of the renormalization group approach based on the conformal field theory of the unperturbed model Ref. 1. Following

the standard procedure of averaging with replicas, it can be shown (see, e.g., Ref. 2) that at the critical point the system under consideration is described by the following continuum-limit replica Hamiltonian:

$$H = \sum_{a=1}^n H_0^a + \sum_{a \neq b}^n g_{ab} \int d^2x e_a(x) e_b(x), \quad (2)$$

where  $H_0$  is the Hamiltonian of the pure system, and the second term represents the couplings of the energy operators  $e_a$  of different replicas. Strictly speaking, after performing replica averaging one obtains the replica symmetric coupling matrix  $g_{ab} = g$  (where  $g$  is proportional to  $g_0$ ). However, according to qualitative physical arguments<sup>5</sup> one can also consider a more general situation in which the replica symmetry is spontaneously broken in the coupling matrix  $g_{ab}$  such that it has the Parisi block-like structure.<sup>6</sup>

The renormalization group for the model (2) (with the replica symmetric  $g_{ab}$ ) has been derived in the two-loop approximation in Ref. 1, and by the technique developed in Ref. 2 these RG equations can be easily generalized for an arbitrary structure of the coupling matrix  $g_{ab}$  (Ref. 3):

$$\frac{d}{d\xi} g_{ab} = \tau g_{ab} + \sum_{c=1}^n g_{ac} g_{cb} + g_{ab}^3 - g_{ab} \sum_{c=1}^n g_{ac} g_{ca} \quad (3)$$

(it is assumed that  $g_{aa} \equiv 0$ ). Here  $\xi$  is the usual RG log-scale parameter, and the small parameter of the theory  $\tau = -3\epsilon$  is related to the deviation  $\epsilon$  of the central charge of the conformal theory for the Potts model from the one for the Ising model. In particular, for the 3-component Potts model  $\epsilon = -2/15$ . In fact, the renormalization group for the Potts model is derived in terms of the  $\epsilon$ -expansion technique.

The critical behavior determined by the replica symmetric fixed point of Eq. (3) has been analyzed in full detail in Refs. 1, 2, and 4. Here we will concentrate on the RSB case. According to the standard technique developed in the mean-field theory of spin glasses,<sup>6</sup> in the limit of the continuous RSB, the matrix  $g_{ab}$  is parametrized in terms of the continuous (and monotonic) function  $g(x)$  defined on the interval  $0 \leq x \leq 1$ . In this case, from the general Eq. (3) one can easily derive the following RG equation for the renormalized function  $g(x; \xi)$  (Ref. 3):

$$\begin{aligned} \frac{d}{d\xi} g(x; \xi) = & \tau g(x; \xi) - 2g(x; \xi) \bar{g}(\xi) - \int_0^x dy [g(x; \xi) - g(y; \xi)]^2 + g^3(x; \xi) \\ & + g(x; \xi) \bar{g}^2(\xi), \end{aligned} \quad (4)$$

where  $\bar{g}(\xi) \equiv \int_0^1 dx g(x; \xi)$  and  $\bar{g}^2(\xi) \equiv \int_0^1 dx g^2(x; \xi)$ . Note that the structure of the corresponding fixed-point equation,  $(d/d\xi) g(x; \xi) = 0$  coincides (with the exception of the last term on the right-hand side of Eq. (4)) with the corresponding saddle-point equation for the Parisi order parameter function in the mean-field theory of spin glasses near the phase transition point.<sup>6</sup> The fixed-point solution of the Eq. (4) is:

$$g_*(x) = \begin{cases} \frac{1}{3}x & \text{at } 0 \leq x \leq x_1 \\ g_1 & \text{at } x_1 \leq x \leq 1, \end{cases} \quad (5)$$

where  $x_1 = 3g_1$ , and the value of  $g_1$  is defined by the equation  $2g_1(1-g_1)^2 = \tau$ , such that  $g_1 \approx \frac{1}{2}\tau$  in the linear order in small  $\tau$ . The critical properties determined by this fixed point are described in detail in Refs. 2 and 3.

Here we would like to study the problem of crossover to the critical regime determined by the RSB fixed point (5). Usually, if one deals with the renormalization group in terms of a finite number of renormalized parameters, this problem is not so difficult. In this case, if the fixed point is stable, the RG trajectories are approaching the fixed point exponentially fast, and therefore the corresponding spatial crossover scale depends on the starting parameters according to some algebraic law (with the crossover exponent determined by the smallest (in absolute value) eigenvalue of the linearized RG equations in the vicinity of the fixed point).

In the present case the RG equation (4) describes the evolution of a *function*, which formally means that we are dealing with an infinite number of renormalized parameters, and correspondingly one finds a whole *spectrum* (infinite number) of eigenvalues of the linearized RG equations. Moreover, it is well known from the mean field theory of spin glasses that this spectrum starts from  $\lambda = 0$ , and therefore it is not so easy to tell right away what must be the typical asymptotic decay of the perturbations near the fixed point. Although the problem of stability of the saddle-point of the type given by Eq. (5) for the corresponding mean-field SG free energy functional is already studied in all detail, and the spectrum of all the eigenvalues is well known,<sup>7</sup> in the present problem we are facing somewhat different situation.

First, in the terminology of the stability analysis of the Parisi-type structures, the RG Eq. (4) actually represents not all possible (in the mean-field spin glasses) deviations, but only the so-called “longitudinal” modes. This makes life much easier because, as it will be shown below (see also<sup>7</sup>), it makes the spectrum of the eigenvalues to be *discrete* (although still accumulating towards zero), unlike the complete spectrum in the corresponding SG problem, which is *continuous*.

Second, unlike spin glasses, where the “dynamical” behavior of the order parameter defined by Eq. (4) makes no sense (the real microscopic spin dynamics can not be reduced to such a simple dynamical equation for the replica order parameter), here it is the asymptotic “dynamical” evolution of the Parisi function in the vicinity of the fixed point which is of the main interest.

Third, in the present problem, described by Eq. (4), we have the additional term  $g(x)\overline{g^2}$ , which is not present in the corresponding saddle-point equation in spin glasses. This term appears to be irrelevant for the structure of the fixed-point solution, but it turns out to be quite relevant for the asymptotic behavior of the deviations near the fixed point.

The linear analysis of the perturbations around the fixed point specified by Eq. (5) is rather simple. Substituting  $g(x; \xi) = g_*(x) + \phi(x; \xi)$  into Eq. (4), in the linear order in the small deviation  $\phi(x; \xi)$  we get

$$\frac{d}{d\xi} \phi(x; \xi) = 2 \int_0^1 dy K(x, y) \phi(y; \xi) + 2g_*(x) \int_0^1 dy g_*(y) \phi(y; \xi), \quad (6)$$

where

$$K(x, y) = \begin{cases} -g_*(y) & \text{for } x > y \\ -g_*(x) & \text{for } x < y. \end{cases} \quad (7)$$

It can be easily checked *a posteriori* that since  $g_* \sim \tau$ , in the leading order in  $\tau \ll 1$  the last term in Eq. (6) is irrelevant, and it will therefore be dropped in the further analysis.

Since  $K(x, y) = K(y, x)$ , the operator  $\hat{K}$  is Hermitian and can be diagonalized. The corresponding equation for the eigenfunctions is:

$$\hat{K} \phi^{(n)} = \lambda_n \phi^{(n)}. \quad (8)$$

Twice taking the derivative of the above equation with respect to  $x$ , we obtain:

$$\frac{d^2}{dx^2} \phi^{(n)}(x) - \frac{g'_*(x)}{\lambda_n} \phi^{(n)}(x), \quad (9)$$

where, according to Eq. (5),  $g'_*(x) = 1/3 = \text{const}$  for  $0 \leq x < x_1$ , and  $g'_*(x) = 0$  for  $x_1 < x \leq 1$ . Thus, the solution for the eigenfunction is:

$$\phi^{(n)}(x) = \begin{cases} \sin(k_n x) & \text{for } 0 \leq x \leq x_1 \\ \phi_1 = \sin(k_n x_1) & \text{for } x_1 \leq x \leq 1, \end{cases} \quad (10)$$

where

$$k_n^2 = -\frac{1}{3\lambda_n}. \quad (11)$$

Substituting these eigenfunctions in the original equation (8) we obtain the equation for the eigenvalues:  $k_n \tan(k_n x_1) = (1 - x_1)^{-1}$ . Since  $x_1 \sim \tau \ll 1$  the solution of this equation gives the following spectrum of the eigenvalues:

$$\lambda_n = -\frac{3\tau^2}{4\pi^2 n^2}. \quad (12)$$

We see that the eigenvalues are accumulating towards zero. Since the characteristic decay scale of the  $n$ th order mode is of the order of  $\xi_n \sim \lambda_n^{-1} \sim n^2/\tau^2$ , the more higher-order modes that the starting function  $g(x; \xi=0)$  contains, the slower it will decay. In the extreme case, if the starting function would be composed of all the modes with equal weight, it would not decay towards the fixed point at all. Thus, if the analysis of the stability of the fixed point would have to be restricted within the linear order, the result would be not quite conclusive. Fortunately, the actual situation appears to be more complicated, and it turns out that the linear analysis is not enough.

The problem is that besides the set of the eigenfunctions described above, there also exists a whole (infinite) spectrum of the so-called “zero-mode” functions, which have the eigenvalue  $\lambda_0 \equiv 0$ . Coming back to the original linear equation (6), one can easily

check that the zero-mode is an arbitrary function  $\phi_0(x)$  such that  $\phi_0(x) \equiv 0$  in the interval  $0 \leq x < x_1$  and  $\int_{x_1}^1 dx \phi_0(x) = 0$ . Apparently, a zero-mode function is orthogonal to all the ‘‘non-zero-mode’’ functions, Eq. (10). Since in the linear order all the deviations which contain the zero-mode function do not decay, a second-order analysis is needed.

Let us explicitly separate the two types of modes:  $\phi(x; \xi) = \phi_1(x; \xi) + \phi_0(x; \xi)$ , where the function  $\phi_1(x; \xi)$  is assumed to be composed of the non-zero-mode functions (10) only. Simple calculation gives the following second-order equations for the functions  $\phi_1(x; \xi)$  and  $\phi_0(x; \xi)$ :

$$\begin{aligned} \frac{d}{d\xi} \phi_1(x; \xi) = & 2 \int_0^1 dy K(x, y) \phi_1(y; \xi) - 2 \phi_1(x; \xi) \overline{\phi_1}(\xi) - \int_0^x dy [\phi_1(x; \xi) \\ & - \phi_1(y; \xi)]^2 + g_*(x) \overline{\phi_0^2}(\xi) \end{aligned} \quad (13)$$

in the interval  $0 \leq x \leq x_1$ ; and

$$\frac{d}{d\xi} \phi_0(x; \xi) = -2 \phi_0(x; \xi) \phi_1(\xi) - \int_{x_1}^x dy [\phi_0(x; \xi) - \phi_0(y; \xi)]^2 \quad (14)$$

in the interval  $x_1 < x \leq 1$ . In Eq. (13) all the terms like  $g_* \overline{g_* \phi_1}, g_* \phi_1^2, \phi_1 \overline{g_* \phi_1}, g_* \overline{\phi_1^2}$  which are small in  $\tau$  have been omitted; and in Eq. (14) we have introduced the notation:  $\phi_1(\xi) \equiv \phi_1(x=x_1; \xi)$ . Below we will show that due to mutual interference of the zero- and non-zero-modes (via the last term in Eq. (13) and the first term in Eq. (14)) the asymptotic behavior of the solutions of the above two equations appears to be quite universal.

The solution of the Eq. (14) can be found exactly for an arbitrary given function  $\phi_1(\xi)$  and for an arbitrary starting function  $\phi_0(x; \xi=0)$ :

$$\phi_0(x; \xi) = \int_0^x dy \left[ \frac{\gamma(\xi) \phi_0'(y; 0)}{1 + h(\xi) \int_{x_1}^y dz (z - x_1) \phi_0'(z; 0)} \right]^2 - \overline{\phi}(\xi), \quad (15)$$

where

$$\gamma(\xi) = \exp \left\{ -2 \int_0^\xi d\xi \phi_1(\xi) \right\} \quad (16)$$

and

$$h(\xi) = \int_0^\xi dt \gamma(t). \quad (17)$$

Here the function  $\overline{\phi}(\xi)$  is fixed by the condition  $\int_{x_1}^1 dx \phi_0(x; \xi) = 0$ , and  $\phi_0'(x; 0)$  is the derivative with respect to  $x$  of a given starting function  $\phi_0(x; \xi=0)$ .

The solution (15) make it possible to derive the asymptotic (at  $\xi \rightarrow \infty$ ) behavior of the functions  $\phi_1$  and  $\phi_0$  without explicit solutions of equation (13). Let us consider three different types of possible asymptotic decays of the function  $\phi_1$ .

1. Let us assume first that the decay of the function  $\phi_1$  is sufficiently fast:  $\phi_1 \sim \xi^{-\alpha}$  with  $\alpha > 1$  (or  $\phi_1$  decays exponentially fast, as it should follow from the linear analysis for the function containing finite number of the eigenfunctions, Eq. (10)). Then, from Eqs. (16) and (17) one finds:  $\gamma(\xi \rightarrow \infty) \rightarrow \text{const}$  and  $h(\xi \rightarrow \infty) \rightarrow (\text{const})\xi$ . In this case it is easy to see from the solution (15) that the function  $\phi_0(x; \xi \rightarrow \infty)$  has a step-like structure: in the narrow interval  $x_1 \leq x < x_1 + \Delta(\xi)$ , where  $\Delta(\xi) \sim \xi^{-1/2}$ , its absolute value is  $\phi^{(*)} \sim \xi^{-1/2}$ , whereas in the rest of the interval,  $x_1 + \Delta(\xi) < x \leq 1$ , its value is much smaller:  $\phi^{(**)} \sim \xi^{-1}$ . Therefore, for the asymptotic behavior of the last term in Eq. (13) we get:  $\overline{\phi_0^2} \sim (\phi^{(*)})^2 \Delta + (\phi^{(**)})^2 \sim \xi^{-3/2}$ . Since the linear and the quadratic terms in Eq. (13) decay as  $\xi^{-(\alpha+1)}$  and  $\xi^{-2\alpha}$ , respectively, where both  $(\alpha+1)$  and  $2\alpha$  are greater than  $3/2$ , the last term, containing  $\overline{\phi_0^2} \sim \xi^{-3/2}$ , must dominate at  $\xi \rightarrow \infty$ . Thus, the asymptotic behavior  $\phi_1 \sim \xi^{-\alpha}$  with  $\alpha > 1$  cannot take place.

2. Let us assume now that the asymptotic decay of the function  $\phi_1$  is slow:  $\phi_1 \sim \xi^{-\alpha}$  with  $\alpha < 1$ . In this case from Eqs. (16) and (17) one finds:  $\gamma(\xi \rightarrow \infty) \sim \exp\{-(\text{const})\xi^{(1-\alpha)}\}$  and  $h(\xi \rightarrow \infty) \rightarrow (\text{const})$ . Therefore, according to Eq. (15), the function  $\phi_0$  must be exponentially small:  $\phi_0 \sim \exp\{-(\text{const})\xi^{(1-\alpha)}\}$ , and the last term in Eq. (13) can be neglected in comparison with the other terms, which depend on the function  $\phi_1$  only. In this case, however, if  $\alpha < 1$ , the second-order terms, being of the order of  $\xi^{-2\alpha}$ , must be dominating over the linear term, which is of the order of  $\xi^{-(\alpha+1)}$ . On the other hand, simple estimates show that the asymptotic solution of equation (13) with only the second-order terms decays as  $\xi^{-1}$ , and one cannot have  $\xi^{-\alpha}$  with  $\alpha < 1$ . Thus, the slow asymptotic behavior  $\phi_1 \sim \xi^{-\alpha}$  with  $\alpha > 1$  cannot take place either.

3. It can be easily checked that the only self-consistent asymptotic decay of the function  $\phi_1$  is  $\phi_1 \sim A\xi^{-1}$ , where  $A$  is some constant. Indeed, using again the general solution (15) for the function  $\phi_0$ , one can easily find that depending on the value of the constant  $A$  there can exist three different regimes:

$$\overline{\phi_0^2} \sim \begin{cases} \xi^{-4A} & \text{if } A > \frac{1}{2} \\ \frac{1}{\xi^2 (\ln \xi)^{3/2}} & \text{if } A = \frac{1}{2} \\ \xi^{-(3+2A)/2} & \text{if } A < \frac{1}{2}. \end{cases} \quad (18)$$

Returning to Eq. (13) for the function  $\phi_1$ , one can easily check that the last term  $\overline{\phi_0^2}$  can be neglected (and only in this case can the asymptotic behavior  $\phi_1 \sim \xi^{-1}$  appear) only in the first two cases, i.e., for  $A \geq 1/2$ .

Thus we conclude that in the above RG approach with continuous RSB, for a generic starting Parisi function  $g(x; \xi=0)$  the deviations of the renormalized function  $g(x; \xi)$  from the fixed point  $g_*(x)$  given by Eq. (5) decay as  $\xi^{-1}$ . This slow asymptotic behavior is essentially different from the usual exponentially fast decay in the vicinity of a stable fixed point in the RSB renormalization group. As a consequence, the crossover scale  $\xi_*$  corresponding to the RSB fixed point (5) is defined by the condition

$\xi_* \sim g_*^{-1} \sim \tau^{-1}$ , and therefore the corresponding spatial crossover scale must be exponentially large:

$$R_* \sim \exp\{\text{const}/\tau\}. \quad (19)$$

It should be noted that the actual value of this crossover scale (which is quite important for reliable interpretation of numerical tests) essentially depends on a nonuniversal constant which is determined by the structure of the starting Parisi function  $g(x; \xi=0)$ . Since the structure of this function remains quite unclear, at the present stage it is hardly possible to derive a more concrete prediction for the RSB crossover scale. Nevertheless, the present study demonstrates that in principle this scale may turn out to be well beyond the sizes accessible in the usual numerical simulations.

This work was supported in part by Russian Fund for Fundamental Research, Grants 96-02-18985 and 96-15-96920. V. D. is grateful to Vl. S. Dotsenko for numerous stimulating discussions. V. D. would also like to thank I. Kondor for a helpful discussion of this work.

<sup>1</sup>A. W. W. Ludwig, Nucl. Phys. B **285**, 97 (1987); Nucl. Phys. B **330**, 639 (1990).

<sup>2</sup>Vl. S. Dotsenko, M. Picco, and M. Pujol, Nucl. Phys. B **455**, 701 (1995).

<sup>3</sup>Vik. S. Dotsenko, Vl. S. Dotsenko, M. Picco, and M. Pujol, Europhys. Lett. **32**, 425 (1995).

<sup>4</sup>Vik. S. Dotsenko, Vl. S. Dotsenko, and M. Picco, preprint <http://xxx.lanl.gov/abs/hep-th/9709136>.

<sup>5</sup>Vik. S. Dotsenko, A. B. Harris, D. Sherrington, and R. B. Stinchcombe, J. Phys. A **28**, 3093 (1995).

<sup>6</sup>M. Mezard, G. Parisi, and M. Virasoro, *Spin-Glass Theory and Beyond*, World Scientific, Singapore, 1987.

<sup>7</sup>C. De Dominicis and I. Kondor, Phys. Rev. B **27**, 606 (1983); I. Kondor, C. De Dominicis and T. Temesvari, Physica A **185**, 295 (1992).

Published in English in the original Russian journal. Edited by Steve Torstveit.

# Mn<sup>55</sup> NMR investigation of the suppression of quantum fluctuations in quasi-one-dimensional antiferromagnets by a magnetic field

A. S. Borovik-Romanov,<sup>a)</sup> S. V. Petrov, and A. M. Tikhonov

*P. L. Kapitza Institute of Physical Problems, Russian Academy of Sciences, 117334 Moscow, Russia*

B. S. Dumesh

*Institute of Spectroscopy, Russian Academy of Sciences, 142092 Troitsk, Moscow Region, Russia*

(Submitted 5 November 1997)

*Pis'ma Zh. Éksp. Teor. Fiz.* **66**, No. 11, 724–729 (10 December 1997)

The NMR of Mn<sup>55</sup> nuclei is measured in the quasi-one-dimensional antiferromagnets CsMnBr<sub>3</sub>, RbMnBr<sub>3</sub>, and CsMnI<sub>3</sub> in magnetic fields up to 8 T at temperatures in the range 1.3–4.2 K. The average moments of the magnetic sublattices and their field dependences, which turned out to be comparatively strong and different for magnetically non-equivalent Mn<sup>2+</sup> ions, are determined from the hyperfine-field data obtained. As a result, the magnetizations of separate sublattices in an external magnetic field ~8 T differ by more than 5%. The results obtained agree qualitatively with the theory of the suppression of quantum fluctuations by a magnetic field. © 1997 American Institute of Physics. [S0021-3640(97)01123-7]

PACS numbers: 75.25.+z, 76.60.-k, 75.50.Ee

The investigation of the deviation of the average moments  $\langle S \rangle$  of magnetic sublattices in antiferromagnets (AFs) from the nominal values  $S$  as a result of quantum fluctuations is one of the standard problems of the physics of antiferromagnetism. Although the general theory of this phenomenon was constructed quite long ago,<sup>1</sup> comparatively few reliable experiments have been performed. The problem is that in 3D antiferromagnets the reduction  $(\langle S \rangle - S)/S \approx 2 - 5\%$  is small and difficult to measure.<sup>b)</sup> The accuracy of the amplitude measurements is, as a rule, inadequate because of the need to make allowance for extinction effects in neutron diffraction. The other well-known method is measurement of the hyperfine fields at the nuclei of the magnetic ions. Thus, in ions of 3d elements

$$H_n = - \frac{A}{\gamma_n h} \langle S \rangle, \quad (1)$$

where  $A$  is the hyperfine constant,  $\gamma_n$  is the nuclear gyromagnetic ratio ( $\gamma_n = 10.6$  MHz/T for Mn<sup>2+</sup>), and  $h$  is Planck's constant. However, the reduction effect is masked by the uncertainty in the hyperfine constant  $A$ , determined from ESR on the same ions in an isomorphous nonmagnetic matrix.

TABLE I.

$\langle S \rangle$	Neutron diffraction	NMR	Other methods	Theory
CsMnBr <sub>3</sub>	1.65 [Ref. 3]	1.8 [Ref. 4]	1.7 [Ref. 5]	1.82 [Ref. 6]
RbMnBr <sub>3</sub>	1.8 [Ref. 7]	1.8 present		
CsMnI <sub>3</sub>	1.85 [Ref. 8]	1.74 work	1.8 [Ref. 9]	1.8; 2 [Ref. 10]

Calculations<sup>2</sup> have shown that the hyperfine constant  $A$  in substances with a low concentration of magnetic ions is smaller than in pure magnets because of effects due to the transfer of an unpaired electron spin from one manganese ion to a neighboring one. Making allowance for covalence effects for the  $\text{Mn}^{2+}$  ion with six nearest neighbors gave a 2–4% increase in the hyperfine field, which limits the accuracy with which  $\langle S \rangle$  in 3D magnets can be determined.

The situation is much better in the case of the investigation of quasi-one-dimensional magnets, where the expected spin reduction can reach 30% and can be measured by different methods. Moreover, in quasi-1D magnets the  $\text{Mn}^{2+}$  ion has only two nearest neighbors and therefore the contribution of the indirect hyperfine interaction to the local field at the nucleus of this ion should be less than the estimate indicated above.

Data on the magnitude of the average spins of  $\text{Mn}^{2+}$  ions in some quasi-1D AFs with triangular magnetic structure are given in Table I.<sup>c)</sup> One can see that the agreement of the results with one another and with the theoretical predictions is good. Moreover, as a result of the large spin reduction, it is now possible to study the suppression of quantum spin fluctuations (correspondingly, a decrease of the reduction) by an external magnetic field. Several recently published theoretical works are devoted to this question.<sup>6,10,12,13</sup> It was possible to explain some features of the field dependences of the magnetization in these substances by the mechanism of suppression of quantum fluctuations: the weak nonlinearity of the increase in magnetization in magnetic fields perpendicular to the plane of the triangle and the magnetization anisotropy above the reorientational phase transition.<sup>6,12</sup> The increase, associated with suppression of quantum fluctuations, of the average spin of the magnetic ions, which was found to be fully measurable<sup>6,13</sup> even in fields  $H < 0.1 H_E$ , was calculated.

On this basis, we undertook an investigation of  $\text{Mn}^{55}$  NMR in these substances. This makes it possible to measure directly the values and field dependences of the microscopic magnetic moments of  $\text{Mn}^{2+}$  ions.

All three substances (CsMnBr<sub>3</sub>, CsMnI<sub>3</sub>, RbMnBr<sub>3</sub>) possess a closely similar crystal structure.<sup>14</sup> The  $\text{Mn}^{2+}$  ions are surrounded by octahedra of halogen atoms, and these octahedra, joined at a common face, form chains along the  $C_6$  axis. These chains are packed hexagonally in the basal plane of the crystal, and the voids thus arising are filled with alkali-metal atoms. The unit cells in CsMnBr<sub>3</sub> and CsMnI<sub>3</sub> contain two formula units and possesses  $D_{6h}^4$  symmetry. All  $\text{Mn}^{2+}$  ions are crystallographically equivalent.<sup>d)</sup> The distance between neighboring  $\text{Mn}^{2+}$  ions along the chains is approximately half the distance between neighbors in the plane. Correspondingly, the value of the exchange

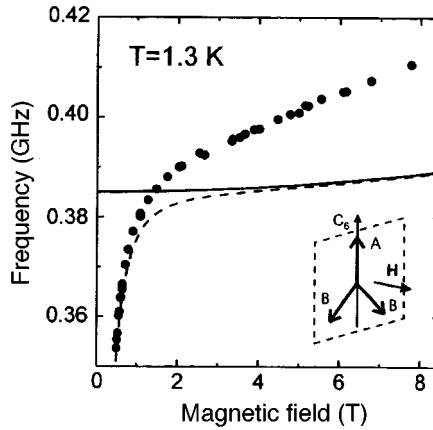


FIG. 1.  $\text{Mn}^{55}$  NMR spectrum of  $\text{CsMnI}_3$  at  $T=1.3$  K and with  $\mathbf{H} \perp C_6$ . Solid line — “unshifted” NMR spectrum with  $H_n = \text{const}$ ; dashed line — allowance for the DFS of NMR. Inset: Arrangement of  $\text{Mn}^{2+}$  spins with  $\mathbf{H} \perp C_6$ .

integral  $J$  between them is several hundreds of times larger. Nonetheless, magnetic ordering with  $T_N \approx 10$  K arises on account of interchain exchange  $J'$ . The Mn spins in the chains are ordered antiferromagnetically and the mutual polarization of the chains is determined by  $J'$  and the anisotropy. Triangular ordering occurs in all substances — in weak fields the spins of neighboring ions in the plane lie on the sides of isosceles triangles (in  $\text{RbMnBr}_3$  in fields  $H > 3$  T).

The NMR of  $\text{Mn}^{55}$  was measured at temperatures 1.3–4.2 K with a cw NMR spectrometer, similar to the one employed in Ref. 15, in the frequency range 200–450 MHz and in magnetic fields 0.5–8 T. All measurements were performed on single-crystalline samples, placed in a helium bath and oriented so that the external and high-frequency magnetic fields were mutually perpendicular and lay in the basal plane. As a rule, the absorption line was recorded by scanning the magnetic field. Preliminary results on NMR in  $\text{CsMnBr}_3$  were published in Ref. 4; a more complete article is published in Ref. 16.

The anisotropy in  $\text{CsMnI}_3$  is of the easy-axis type. For this reason, the triangles of  $\text{Mn}^{2+}$  spins lie in a plane passing through the  $C_6$  axis. When a magnetic field perpendicular to the  $C_6$  axis is switched on, the planes of the triangles rotate so that the spins are perpendicular to  $\mathbf{H}$ . The  $\text{Mn}^{55}$  NMR spectrum is presented in Fig. 1. To a first approximation, it should be described by the formula

$$\frac{\omega_n}{\gamma_n} = |\mathbf{H}_n + \mathbf{H}| = H_n \left[ 1 + \frac{H^2}{H_n^2} \left( 1 - \frac{2H_n}{H_E} \right) \right]^{1/2}. \quad (2)$$

Here  $H_E$  is the exchange field and  $H$  is the external magnetic field. We took account of the fact that the  $\text{Mn}^{2+}$  spins are tilted with respect to the external field by the small angle  $\sim H/H_E$  ( $H_E \approx 140$  T). This dependence with  $H_n = \text{const}$  is presented in Fig. 1 (solid line).

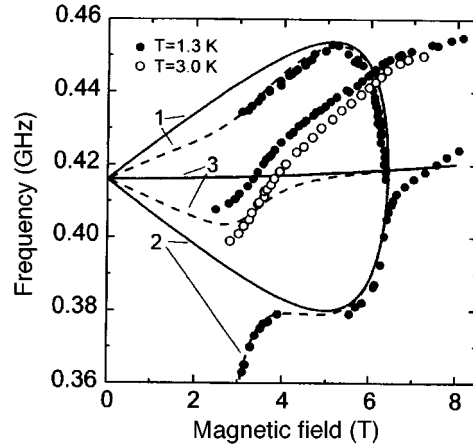


FIG. 2.  $\text{Mn}^{55}$  NMR spectrum of  $\text{CsMnBr}_3$  with  $\mathbf{H} \parallel C_6$ ,  $T = 1.3 \text{ K}$  ( $\bullet$ ),  $T = 3.0 \text{ K}$  ( $\circ$ ) (only the middle branch is shown). Solid line — ‘‘unshifted’’ NMR spectrum with  $H_n = \text{const}$ ; dashed line — allowance for DFS of NMR.

In weak fields the spectrum is deformed by the interaction with the Goldstone branch of the AFMR (so-called dynamic frequency shift (DFS) of NMR). The NMR spectrum under the condition  $\omega_n^2 \ll \omega_e^2$  is described well by the expression<sup>17</sup>

$$\frac{\omega_n^2}{\gamma_n^2} = H_n^2 \left( 1 + \frac{\omega_T^2}{\omega_e^2} \right)^{-1}. \quad (3)$$

Here  $\omega_e$  is the unshifted AFMR frequency and  $\omega_T$  is the coupling frequency. The frequencies  $\omega_e$  and  $\omega_T$  were taken from the AFMR data presented in Ref. 9. Although Eq. (3) was introduced for two-sublattice AFs, the calculation performed in Ref. 9 showed that for  $\text{CsMnI}_3$  it holds up to terms  $\approx 10^{-5} H_n^2$ . However, in strong fields, where the DFS is negligibly small, a substantial increase of the NMR frequency is observed. This increase can be interpreted, in accordance with Eq. (2), as an increase in the hyperfine field. The field dependence  $H_n(H)$  obtained is presented in Fig. 3 (see below).

In  $\text{CsMnBr}_3$  the spins lie in the basal plane. When an external field is applied, the spins become oriented in a manner so that the field lies in the direction of the bisector of the triangle on whose sides the spins lie. As the field increases, the angles at the base of the triangle start to decrease as<sup>18</sup>

$$\cos(\alpha) = \frac{1}{2 - H^2/H_C^2}, \quad (4)$$

where  $H_C = 6.4 \text{ T}$  is the reorientational phase transition field. A collinear structure consisting of antiferromagnetically ordered ferrimagnetic planes (with spin ratio 2:1) arises above the transition. To within the tilt angles  $\sim H/H_E$  ( $H_E \approx 150 \text{ T}$ ), all spins are perpendicular to the magnetic field.

The NMR spectrum in  $\text{CsMnBr}_3$  is presented in Fig. 2. It consists of three branches,

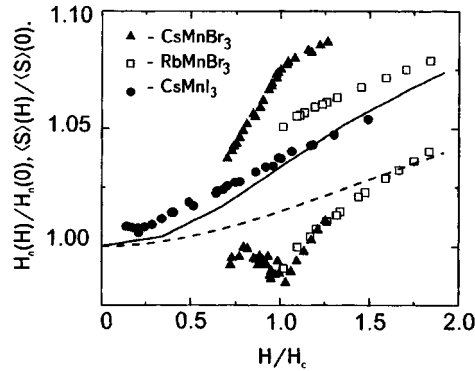


FIG. 3. Field dependences of the hyperfine field at  $\text{Mn}^{55}$  nuclei with  $\mathbf{H} \perp C_6$ ,  $T = 1.3$  K in  $\text{CsMnBr}_3$  ( $\Delta$ ),  $\text{RbMnBr}_3$  ( $\square$ ), and  $\text{CsMnI}_3$  ( $\bullet$ ). Dashed line —  $\langle S \rangle(H/H_C)$  in  $\text{CsMnBr}_3$  with  $\mathbf{H} \parallel C_6$ ;<sup>6</sup> solid line —  $\langle S \rangle(H/H_C)$  for  $\text{CsMnI}_3$  with  $\mathbf{H} \perp C_6$ .<sup>13</sup>

corresponding to different relative arrangements of the hyperfine and external fields,

$$\frac{\omega_{1,2}}{\gamma_n} = H_n \left[ 1 + \frac{H^2}{H_n^2} + 2 \frac{H}{H_n} \left( \pm \sin(\alpha) - \frac{H}{H_E} \cos^2(\alpha) \right) \right]^{1/2}, \quad (5)$$

$$\frac{\omega_3}{\gamma_n} = H_n \left[ 1 + \frac{H^2}{H_n^2} \left( 1 - \frac{2H_n}{H_E} \right) \right]^{1/2}, \quad (6)$$

for  $H > H_C$  and constant  $H_n$  a single branch, described by Eq. (6) (solid curve 3 in Fig. 2), remains. The dashed lines indicate the NMR spectrum with allowance for the DFS, calculated in Ref. 16. One can see that up to  $H_C$  the branches 1 and 2 agree satisfactorily with the calculation, while the frequency of the branch perpendicular to the magnetic field increases with field similarly to  $\text{CsMnI}_3$ . Above  $H_C$  the increase in the frequency of this branch slows down, though appreciable growth of the bottom branch is observed for spins which in weak fields comprised the lateral faces of the triangle. The corresponding field dependences  $H_n(H)$  are presented in Fig. 3. This figure also shows the dependences  $H_n(H)$  on  $\text{Mn}^{55}$  nuclei for the collinear phase of  $\text{RbMnBr}_3$  in fields  $H > H_C \approx 4$  T. This is also an easy-plane AF, in which a complicated spin structure, incommensurate with the lattice, is realized in weak fields, but in  $H \approx 3$  T it transforms into a commensurate phase with triangular spin ordering and subsequently behaves just as in  $\text{CsMnBr}_3$ .<sup>11</sup> One can see that similarly to  $\text{CsMnBr}_3$  the nonequivalent  $\text{Mn}^{2+}$  spins in the magnetic plane are characterized by different values of  $H_n$ , which depend quite strongly on the external field.

In summary, strong growth of the hyperfine field on  $\text{Mn}^{55}$  nuclei is observed in all three materials with the application of an external magnetic field. This dependence is different for magnetically nonequivalent ions and leads to splitting of the NMR in the collinear magnetic phase. Such a growth cannot be explained by a change in the hyperfine constant of the ion itself on account of magnetostriction, since the orbital contribution to it  $A_L \sim (g-2) \approx 0.004$  is very small ( $g$  is the  $g$  factor of the ion) and the contri-

bution due to core polarization depends extremely weakly on the distance up to the ligands.<sup>19</sup> The well-known instability arising in the crystal structure of these compounds as a result of the shift in the neighboring octahedral chains relative to the  $C_6$  axis also has a weak effect on the hyperfine constant, since it does not change the nearest neighbor environment of the magnetic ions. The nature of the contribution of the indirect hyperfine interaction of neighboring magnetic ions is close to that of the exchange interaction. For this reason, the change in  $A$  due to reorientation of neighboring Mn spins in the plane should be  $J'/J$  times less than the correction calculated in Ref. 2. For this reason, it can be asserted that the change in the average spins  $\langle S \rangle$  of the  $\text{Mn}^{2+}$  ions makes the main contribution to the change in the hyperfine fields.

Thermal fluctuations of the spins also make a definite contribution to  $\langle S \rangle$ . However, they are small at temperatures  $T \approx 1.3$  K. According to our data on the temperature dependence of  $H_n$  in  $\text{CsMnBr}_3$  at  $H=0$ ,  $\langle S \rangle(0) - \langle S \rangle(1.3 \text{ K}) \leq 0.01 \langle S \rangle(0)$  (Ref. 16). Moreover, temperature fluctuations become frozen out when  $\hbar \omega_e(H) > kT$ , i.e., in comparatively weak magnetic fields. The field dependence of the frequency of the middle branch of  $\text{Mn}^{55}$  NMR in  $\text{CsMnBr}_3$  at  $T \approx 3$  K is presented in Fig. 2. One can see that it is appreciably steeper in weak fields, and for  $H > 6.0$  T the temperature correction becomes very small.

It is difficult to make a quantitative comparison between our results and the theory of the suppression of quantum fluctuations, since no calculations have been performed for our experimental situation. The dashed curve in Fig. 3 shows the dependence  $\langle S \rangle \times (H/H_C)$  calculated in Ref. 6 for  $\text{CsMnBr}_3$  but with  $\mathbf{H} \parallel C_6$  (in this geometry all  $\text{Mn}^{2+}$  spins are equivalent and there is no splitting). The solid curve shows the  $\langle S \rangle (H/H_C)$  ( $\mathbf{H} \perp C_6$ ) for  $\text{CsNiCl}_3$  (analog of  $\text{CsMnI}_3$ ) from Ref. 13. One can see that the increase in magnetization of the sublattices corresponds in order of magnitude to our experiment.

In Ref. 10, it was pointed out that in quasi-one-dimensional AFs with easy-axis anisotropy the magnetic ions are nonequivalent even in the absence of an external field, since only one third of them are oriented parallel to the easy axis  $C_6$  (spins  $A$ ) and the remaining spins are tilted from the axis by an angle  $\sim 50^\circ$  (spins  $B$ ) (see inset in Fig. 1). In consequence the average spins are different, the difference  $\langle S_A \rangle - \langle S_B \rangle \approx 0.2$  for  $\text{CsMnI}_3$ . The corresponding splitting of  $\text{Mn}^{55}$  NMR  $\approx 50$  MHz is close in order of magnitude to the splitting we observed in  $\text{CsMnBr}_3$  and  $\text{RbMnBr}_3$ . Unfortunately, the NMR line corresponding to  $A$  spins in  $\text{CsMnI}_3$  is very weak and we could not detect it.<sup>e)</sup>

In summary, we have measured the field dependences of the average spins of  $\text{Mn}^{2+}$  ions in quasi-one-dimensional AFs  $\text{CsMnI}_3$ ,  $\text{CsMnBr}_3$ , and  $\text{RbMnBr}_3$ . These dependences were found to be not only strong enough to be observed by the NMR method but also different for magnetically nonequivalent  $\text{Mn}^{2+}$  ions. The results obtained are in qualitative agreement with the theory.<sup>6,10,13</sup>

In closing, we wish to express our heartfelt gratitude to I. A. Zaliznyak, M. I. Kurkin, L. A. Prozorov, S. S. Sosin, and I. A. Fomin for fruitful discussions. We wish to thank especially A. I. Smirnov, whose helpful remarks were taken into account in the final variant of the manuscript.

This work was supported in part by Grant 95-02-04555-a from the Russian Fund for Fundamental Research and Grant RP1-207 from the U. S. Civilian Research and Devel-

opment Foundation for the Independent States of the former Soviet Union (CRDF). A. M. Tikhonov also thanks Forschungszentrum Jülich GmbH.

<sup>a)</sup>Deceased.

<sup>b)</sup>The reduction in AFs with spin 1/2 should be much greater, but experiments with such ions ( $\text{Cu}^{2+}$ ) are difficult to interpret because of the difficulty of taking into account accurately the effect of the large orbital magnetic moment  $L=2$ . For this reason, in what follows, we shall discuss substances with  $\text{Mn}^{2+}$  ions ( ${}^6S_{5/2}$  state).

<sup>c)</sup>The magnetic properties of these compounds are discussed in greater detail in Ref. 11.

<sup>d)</sup>The structure in  $\text{RbMnBr}_3$  is more complicated because of orthorhombic distortions.<sup>11</sup>

<sup>e)</sup>While this paper was being prepared for publication, we observed this NMR branch. Its frequency in the absence of a magnetic field equals 417 MHz.

---

<sup>1</sup>P. W. Anderson, Phys. Rev. Lett. **86**, 694 (1952).

<sup>2</sup>J. Owen and D. R. Taylor, Phys. Rev. Lett. **16**, 1164 (1966); Nai Li Huang, R. Orbach, and E. Simanek, Phys. Rev. Lett. **17**, 134 (1966).

<sup>3</sup>M. Eibshutz, R. C. Sherwood, F. S. L. Hsu, and D. E. Cox, AIP Conf. Proc. **17**, 864 (1972).

<sup>4</sup>A. S. Borovik-Romanov, B. S. Dumesh, S. V. Petrov, and A. M. Tikhonov, JETP Lett. **64**, 225 (1996).

<sup>5</sup>S. I. Abarzhi, A. N. Bazhan, L. A. Prozorova, and I. A. Zaliznyak, J. Phys.: Condens. Matter **4**, 3307 (1992).

<sup>6</sup>M. Zhitomirskiĭ and I. Zaliznyak, Phys. Rev. B **53**, 3428 (1996).

<sup>7</sup>C. J. Glinka, V. J. Minkiewicz, D. E. Cox, and C. P. Khattak, in *Magnetism and Magnetic Materials*, 1972 (Denver), edited by C. D. Graham and J. J. Rhyne, AIP Conf. Proc. No. 10, AIP, New York, 1973, p. 659.

<sup>8</sup>H. W. Zandbergen, J. Solid State Chem. **35**, 367 (1980).

<sup>9</sup>L. A. Prozorova, S. S. Sosin, D. V. Efremov, and S. V. Petrov, Zh. Éksp. Teor. Fiz. **112**, 11 (1997) [*sic*].

<sup>10</sup>Y. Watabe, T. Suzuki, and Y. Natsume, Phys. Rev. B **52**, 3400 (1995).

<sup>11</sup>M. Zhitomirsky, O. Petrenko, and L. Prozorova, Phys. Rev. B **52**, 3511 (1995).

<sup>12</sup>A. G. Abanov and O. A. Petrenko, Phys. Rev. B **50**, 6271 (1994); P. Santini, G. Fáth, Z. Domański, and P. Erds, Phys. Rev. B **56**, 5373 (1997).

<sup>13</sup>T. Ohyama and Hiroyuki Shiba, J. Phys. Soc. Jpn. **63**, 3454 (1994).

<sup>14</sup>K. S. Aleksandrov, N. F. Fedoseev, and I. P. Spevakova, *Magnetic Phase Transitions in Halide Crystals* [in Russian], Nauka, Novosibirsk, 1983.

<sup>15</sup>B. S. Dumsh, Prib. Tekh. Éksp., No. 1, 135 (1986).

<sup>16</sup>A. S. Borovik-Romanov, B. S. Dumesh, S. V. Petrov, and A. M. Tikhonov, Zh. Éksp. Teor. Fiz. **113**, No. 1–2 (1998) [JETP **86**, No. 1–2 (1998)] (in press).

<sup>17</sup>E. A. Turov and M. P. Petrov, *Nuclear Magnetic Resonance in Ferro- and Antiferromagnets*, Halsted Press, New York, 1972 [Russian original, Nauka, Moscow, 1963].

<sup>18</sup>A. V. Chubukov, J. Phys. C: Solid State Phys. **21**, L441 (1988).

<sup>19</sup>S. Ogava, J. Phys. Soc. Jpn. **15**, 1475 (1960); S. Geschwind, in *Hyperfine Interaction*, edited by A. J. Freeman, Academic Press, N. Y., 1967, No. 9, p. 103.

Translated by M. E. Alferieff

## Charged and neutral excitonic complexes in GaAs/AlGaAs quantum wells

O. V. Volkov,<sup>a)</sup> V. E. Zhitomirskiĭ, I. V. Kukushkin, and V. E. Bisti

*Institute of Solid-State Physics, Russian Academy of Sciences, 142432 Chernogolovka, Moscow Region, Russia*

K. von Klitzing and K. Eberl

*Max-Planck-Institut für Festkörperforschung, 70569 Stuttgart, Germany*

(Submitted 5 November 1997)

*Pis'ma Zh. Éksp. Teor. Fiz.* **66**, No. 11, 730–735 (10 December 1997)

The temperature and magnetic-field dependences of the recombination line of multiparticle excitonic complexes in undoped and lightly doped GaAs/AlGaAs quantum wells are investigated. These dependences have previously been attributed to free charged excitons (trions). It is shown that this line corresponds to a bound state of a complex, specifically, to an exciton bound on a neutral donor in a barrier. It is found that as the temperature or pump power is raised, there appear in the recombination spectrum not only a cyclotron replica shifted downward in energy but also a replica which is symmetrically shifted upwards in energy by an amount equal to the cyclotron energy and which is due to emission from an excited state of an impurity complex. The behavior of the cyclotron replicas is studied as a function of the electron density and temperature. © 1997 American Institute of Physics.

[S0021-3640(97)01223-1]

PACS numbers: 71.35.Cc, 78.66.Fd

1. Excitonic complexes play an important role in undoped and lightly doped quasi-two-dimensional (2D) systems. Moreover, they are extremely interesting from the standpoint of studying the role of the Coulomb interaction in a system consisting of several electrons. An example of such complexes are charged excitons or trions. Positively and negatively charged excitons were predicted theoretically in Ref. 1. These formations ( $X^-$  and  $X^+$ ) are similar to the hydrogen ions  $H^-$  and  $H_2^+$  and have a very low energy of dissociation into an exciton and a free particle. Charged excitons in the three-dimensional (3D) case have never been reliably established, and no spectroscopically resolved line of such complexes has ever been observed. In a 2D system, both excitons and trions have a high binding energy and are accordingly highly stable, since the limitation of the motion of the charge in the transverse direction has the effect of an increase in the Coulomb interaction. The presence of a second electron is responsible for some specific properties of such a system, specifically, a negative diamagnetic shift of the recombination line in a weak magnetic field and the existence of a cyclotron replica due to the transfer of a quantum of cyclotron energy to the second electron in the process of electron-hole recombination. A number of authors claim to have discovered a free trion and assigned to it the emission line in the luminescence spectra of quantum wells.<sup>2</sup> Nonetheless, the

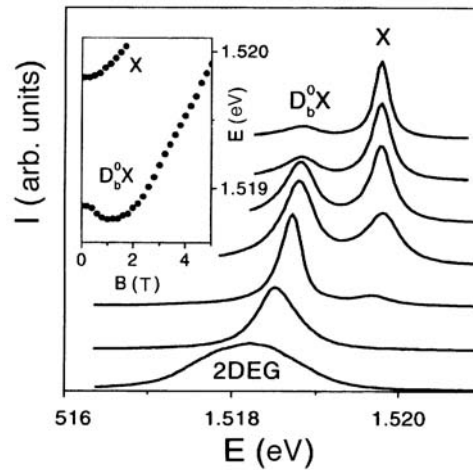


FIG. 1. Photoluminescence spectra obtained for a lightly doped 300 Å SQW with 2D-electron density varying from 0 to  $5 \times 10^{10} \text{ cm}^{-2}$ . Inset: Recombination energy of a free exciton and an excitonic complex versus magnetic field, measured with zero 2D-electron density.

proofs presented in Refs. 2–4 in favor of such an interpretation are ambiguous and there are a number of discrepancies with the theoretical predictions, for example, in the experimentally obtained temperature and magnetic-field dependences of the emission spectrum of a free trion. To resolve this question, we investigated several undoped and lightly doped GaAs/AlGaAs single quantum wells (SQWs) with widths of 150, 200, and 300 Å. We show on the basis of the temperature and magnetic field dependences of the luminescence spectra that the recombination line attributed to free triions most likely corresponds to the radiation of an exciton bound on a neutral donor in a barrier.

2. We investigated 150 and 200 Å wide undoped SQWs and a 300 Å (800 Å spacer) lightly doped SQW. The samples were grown by molecular-beam epitaxy on a GaAs substrate (see Ref. 5). Optical excitation of the system was performed with a tunable Ti/Sp laser and/or He/Ne laser. A Ramanor U-1000 double monochromator (which, when combined with a CCD detector, provided a resolution of 0.03 meV) served as a spectrometer.

3. The photoluminescence spectra obtained for a lightly doped 300 Å SQW with different 2D-electron densities are shown in Fig. 1. The electron density was changed by varying the intensity of the He/Ne laser illumination, giving rise to neutralization of the charge of the impurities in the doping layer by photoexcited carriers. With a zero 2D-electron density (top spectrum) the recombination line of a free heavy-hole exciton (X) dominates the spectrum (similar spectra were also obtained for undoped samples). As the 2D-electron density increases, a low-energy line due to recombination of an excitonic complex (designated as  $D_b^0X$ ) starts to buildup in the emission spectrum. This line was attributed in Refs. 2 and 3 to recombination of a free trion. At some 2D-electron density the free-exciton line vanishes completely from the spectra; this is accompanied by a metal–insulator transition in the electronic system. Further increase of the 2D-electron

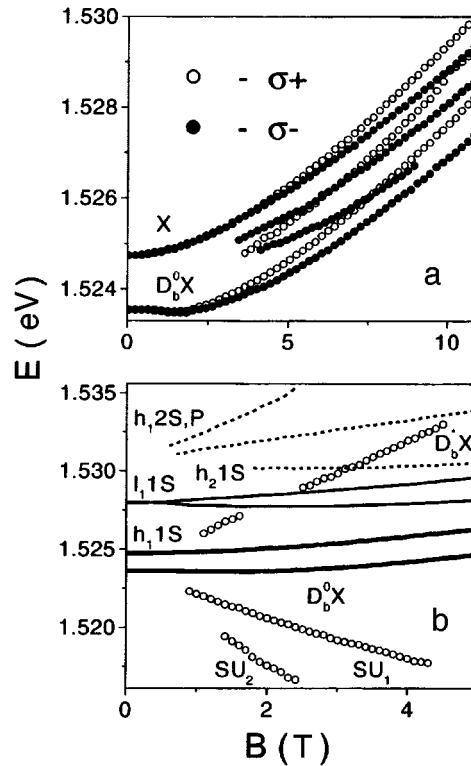


FIG. 2. (a) Spectral position of recombination lines of free and bound excitons versus magnetic field, measured in two polarizations for a 200 Å SQW. (b) Diagram of optical transitions for the same sample. Recombination lines of free and bound excitons (solid lines), cyclotron replicas (dots), and recombination lines of excited excitonic states (dashed lines) are shown.

density results in broadening of the low-energy line and transformation of this line into a recombination line of the 2D-electron gas, the latter line splitting in a perpendicular magnetic field into Landau levels. So, at a density corresponding to the bottom spectrum well-resolved Landau levels are observed even in a magnetic field of 0.25 T (filling factor equals 8), indicating that the experimental structure is of high quality. At this density the mobility of the 2D-electrons equals  $2.6 \times 10^6 \text{ cm}^2/\text{V} \cdot \text{s}$ .

To determine the nature of the low-energy line at low 2D-electron densities (before the transition into the metallic state), we studied the magnetic-field dependence of the spectral position of the excitonic lines. Such a dependence, measured in two circular polarizations for a 200 Å SQW, is presented in Fig. 2a. We obtained similar results with identical polarization and spectral features for a 150 Å SQW and a lightly doped 300 Å SQW (inset in Fig. 1). They are completely identical to the results obtained by other authors<sup>2,3</sup> and employed by them as proof of the trionic nature of the  $D_b^0 X$  line. A characteristic feature of this line is the negative diamagnetic shift, observed in a weak magnetic field. This shift is explained<sup>4</sup> by the fact that in weak magnetic fields the internal energy of a trion is virtually field-independent, and the energy of the transition

corresponding to recombination of the trion is determined by the difference of the cyclotron energy of the entire complex and the free electron remaining after recombination. Since the electron mass is much smaller than the trion mass, the transition energy in weak magnetic fields should undergo a negative cyclotron shift of the order of  $\frac{1}{2}\hbar\omega_c$ . A similar dependence is also observed in our experiment (see Fig. 2a and inset in Fig. 1), but the magnitude of the shift is much less than  $\frac{1}{2}\hbar\omega_c$ , and it is absent completely in fields weaker than 0.5 T. This behavior can be explained by localization of a trion on a charged donor center, as one would naturally expect for a heavy charged particle at low densities and low temperatures.

To check this conjecture, we studied the temperature dependence of the shape of the recombination line of the excitonic complex. On account of recoil, the existence of a second electron in a free trion allows recombination of a complex possessing a nonzero total quasimomentum  $k$  (which is forbidden for a direct-band exciton). The energy of the emitted photon is less by the amount  $\Delta E = E(k)[M/m_e - 1]$ , where  $E(k)$  is the trion kinetic energy,  $M$  is the trion mass, and  $m_e$  is the mass of the electron remaining after recombination. Substituting  $M \approx 2m_e + m_h$ , where  $m_h$  is the hole mass, we obtain  $\Delta E = E(k)[m_h/m_e + 1]$ . Since  $m_h > m_e$ , we obtain  $\Delta E > 2E(k)$ . Therefore the recombination line of a free trion should be asymmetrically broadened on the low-energy edge at least by the amount  $2k_bT$ . This conclusion directly contradicts the experimental results. Figure 3a shows the orthonormalized recombination spectra of a complex which were measured at three different temperatures in zero magnetic field for a 200 Å SQW. As one can see from the figure, the line has a symmetric shape and its width is virtually temperature-independent in the range 1.5–10 K. In accordance with the estimate presented above, the width of the recombination line for a 10 K bath corresponds to an effective trion temperature of not greater than 2 K, which can be explained only by localization of the complex. Figure 3b shows our computational results for the shape of the recombination line of a free trion for 2D-electron gas density  $5 \times 10^{10} \text{ cm}^{-2}$ . Comparing Figs. 3a and 3b demonstrates that the free-trion model is completely untenable in the explanation of the experimentally observed temperature dependence. This fact confirms the conjecture that the investigated recombination line corresponds to the state of a complex localized on an impurity center. In this case, quasimomentum conservation is not required in the recombination of a bound exciton; this is why the width of the luminescence line is small. It should be noted that increasing the temperature does not result in the appearance of free trions, since an additional wide temperature-sensitive line does not arise in the emission spectrum, attesting against trion localization by distant charged donors.

Thus, it is logical to conjecture that the low-energy excitonic line corresponds to recombination of a trion localized on a charged donor in a barrier (most likely, near a heterointerface), since the density of residual doping with donors is relatively high in the AlGaAs spacer. However, such an electron–hole complex is nothing more than an exciton bound on a neutral donor located in a barrier near a well. We note that the spectral splittings of the line in a magnetic field (including the triplet state) and their polarization properties are virtually identical for a free trion and for a trion localized on a positively charged donor (in other words, for an exciton bound on a neutral donor), since the presence of an impurity center does not change optical transitions. The second electron,

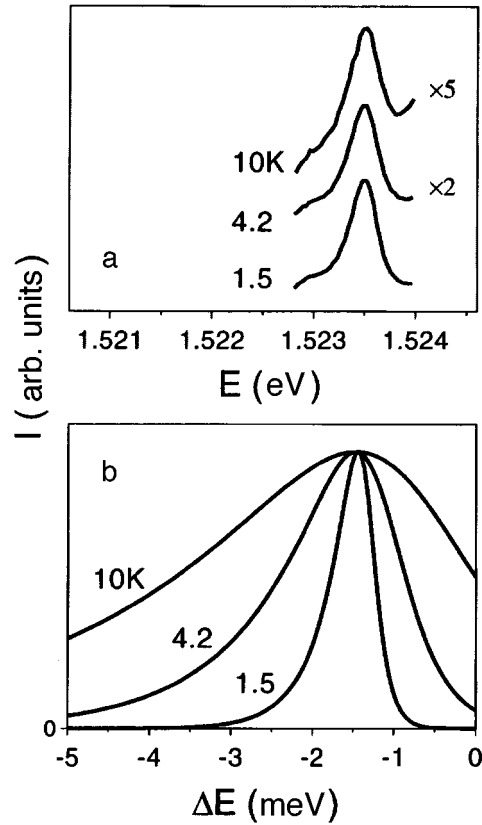


FIG. 3. (a) Orthonormalized recombination spectra of an excitonic complex ( $D_b^0X$  line), measured in 200 Å SQW at different temperatures. (b) Temperature dependence of the shape of the emission line of a free trion in the presence of a 2D-electron gas with density  $5 \times 10^{10} \text{ cm}^{-2}$ , calculated for the same temperatures.

which is responsible for neutralization of the donor, in the  $D_b^0X$  complex determines the properties of the complex, which are analogous to properties of the recombination line of a free trion, specifically, a negative diamagnetic shift and the appearance of cyclotron replicas ( $SU$ ) in a magnetic field. The appearance of replicas is explained by the fact that if in the recombination of a system with two electrons the remaining electron acquires one or several cyclotron energy quanta, then the recombination line is shifted to lower energies by one or several  $\hbar \omega_c$ .<sup>4</sup> We observed such replicas on all experimental samples; for 200 Å SQW they are shown in Fig. 2b. It should be underscored that the character of the magnetic field dependence of the spectral position of these replicas and the diamagnetic shift of the recombination line itself of the complex should depend strongly on the position of the impurity center — in a well or in a barrier. It is known that the ground state of an impurity complex in a 3D semiconductor has a  $1S$ -type wave function. The appearance of replicas (dielectronic satellites), including cyclotron transitions, in the process of recombination of a complex  $D^0X$  is due to excitation of the  $2P$  state of the impurity, so that they are shifted downwards by the transition energy of the donor into an

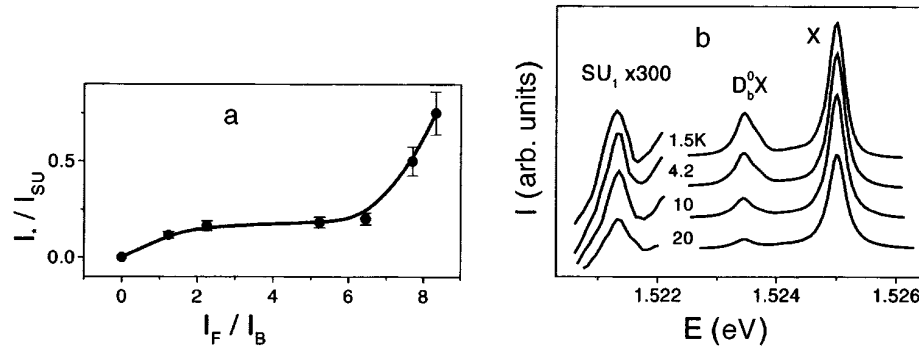


FIG. 4. (a) Ratio of the intensities of the top and bottom (in energy) cyclotron replicas versus the ratio of the intensities of free and bound exciton lines, measured with variation of the 2D-electron density in a lightly doped 300 Å SQW. (b) Recombination spectra of a free exciton and an excitonic complex as well as a  $SU_1$  replica, measured at different temperatures in a magnetic field of 1.5 T for 200 Å SQW.

excited state.<sup>6</sup> The absence of such a shift in our case could be due to breakdown of the symmetry of the complex as a result of the fact that the impurity center is located in a barrier next to a well. The ground state of the impurity center has a  $P$ -type wave function<sup>7,8</sup> and the splitting between the ground and excited states is almost zero.<sup>9</sup> Under these conditions the energy shift of the cyclotron replicas in the zero magnetic field limit should also be close to zero, as is observed experimentally. The interpretation of the excitonic complex as an exciton localized on a neutral donor in a barrier is also confirmed by comparing with the recombination spectra obtained in Ref. 10 for the complex  $D^0X$  under conditions of  $\delta$ -doping of the barrier material. These spectra show detailed similarity with our spectra.

The recombination spectra which we measured at high temperature ( $\sim 10$  K) or high pump power ( $\sim 1$  W/cm<sup>2</sup>), together with the cyclotron replicas shifted downward in energy, demonstrate the appearance of a replica symmetrically shifted upwards in energy by  $\hbar\omega_c$  (Fig. 2b). This replica is evidently associated with recombination of the excited state of the excitonic complex (designated by  $D_b^*X$ ), since the lines associated with recombination of the excited states of the excitons are strongly shifted upwards in energy. These lines are shown in Fig. 2b by the dashed line. Their spectral position depends on the well width and is in good agreement with the theoretical calculations.<sup>11</sup> As the 2D-electron density increases, the intensity of the top cyclotron replica decreases, and after the system passes into the metallic state the replica completely vanishes from the spectra, while the bottom cyclotron replicas ( $SU$ ) decrease only somewhat in intensity and become wider. Figure 4a shows the dependence of the ratio of the intensities of the top and bottom cyclotron replicas ( $D_b^*X$  and  $SU_1$ ) on the 2D-electron density; here the ratio of the intensities of the recombination lines of a free exciton ( $I_{Fr}$ ) and an excitonic complex ( $I_B$ ) is used as the parameter characterizing the density. Vanishing of the top cyclotron replica at a transition of the system into the metallic state ( $I_{Fr}/I_B=0$ ) confirms the conjecture that the complex is localized in an external Coulomb potential. The fact that the bottom cyclotron replicas remain as the 2D-electron density increases attests to the fact that complete localization of the system does not necessarily occur for them. For

example, the same mechanism leading to the appearance of replicas can also work for a degenerate 2D-electron gas regime with a collision of a free exciton with an electron localized in an external Coulomb potential. This conjecture is also confirmed by the temperature dependence of the spectra of the cyclotron replica ( $SU_1$ ) shown in Fig. 4b together with the spectra of the main excitonic lines. As one can see from the figure, the intensity of the cyclotron replica decreases with increasing temperature much less than does the intensity of the recombination line of the excitonic complex.

**4.** In summary, we have shown on the basis of an investigation of the temperature and magnetic-field dependences of a recombination line of multiparticle excitonic complexes in undoped and lightly doped GaAs/AlGaAs quantum wells that this line corresponds to a bound state of a complex, specifically, an exciton bound on a neutral donor in a barrier, and not a free trion, as previously assumed.

This work was supported under the program ‘‘Physics of Solid-State Nanostructures’’ (Grant 1-062/3) and by the Volkswagen Foundation.

<sup>a)</sup>e-mail: volkov@issp.ac.ru

---

<sup>1</sup>M. A. Lampert, Phys. Rev. Lett. **1**, 450 (1958).

<sup>2</sup>A. J. Shields, M. Pepper, D. A. Ritchie, and M. Y. Simmons, Adv. Phys. **44**, 47 (1995).

<sup>3</sup>G. Finkelstein, H. Shtrikman, and I. Bar-Joseph, Phys. Rev. B **53**, 1709 (1996).

<sup>4</sup>G. Finkelstein, H. Shtrikman, and I. Bar-Joseph, Phys. Rev. B **53**, 12593 (1996).

<sup>5</sup>O. V. Volkov, V. E. Zhitomirskii, I. V. Kukushkin *et al.*, JETP Lett. **65**, 38 (1997).

<sup>6</sup>J. Rorison, D. C. Herbert, P. J. Dean and M. S. Skolnik, J. Phys. C **17**, 6435 (1984).

<sup>7</sup>J. Levine, Phys. Rev. A **140**, 586 (1965).

<sup>8</sup>G. Bastard, Phys. Rev. B **24**, 4714 (1981).

<sup>9</sup>J. M. Shi, F. M. Peeters, G. Q. Hai, and J. T. Devreese, Phys. Rev. B **44**, 5692 (1991).

<sup>10</sup>D. C. Reynolds, C. E. Leak, K. K. Bajaj *et al.*, Phys. Rev. B **40**, 6210 (1989).

<sup>11</sup>G. E. W. Bauer and T. Ando, Phys. Rev. B **38**, 6015 (1988).

Translated by M. E. Alferieff

# Coherent-states quantum cryptography based on a quantum comparator

S. N. Molotkov

*Institute of Solid-State Physics, Russian Academy of Sciences, 142432 Chernogolovka, Moscow Region, Russia*

(Submitted 16 September 1997; resubmitted 28 October 1997)

*Pis'ma Zh. Éksp. Teor. Fiz.* **66**, No. 11, 736–741 (10 December 1997)

A quantum cryptosystem based on comparing an input signal from a communication channel with a reference state prepared at the receiving end is proposed. © 1997 American Institute of Physics.

[S0021-3640(97)01323-6]

PACS numbers: 03.65.-w, 89.70.+c

Quantum cryptosystems as information carriers employ quantum states. The secrecy of the key in quantum cryptography is based on two facts — the prohibition of cloning (ideal copying) of a previously unknown quantum state<sup>1</sup> and the impossibility of obtaining any information about the states without perturbing them, if they are nonorthogonal.<sup>2</sup> The protocol for distribution of the key must be set up so that measurements by authorized users would permit detection of any attempts at eavesdropping.

The idea of the proposed quantum cryptosystem is based on comparing a state entering from the communication channel with a reference state prepared at the receiving end. A quantum cryptosystem based on two coherent states (one high-intensity reference state and a weak information state) was discussed in Ref. 3. A substantial difference between the proposed system and the scheme described in Ref. 3 is that the present protocol employs explicitly the circumstance that a beam splitter converts coherent radiation into coherent radiation.

Everywhere below, the communication channel is assumed to be ideal.

Let us consider a 50/50 optical beam splitter (Fig. 1). Let two states of a field in a coherent state enter the beam splitter. The coherent state of the field describes radiation at the output of an ideal laser.<sup>4</sup> The state at the input of the beam splitter is represented as

$$|\psi\rangle_{\text{in}} = |\alpha\rangle_{\text{in},a} \otimes |\beta\rangle_{\text{in},b}, \quad \hat{\rho}_{\text{in}} = |\psi\rangle_{\text{in}} \langle\psi|, \quad (1)$$

where  $|\alpha\rangle_{\text{in}}$  and  $|\beta\rangle_{\text{in}}$  are coherent states at the input of the optical beam splitter. By definition of the latter states we have

$$|\alpha\rangle_{\text{in}} = \hat{D}(\hat{a}_{\text{in}})|0\rangle_{\text{in}}, \quad \hat{D}(\hat{a}_{\text{in}}) = \exp(\alpha\hat{a}_{\text{in}}^+ - \alpha^*\hat{a}_{\text{in}}), \quad (2)$$

where  $\hat{D}(\hat{a}_{\text{in}})$  is the shift operator along the group of coherent states,  $\hat{a}_{\text{in}}$  and  $\hat{a}_{\text{in}}^+$  are annihilation and creation operators for a mode of the field, and  $|0\rangle_{\text{in}}$  is the vacuum state for a mode of the field at the input  $a_{\text{in}}$ . Similarly for the input  $b_{\text{in}}$ . As is well known,<sup>5</sup> a coherent state is an eigenstate of the annihilation operator

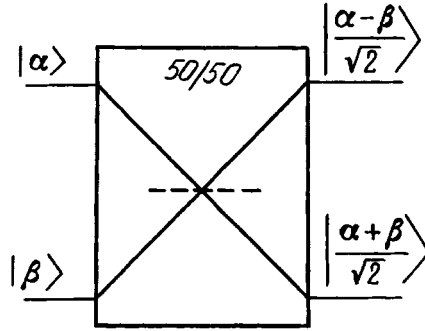


FIG. 1.

$$\hat{a}_{\text{in}}|\alpha\rangle_{\text{in}} = \alpha|\alpha\rangle_{\text{in}} \quad \text{and} \quad {}_{\text{in}}\langle\alpha|\hat{a}_{\text{in}}^{\dagger} = {}_{\text{in}}\langle\alpha|\alpha^*, \quad (3)$$

$$|\alpha\rangle_{\text{in}} = \exp(-|\alpha|^2/2) \sum_{n=0}^{\infty} \frac{\alpha^n}{\sqrt{n!}} |n\rangle,$$

where  $|n\rangle$  is the Fock state with  $n$  photons. Any two coherent states are nonorthogonal because they have a vacuum component, even if they have different carrier frequencies:

$${}_{\text{in}}\langle\beta|\alpha\rangle_{\text{in}} = \exp(-|\alpha - \beta|^2).$$

The beam splitter is a unitary converter of input states of the field into output states. Its action is described by a  $2 \times 2$  unitary matrix. We have

$$\begin{pmatrix} \hat{a}_{\text{out}} \\ \hat{b}_{\text{out}} \end{pmatrix} = \frac{1}{\sqrt{2}} \begin{pmatrix} 1 & -1 \\ 1 & 1 \end{pmatrix} \begin{pmatrix} \hat{a}_{\text{in}} \\ \hat{b}_{\text{in}} \end{pmatrix} = \hat{U} \begin{pmatrix} \hat{a}_{\text{in}} \\ \hat{b}_{\text{in}} \end{pmatrix}. \quad (4)$$

An approach in which the optical scheme transforms field operators and leaves the states themselves unchanged corresponds to the Heisenberg picture. A different approach is possible (the Schrödinger representation), where the optical channel transforms the states of the field but not the operators.<sup>6</sup>

The photon number operators at the outputs of the beam splitter are

$$\hat{a}_{\text{out}}^{\dagger} \hat{a}_{\text{out}} = \left( \frac{\hat{a}_{\text{in}}^{\dagger} - \hat{b}_{\text{in}}^{\dagger}}{\sqrt{2}} \right) \left( \frac{\hat{a}_{\text{in}} - \hat{b}_{\text{in}}}{\sqrt{2}} \right), \quad (5)$$

$$\hat{b}_{\text{out}}^{\dagger} \hat{b}_{\text{out}} = \left( \frac{\hat{a}_{\text{in}}^{\dagger} + \hat{b}_{\text{in}}^{\dagger}}{\sqrt{2}} \right) \left( \frac{\hat{a}_{\text{in}} + \hat{b}_{\text{in}}}{\sqrt{2}} \right).$$

The *average* number of photons at the outputs  $a$  and  $b$ , using expressions (3) and (5), respectively, equal (it is understood below that the carrier frequencies for the input states are identical)

$$N_{a,\text{out}} = \text{Tr}\{\hat{\rho}_{\text{in}}\hat{a}_{\text{out}}^+\hat{a}_{\text{out}}\} = \left| \frac{\alpha - \beta}{\sqrt{2}} \right|^2, \quad (6)$$

$$N_{b,\text{out}} = \text{Tr}\{\hat{\rho}_{\text{in}}\hat{b}_{\text{out}}^+\hat{b}_{\text{out}}\} = \left| \frac{\alpha + \beta}{\sqrt{2}} \right|^2.$$

Therefore, the beam splitter operates as a quantum comparator for input signals in a *coherent state* (and only for them). If the input states are identical, then complete compensation of the signals — total destructive interference — occurs at one of the outputs (the “subtracting” one). In this case total constructive interference occurs at the “summing” output.

When the states at the inputs are identical, the probability of detecting a photon at the “subtracting” output of the photodetector equals *identically* zero, since the state of the “subtracting” output corresponds to the vacuum state, which is an *eigenstate* of the photon-number operator with eigenvalue  $N_{a,\text{out}} = 0$ . If the states at the inputs of the beam splitter are not identical, then the output states at the outputs  $|\alpha - \beta/\sqrt{2}\rangle_{a,\text{out}}$  and  $|\alpha + \beta/\sqrt{2}\rangle_{b,\text{out}}$  are *not* eigenstates of the photon-number operator. The latter means physically that  $N_{a,\text{out}}$  and  $N_{b,\text{out}}$  are the *average* number of photons detected by a photodetector in a large series of measurements. In each individual measurement (when the signals at the inputs are not identical) any number of photons can be detected in each output. Consequently, events in which a photodetector will not be triggered at the “subtracting” output (zero photons are detected) will be inevitable. In addition, the fraction of such events will be all the larger, the closer the difference  $\alpha - \beta$  is to zero (the closer the states are to one another or, equivalently, the more nonorthogonal they are). Therefore if a photodetector is not triggered at the “subtracting” output, then this event does not make it possible to draw a definite conclusion about the second input state with a known reference (so-called inconclusive result). At the same time, if it is known which state should be at the second input and if it is identical to the reference state, then triggering of the photodetector at the “subtracting” output gives an *unequivocal* conclusion that the state at the second input was altered by an eavesdropper.

In summary, we arrive at the conclusion that if both detectors are triggered simultaneously, then this event means that the reference state is not identical to the probe state. But if only the bottom detector is triggered, then a definite conclusion about the probe state cannot be drawn. This circumstance (which is a consequence of the nonorthogonality of the states) essentially has the effect that an eavesdropper will inevitably err.

Let us now discuss the application of this quantum comparator for distribution of the key (a random sequence of zeros and ones) between two users. A schematic diagram of the quantum cryptosystem is displayed in Fig. 2. The users *A* and *B* have two identical sources that can prepare, by choice, the states  $|\alpha\rangle_{\text{in}}$  or  $|\beta\rangle_{\text{in}}$  ( $\alpha \neq \beta$ ). Moreover, user *B* has a delay line whose length equals that of the communication line. It is assumed that the user clocks are synchronized in each transmission. The key generation protocol is as follows.

The users *A* and *B* randomly and independently of one another prepare states  $|\alpha\rangle_{\text{in}}$  and  $|\beta\rangle_{\text{in}}$  corresponding to a logical 0 or 1.

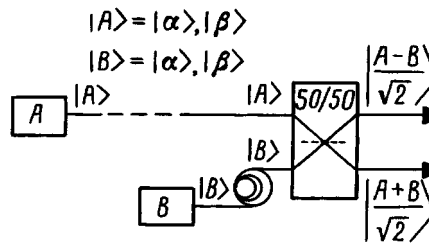


FIG. 2.

After making a series of transmissions, for some of them the user  $A$  reports through an open communication channel the number of measurements in which  $|\alpha\rangle_{\text{in}}$  was transmitted and in which  $|\beta\rangle_{\text{in}}$  was transmitted. User  $B$  checks the outcomes of measurements in which the transmission from  $A$  was identical to his reference state. If there is no eavesdropping, then for these measurements the outcome at the ‘‘subtracting’’ output of the comparator should be zero. The first nonzero outcome with an ideal communication channel indicates the presence of an eavesdropper.

After the absence of eavesdropping is established, the remaining measurements serve for generation of a secret key. For this, the user  $B$  reports the number of measurements for which a nonzero result was obtained at both comparator outputs but he does not report which reference state he used ( $|\alpha\rangle_{\text{in}}$  or  $|\beta\rangle_{\text{in}}$ ). This information is sufficient for the users to have an identical secret key. Indeed, if in a given measurement a nonzero outcome was obtained at both outputs and, for example, the user  $B$  used as the reference state  $|\alpha\rangle_{\text{in}}$  (logical 0), then this could occur only when user  $A$  transmitted the state  $|\beta\rangle_{\text{in}}$  and vice versa. In this case the users accept into the key a logical 0. Similarly for a logical 1. As a result, an identical and secret sequence of 1s and 0s arises.

Different variants of exchange protocols for quantum cryptosystems were recently proposed.<sup>2,3,7-13</sup> However, only the systems of Refs. 14–17, which are based on the protocol proposed in Ref. 2, have been realized experimentally. These systems consist of a quite complicated interferometer with time division (so-called time division interferometer<sup>14-17</sup>), in which to guarantee secrecy the signal must be attenuated to the level of a single photon per pulse. In real experiments,<sup>14-17</sup> radiation is attenuated to the level 0.1–0.2 photons per transmission.

In my view, the main difficulty in implementation consists of the following. Formally, to implement a quantum cryptosystem it is sufficient to have as carriers any pair of nonorthogonal states,<sup>2</sup> for example,  $|u_0\rangle$  and  $|u_1\rangle$ , and a measurement ‘‘device’’ that implements the projectors  $\bar{P}_0 = 1 - |u_0\rangle\langle u_0|$  and  $\bar{P}_1 = 1 - |u_1\rangle\langle u_1|$ . Measurements with these projectors make it possible to discover *any* changes in the states  $|u_0\rangle$  and  $|u_1\rangle$ . This guarantees the secrecy of the cryptosystem. However, there is no general prescription that would make it possible to produce, according to the projector written, an experimental apparatus that implements it. It is especially difficult to realize projectors if they do not correspond to a physical observable.

It is most convenient to use coherent laser radiation as information carriers, for

example,  $|\alpha\rangle$  and  $|\beta\rangle$  ( $|\alpha\rangle$  and  $|\beta\rangle$  are nonorthogonal when  $\alpha \neq \beta$ , which is achieved simply by changing the intensity of the radiation in different transmissions). However, it is quite difficult to implement a “negation” projector for a coherent state  $\bar{P}(\alpha) = 1 - |\alpha\rangle\langle\alpha|$  and  $\bar{P}(\beta) = 1 - |\beta\rangle\langle\beta|$ . It is only known how to implement a projector-valued measure for a coherent state  $\hat{M}(d\alpha) = |\alpha\rangle\langle\alpha|d^2\alpha/\pi$  using a quite delicate homodyne detection method,<sup>18</sup> but by no means the projector  $\bar{P}(\alpha)$ . In addition, such a projector-valued measure can be implemented for ideal homodyne detection, where the phase of the reference signal (“local oscillator”) is strictly fixed, which is achieved formally only with an infinite intensity of the reference signal.

For this reason, it is actually necessary to decrease the intensity of the signal to the one-photon level. If only one Fock state  $|n\rangle$  ( $n=1$ ) is present in the signal, then the projector onto such a state can be implemented quite simply with a standard photodetector. If  $n > 1$ , then for the time being there are no photodetectors that would make it possible to distinguish states with different numbers of photons. Moreover, a single-photon state is obtained in experiments (see Refs. 14–17 for details) by strong attenuation of the laser radiation, i.e., the signal has the form  $|\alpha\rangle \approx |0\rangle + \alpha|1\rangle + \dots$  (for  $\alpha \ll 1$ ).<sup>17</sup> For this reason, strictly speaking, it is necessary to implement a projector onto such a state, which an ordinary photodetector does not give.

Moreover, there is another annoyance in using laser radiation that is attenuated to the one-photon level. In principle, such attenuation cannot give any guarantee that one and not two or more photons are present in the transmission. Of course, the probability of the presence of  $n$  photons decreases with  $\alpha$ . The presence of more than one photon in a transmission can be used to eavesdropping by “diverting” some of the photons. In addition, such attempts are not detected in the implementations used in Refs. 14–17.

In my view, the difficulties mentioned above are not present in the scheme proposed in this letter because the scheme operates as a quantum comparator (it performs “subtraction” of the arguments in the coherent input states in one channel and “addition” in the second channel —  $|\alpha\rangle \otimes |\beta\rangle \rightarrow |\alpha - \beta/\sqrt{2}\rangle \otimes |\alpha + \beta/\sqrt{2}\rangle$ ). At the final stage of the measurements the photodetector measures the observable  $N_{a,\text{out}} = \text{Tr}\{\hat{\rho}_{\text{in}}\hat{a}_{\text{out}}^+\hat{a}_{\text{out}}\}$  and  $N_{b,\text{out}} = \text{Tr}\{\hat{\rho}_{\text{in}}\hat{b}_{\text{out}}^+\hat{b}_{\text{out}}\}$  — the number of photons in the states  $|\alpha - \beta/\sqrt{2}\rangle$  and  $|\alpha + \beta/\sqrt{2}\rangle$  already converted by the comparator — and not the projectors  $\text{Tr}\{\hat{\rho}\bar{P}(\alpha)\}$  and  $\text{Tr}\{\hat{\rho}\bar{P}(\beta)\}$ . In addition, for the protocol it is not necessary to distinguish between events with a different number of photons; only the fact of detection or no detection is sufficient. Likewise, there is no need to attenuate the laser radiation to the one-photon level; signals of any intensity can be used. Although interference from two unknown sources is not formally prohibited, if the sources are ideally synchronized, in the experimental implementation this circumstance can present appreciable difficulties (just as in the implementation of the scheme of Ref. 3).

In my view, the present scheme differs substantially from other schemes in that it *explicitly employs the fact that a coherent state is not destroyed by the beam splitter* (the state remains coherent at the output but with a different parameter). The application of this nontrivial property of coherent radiation, well-known in quantum optics and not previously used in other works on quantum cryptography, could simplify the experimen-

tal implementation of quantum cryptosystems. Other states of the field are not converted by the beam splitter into similar states. This signifies the impossibility of a quantum comparator based on a beam splitter for arbitrary states of radiation, including also the single-photon state.

I wish to thank S. V. Iordanskiĭ, V. F. Klyuev, and S. S. Nazin for helpful discussions in the course of this work. This work was supported by the Russian Fund for Fundamental Research (Project 96-02-18918) and by Grant No. 110/57/1–3 from the program “Promising Technologies in Micro- and Nanoelectronics.”

- <sup>1</sup>W. K. Wootters and W. H. Zurek, *Nature* **299**, 802 (1982).
- <sup>2</sup>C. H. Bennett, *Phys. Rev. Lett.* **68**, 3132 (1992); C. H. Bennett, G. Brassard, and N. D. Mermin, *Phys. Rev. Lett.* **68**, 557 (1992).
- <sup>3</sup>B. Huttner, N. Imoto, N. Gisin, and T. Mor, *Phys. Rev. A* **51**, 1863 (1995).
- <sup>4</sup>F. T. Arecchi, M. O. Scully, H. Haken, and W. Weidlick, in *Quantum Optics*, edited by R. J. Glauber, Academic Press, New York, 1969 [Russian translation, Mir, Moscow, 1974].
- <sup>5</sup>V. V. Dodonov and V. I. Man'ko, *Invariants and Evolution of Nonstationary Quantum Systems* [in Russian], Proceedings of the Physicotechnical Institute, 1987, Vol. 183.
- <sup>6</sup>D. N. Klyshko, *Usp. Fiz. Nauk* **164**, 1187 (1994).
- <sup>7</sup>A. K. Ekert, *Phys. Rev. Lett.* **67**, 661 (1991).
- <sup>8</sup>A. K. Ekert, J. G. Rarity, P. R. Tapster, and G. M. Palma, *Phys. Rev. Lett.* **69**, 1293 (1992).
- <sup>9</sup>L. Goldenberg and L. Vaidman, *Phys. Rev. Lett.* **75**, 1239 (1995).
- <sup>10</sup>M. Koashi and N. Imoto, *Phys. Rev. Lett.* **77**, 2137 (1996).
- <sup>11</sup>E. Biham, B. Huttner, and T. Mor, *Phys. Rev. A* **54**, 2651 (1996).
- <sup>12</sup>A. Muller, J. Brequet, and N. Gisin, *Europhys. Lett.* **30**, 809 (1994).
- <sup>13</sup>M. Koashi and N. Imoto, *Phys. Rev. Lett.* **79**, 2383 (1997).
- <sup>14</sup>C. Marand and P. D. Townsend, *Opt. Lett.* **20**, 1695 (1995).
- <sup>15</sup>R. J. Hughes, D. M. Alde, P. Dyer *et al.*, *Contemp. Phys.* **36**, 149 (1995).
- <sup>16</sup>S. J. D. Phoenix and P. D. Townsend, *Contemp. Phys.* **36**, 165 (1995).
- <sup>17</sup>A. Muller, T. Herzog, B. Huttner *et al.*, *Appl. Phys. Lett.* **70**, 793 (1997).
- <sup>18</sup>H. P. Yuen and J. H. Shapiro, *IEEE Trans. Inf. Theory* **IT-26**, 78 (1980); H. P. Yuen and V. W. S. Chan, *Opt. Lett.* **8**, 177 (1983).

Translated by M. E. Alferieff

## Nonstationary-states quantum cryptography

S. N. Molotkov and S. S. Nazin

*Institute of Solid-State Physics, Russian Academy of Sciences, 142432 Chernogolovka, Moscow Region, Russia*

(Submitted 16 September 1997; resubmitted 28 October 1997)

Pis'ma Zh. Éksp. Teor. Fiz. **66**, No. 11, 742–745 (10 December 1997)

A quantum cryptosystem is proposed in which a pair of nonstationary states differing in their times of preparation is used as the information carriers. © 1997 American Institute of Physics.

[S0021-3640(97)01423-0]

PACS numbers: 03.65.-w, 89.70.+c

The secrecy of quantum cryptosystems is based on the impossibility, in the general case, of reliably distinguishing by means of one measurement two states  $\rho_0$  and  $\rho_1$  (for example, two nonorthogonal pure states) employed for encoding information.<sup>1</sup> The key generation protocol for two users  $A$  and  $B$  is chosen in a manner so that measurements performed by both users (or by one of them) would be sufficient to discover an eavesdropper in the quantum communication channel between  $A$  and  $B$ . Thus, the quantum cryptosystem proposed in Ref. 2 employs a pair of pure nonorthogonal quantum states  $|u_0\rangle$  and  $|u_1\rangle$  (they correspond to the density matrix  $\rho_{0,1} = |u_{0,1}\rangle\langle u_{0,1}|$ ). The scheme of Ref. 2 employs two measurements, to which correspond the projectors  $\bar{P}_0 = 1 - P_0$  and  $\bar{P}_1 = 1 - P_1$ , where  $P_{0,1} = |u_{0,1}\rangle\langle u_{0,1}| \equiv \rho_{0,1}$ . The projectors  $\bar{P}_{0,1}$  project onto subspaces orthogonal to  $|u_0\rangle$  and  $|u_1\rangle$ , respectively, and therefore

$$\text{Tr}\{\bar{P}_0\hat{\rho}_0\} = 0, \quad \text{Tr}\{\bar{P}_1\hat{\rho}_1\} = 0, \quad (1)$$

$$\text{Tr}\{\bar{P}_{0,1}\hat{\rho}_{1,0}\} = 1 - |\langle u_0|u_1\rangle|^2 \neq 0, \quad \hat{\rho}_{0,1} = |u_{0,1}\rangle\langle u_{0,1}|.$$

Measurements with projectors  $\bar{P}_{0,1}$  make it possible to detect any changes in the pure states  $|u_0\rangle$  and  $|u_1\rangle$  in control transmissions, when both users know which state was transmitted.<sup>2</sup> Here it is implicitly assumed that the states  $|u_0\rangle$  and  $|u_1\rangle$  are stationary, since otherwise their temporal evolution would make it necessary to perform, at different times  $t_m$ , measurements corresponding to different projectors  $\bar{P}_{0,1}(t_m) = 1 - |u_{0,1}(t_m)\rangle\langle u_{0,1}(t_m)|$ . Note also that the requirement that the states  $|u_0\rangle$  and  $|u_1\rangle$  be nonorthogonal has the effect that these states must have the same energy. Otherwise, stationary states with different energy would be automatically orthogonal.

In the present letter we wish to show, for the example of a very simple quantum system, how to construct a quantum cryptosystem that is based on stationary states and on the measurement of the observed time. The required measurements can be performed by the user  $B$  at any fixed moment in time chosen by him.

Let us consider a two-level system with a time-independent Hamiltonian  $H$  diagonalized in the basis  $|e_0\rangle$  and  $|e_1\rangle$  (the energies  $E_0 = 0$  and  $E_1 = \omega$ ; we assume that  $\hbar = 1$ ).

By analogy with the case of a continuous spectrum,<sup>3</sup> we shall consider the expansion of the number 1 on the interval  $[0, T)$  ( $T = 2\pi/\omega$ ):

$$M(d\tau) = \frac{d\tau}{T} \sum_{k,l=0,1} |e_k\rangle\langle e_l| \exp i(E_k - E_l)\tau, \quad (2)$$

which corresponds to a covariant measurement of the observed time  $\tau$ . The limitation  $0 \leq \tau < T$  is due to the fact that any state of the unperturbed two-level system is periodic in time with period  $T$ . It is convenient to rewrite the expansion (2) of the number 1 in the form

$$M(d\tau) = (\sigma_0 + \sigma_1 \cos \omega\tau + \sigma_2 \sin \omega\tau) \frac{d\tau}{T}, \quad (3)$$

where  $\sigma_i$  ( $i = 1, 2, 3$ ) are Pauli matrices and  $\sigma_0$  is a  $2 \times 2$  unit matrix.

Let us now assume that the user  $A$  has at his disposal two states  $\rho_0$  and  $\rho_1$  (not necessarily pure; the scheme described below is equally applicable to pure and mixed states) that differ only in respect of the preparation time and that user  $A$  transmits along a quantum transmission channel to user  $B$ , i.e.,

$$\rho_i(t) = e^{-iH(t-t_i)} \rho_g e^{iH(t-t_i)}, \quad i = 0, 1; \quad 0 \leq t_0 < t_1 < T, \quad (4)$$

where  $\rho_g$  is a fixed ‘‘generating’’ state. Let us use for  $\rho_i$  the representation

$$\rho_i(t) = \frac{1}{2} (\sigma_0 + v_i^k(t) \sigma_k), \quad (5)$$

where  $v^k$  are the components of a vector  $|\mathbf{v}| \leq 1$ , i.e.,  $((v^1)^2 + (v^2)^2 + (v^3)^2)^{1/2} \leq 1$ . The evolution of the vector  $\mathbf{v}$  in the case of an unperturbed system is determined by the equation  $\dot{\rho} = i[\rho, H]$  with  $H = \omega(\sigma_0 - \sigma_3)/2$  and corresponds to the precession of the vector  $\mathbf{v}$  around the  $z$  axis with frequency  $\omega$ .

It is now clear that the probability of obtaining a result in the interval  $(\tau, \tau + d\tau)$  with a measurement  $M(d\tau)$  performed on the state  $\rho$  at time  $t_m$  is

$$P_M(\tau) d\tau = \text{Tr}(\rho M(d\tau)) = (1 + v^1(t_m) \cos \omega\tau + v^2(t_m) \sin \omega\tau) \frac{d\tau}{T}. \quad (6)$$

Therefore, the distribution function  $P_M(\tau)$  is the sum of the constant  $1/T$  and the linear combination  $v^1(t_m) \cos \omega\tau + v^2(t_m) \sin \omega\tau$ . Knowing the distribution function  $P_M(\tau)$ , the coefficients  $v^1(t_m)$  and  $v^2(t_m)$  of the cosine and sine can be easily determined. This establishes two of the three parameters determining the density matrix of the system. Moreover, a measurement of the energy of the states received by the user (i.e., a measurement of the observable corresponding to the Hamiltonian  $H$ ) gives results 0 and  $\omega$  with probabilities  $P = (1 \pm v^3)/2$  (a measurement of the energy formally corresponds to an expansion of unity  $M(d\epsilon)$  on a straight line concentrated at two points — 0 and  $\omega$ ). Therefore, knowledge of the complete statistics of the measurements  $M(d\tau)$  and  $M(d\epsilon)$  makes possible complete reconstruction of the state  $\rho$ . This circumstance can be used to discover an eavesdropper in the quantum communication channel along which the user  $A$  transmits the states  $\rho_0$  and  $\rho_1$  to the user  $B$ . Indeed, if the states  $\rho_0$  and  $\rho_1$  are such that

they cannot be distinguished reliably in one measurement (for example, if they correspond to two nonorthogonal pure states, when  $|\mathbf{v}_i|=1$ ), then the following key generation protocol can be proposed.

Let the entire time axis be divided into equal intervals of duration  $T$  (we assume that the user clocks are synchronized) and in each interval the user  $A$  randomly prepares and transmits to user  $B$  one of the states  $\rho_0$  or  $\rho_1$  (in each transmission the parameters  $t_0$  and  $t_1$  are measured from the start of the corresponding interval). The user  $B$  randomly chooses, independently of  $A$ , the type of measurement which he performs —  $M(dt)$  or  $M(d\epsilon)$  (at some fixed, i.e., identical for all transmissions, moment in time  $t_m$ ). The result of a measurement is  $\tau$  with probability  $P_M(\rho; d\tau)$  in the first case or the energy  $E$  (taking on values from the set  $\{0, \omega\}$ ) with probability  $P(\rho; E)$ . As usual, it is assumed that the parameters  $t_0$  and  $t_1$  and the generating state  $\rho_g$  are known beforehand to all, including the eavesdropper, but it is unknown whether user  $A$  will transmit  $\rho_0$  or  $\rho_1$  in each specific transmission. The presence of an eavesdropper in the communication channel is discovered as follows. After a sufficiently long series of measurements, the user  $A$  reports for some portion of the measurements (for example, half) the cases in which he transmitted  $\rho_0$  and the cases in which he transmitted  $\rho_1$ . Among these transmissions the user  $B$  looks only at those in which the state  $\rho_0$  was transmitted and he performed the measurements  $M(d\tau)$ . Let the number of such measurements be  $N$ . Next, he chooses an arbitrary  $0 \leq \theta < T$  and counts the number of cases  $N_\theta$  when as a result of measurements the values  $\tau \leq \theta$  were obtained. I now introduce the distribution function  $F(\tau) = \int_0^\tau d\tau' P_M(\tau')$  (according to which, just as according to  $P_M(\tau)$ , the parameters  $v^1$  and  $v^2$  of the density matrix are uniquely reconstructed) and the random variable  $\xi$ , which equals 1 if the value  $\tau \leq \theta$  is obtained in a given measurement and 0 otherwise. Then, from the Chebyshev inequality for a sum of  $N$  random variables  $\xi_k - p$ , where  $p = F(\theta)$ , it follows that for any  $\epsilon$

$$\Pr \left\{ \left| \frac{N_\theta}{N} - p \right| \geq \epsilon \right\} \leq \frac{p(1-p)}{N\epsilon^2} \leq \frac{1}{4N\epsilon^2}. \quad (7)$$

Therefore, as  $N \rightarrow \infty$ , the probability that the empirical distribution function  $F_N(\theta) = N_\theta/N$  deviates from the distribution function  $F(\theta)$  known beforehand uniformly approaches 0 in  $\theta$  as  $N^{-1}$ . Having chosen a sufficiently small value of  $\epsilon_0$ , the user  $B$  can assume that an eavesdropper is present in the communication channel if at least for one  $\theta$  the inequality  $|N_\theta/N - p| \leq \epsilon_0$  is violated. Indeed, since the parameters  $v^1$  and  $v^2$  of the density matrix are reconstructed uniquely according to the function  $F(\tau)$ , the deviation of  $F_N(\tau)$  from  $F(\tau)$  indicates that the measurements performed by the user  $B$  were performed on states for which at least one of the parameters  $v^1$  or  $v^2$  is different from the corresponding parameter  $\rho_0(t_m)$ . A similar procedure can be used to analyze the distribution of the results of measurements of the energy for cases when the states  $\rho_0$  were transmitted; this makes it possible to determine a deviation of the parameter  $v^3$  from  $v_0^3(t_m)$ . Since the parameters  $v^{1,2,3}$  completely fix the state of the two-level system under study, the procedure described above makes it possible to detect any attempt by an eavesdropper to substitute secretly the state transmitted by the user  $A$ .

After the absence of an eavesdropper has been established with a prescribed probability, the set of measurements  $M(d\tau)$  remains at the disposal of the user  $B$ . As a result

of nonorthogonality of the states  $\rho_0$  and  $\rho_1$ , the measurements  $M(d\tau)$  do not permit distinguishing 0 from 1 reliably in each individual attempt. The reliable information about the secret key (a sequence of 0s and 1s) that the users retain as a result of using, for example, a random block code amounts to less than one bit per transmission. This quantity is described by the mutual information, which in our case is given by a formula for a symmetric binary channel:<sup>4,5</sup>

$$I = 1 + q \log_2 q + (1 - q) \log_2 (1 - q), \quad (8)$$

where  $q$  is the probability of an error, i.e.,  $q = P(1|0) = p(0|1)$  is the conditional probability that a 0 was transmitted and interpreted as 1 on reception and vice versa. Correspondingly, the probability of a correct interpretation is  $1 - q = P(1|1) = P(0|0)$ . The concrete values of the quantities  $P(i|j)$  are determined by the strategy that the user  $B$  chooses for interpreting the results of measurements  $M(d\tau)$  obtained by him.

I wish to thank S. V. Iordanskiĭ and V. F. Klyuev for helpful discussions in the course of this work. This work was supported by the Russian Fund for Fundamental Research (Project 96-02-19396).

<sup>1</sup>W. K. Wootters, W. H. Zurek, *Nature* **299**, 802 (1982).

<sup>2</sup>C. H. Bennett, *Phys. Rev. Lett.* **68**, 3132 (1992); C. H. Bennett, G. Brassard, and N. D. Mermin, *Phys. Rev. Lett.* **68**, 557 (1992).

<sup>3</sup>A. S. Kholevo, *Probabilistic and Statistical Aspects of Quantum Theory* [in Russian], Nauka, Moscow, 1980.

<sup>4</sup>C. E. Shannon, *Bell Syst. Tech. J.* **27**, 379 (1948); *Bell Syst. Tech. J.* **27**, 623 (1948).

<sup>5</sup>I. Csiszár and J. Körner, *Information Theory: Coding Theorems for Discrete Memoryless Systems*, Akademiai, Kiado–Budapest, 1981.

Translated by M. E. Alferieff